

**FOSTERING THE DEVELOPMENT OF TECHNOLOGIES AND
PRACTICES TO REDUCE THE ENERGY INPUTS INTO THE
REFRIGERATION OF FOOD**

Reviews of Alternative Refrigeration Technologies

J.S. Lewis, I. Chaer and S.A. Tassou

Centre for Energy and Built Environment Research
School of Engineering and Design
Brunel University

July 2007

CONTENTS

1.	ADSORPTION REFRIGERATION	1
2.	AIR CYCLE REFRIGERATION.....	39
3.	MAGNETIC REFRIGERATION.....	63
4.	STIRLING CYCLE REFRIGERATION	75
5.	THERMOELECTRIC REFRIGERATION.....	90

1. ADSORPTION REFRIGERATION

Basic Concept Description

Adsorption is the process by which molecules of a fluid are fixed on the walls of a solid material via connections of the Van der Waals type, Ruthven (1984). The adsorbed molecules undergo no chemical reaction but simply lose energy when being fixed to the adsorption bed resulting in an exothermic energy output.

This report is not intended to give a comprehensive description of adsorption technologies. The reader is referred to the relevant literature such as Wang and Oliveira (2006) and Critoph et al (2000). Nevertheless, the general principle of the basic adsorption refrigeration cycle is given in Figure 1.1. The refrigeration circuit usually consists of three main components; a solid adsorbent bed, a condenser and an evaporator. Some systems employ isolating valves between the various components and some utilize expansion valves between the condenser and the evaporator. The adsorption refrigeration cycle relies mainly on the natural affinity of the adsorbent bed (when at low temperature) to attract the refrigerant vapour from the evaporator thus creating a lower pressure in the evaporator. Once the adsorbent bed is close to the saturation point, the valve between the evaporator and the adsorber is closed and heat is applied to the adsorbent bed, thus releasing the refrigerant vapour which then gets collected and condensed in the condenser before returning to the evaporator. Once this cycle is completed the heat on the adsorbent bed is removed and in some cases forced cooling is introduced onto the adsorber until the adsorption conditions are established then the valve between the evaporator and the adsorbed is reopened.

Figure 1.2 presents a schematic vapour pressure diagram of the basic adsorption cycle. The refrigerant uptake (x) is defined as the ratio of the mass of the adsorbed refrigerant to the mass of dry adsorbent. Starting with the state point 1, in which the adsorbent is cold and saturated with the refrigerant, heat is applied to the adsorber–desorber heat exchanger. This results in heating up the adsorbent, which consequently results in desorbing a certain amount of the refrigerant. Accordingly, the system pressure increases, ideally without changing the refrigerant uptake (so-called isosteric preheating), until the minimum desorption temperature is reached (state point 2). At this temperature the system pressure becomes equal to the saturation pressure corresponding to the temperature (T_{con}) of the heat sink available for receiving the heat of condensation. The desorption process starts from this point on and the refrigerant is condensed, ideally at a constant pressure (processes 2 and 3 in Figure 1.2). The desorption process proceeds until the adsorbent temperature reaches the maximum available desorption temperature and the refrigerant uptake reaches the cycle minimum uptake (x_{min}) (state point 3).

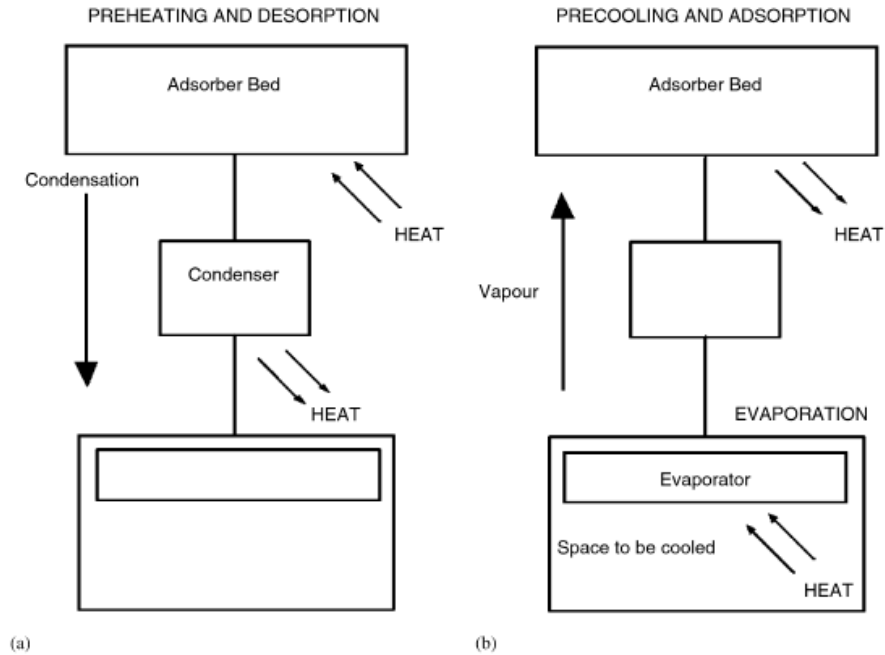


Figure 1.1. Schematic of an adsorption system, Wang and Oliveira (2006).

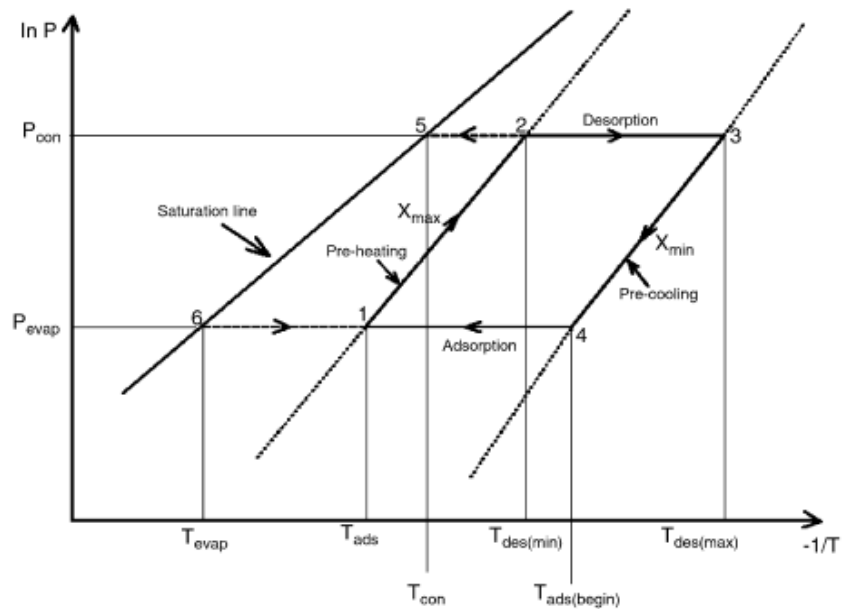


Figure 1.2. Schematic of an adsorption system, Critoph et al (2000).

The second working phase begins as the adsorber–desorber heat exchanger is cooled by rejecting its heat to the ambient. The adsorbent is pre-cooled and becomes able to adsorb

refrigerant vapour. This results in decreasing the system pressure, ideally without changing the refrigerant uptake within the adsorbent. As the adsorber–desorber heat exchanger is further pre-cooled a portion of the previously desorbed and condensed refrigerant is adsorbed and the latent heat of vaporization is drawn from the remaining liquid refrigerant in the evaporator. This results in decreasing the refrigerant temperature from state point 5 to state point 6 at the end of the pre-cooling process (3 -4). The adsorption process, within which the cooling effect is produced, starts from state point 4 and proceeds by further cooling the adsorber–desorber heat exchanger until the whole amount of refrigerant is evaporated upon removing the cooling load from the surrounding space (refrigerator’s cabin) and adsorbed in the adsorbent.

Unlike vapour compression and absorption refrigeration, the basic adsorption/desorption process is not a continuous one. An adsorption bed” is charged with refrigerant at low temperature and pressure; when adsorption slows down or stops, the adsorption bed is heated and high temperature and pressure gas is released from the bed. To obtain a continuous cooling effect from an adsorption refrigeration system normally two or more adsorbent beds are used in the system. In a typical Two-bed cycle, the evaporator and the condenser would be connected to both beds through a series of valve. The heated bed would be opened to the condenser to allow desorption while the other would be opened to the evaporator to allow for adsorption. The heating and cooling of the beds and valve directions would be swapped between the two every cycle to provide “continuous” heating or cooling (actually oscillating between high and low cooling rates). The addition of more adsorption beds allows a steadier cooling rate and also permits the use of heat rejected from the adsorption process to be used as part of the energy input for the regeneration of the fully charged beds. These “advanced” cycles improve efficiency at the cost of adding a pump and heat recovery loops.

Working Pairs

Adsorption refrigeration differs fundamentally in the adsorbent-adsorbate pairs that are chosen and the molecular forces underlying the interaction of the pairs. The most common adsorption pairs are: Silica Jell and water, Zeolites and water, Zeolites and methanol and Active carbon and ammonia.

The refrigerant is normally selected based on its heat capacity, evaporating and melting temperatures and pressures, environmental impact and its ability to be adsorbed on solid beds. Ideally compounds with high heat capacity per unit volume of adsorbed phase and low environmental impact are normally selected. The non-toxicity and high latent heat of evaporation of water (2200 kJ/kg) promotes it as the ideal refrigerant. However, its freezing point and low vapour pressure limits its application to air-conditioning.

Ammonia on the other hand has lower latent heat of vaporization (1368 kJ/kg) than water and so is not thermodynamically efficient but its high vapour pressure ensures that there are no mass transfer limitations. It is also environmentally friendly, stable in the presence of adsorbents to at least 200 °C and maybe used for cooling down to -34 °C. The high toxicity effect of ammonia limits the system material to steel and aluminium and prevents its use within confined public spaces

Ethanol is another refrigerant with higher vapour pressure than water (although sub-atmospheric). The low latent heat of vaporization of ethanol is 838 kJ/kg and its normal boiling and low melting points are 78 °C and -115 °C, respectively.

Methanol has higher vapour pressure than water and ethanol (although still sub-atmospheric). The high normal boiling point of Methanol is 64.7 °C and the low melting point is -93.9 °C. Hence, it could be used for sub-zero temperatures it is also more compatible and less toxic than ammonia. However, its latent heat of evaporation (about 1100 kJ/kg) is only half that of water and is unstable at temperatures above 120 °C, dissociation problems have been encountered with active carbon–methanol at higher temperatures. This puts Methanol operating range somewhat in the middle between Ammonia and Water. Also with methanol, the machine is always at pressures lower than atmospheric. This is also an important safety factor because it means that, when there is a leak, air comes into the machine and can be detected by an abnormal increase in pressure and poor performance. There is thus adequate warning before methanol can flow out of the pipes.

Butane and R123 are alternative adsorption refrigerants. However, they both have low latent heat that would lead to very low COPs. Critoph (2004)

According to Critoph (2003-Performance limitation), methanol, acetonitrile, methyl amine, and NO₂ are all suitable sub-atmospheric refrigerants at -10°C, with methanol giving the best COPs (COP of 0.5 was reported in a single-stage cycle). Of the refrigerants above atmospheric pressure at -10°C, ammonia, formaldehyde, and SO₂ are suitable. Overall, methanol gives the best COP, with.

The properties of the adsorbent are also important when considering the system as complete package. Compared with other adsorbents, silica-gel can be regenerated at a relatively low temperature (below 100 °C and typically about 85 °C) and is also suitable to be utilized in a closed cycles at sub atmospheric pressure, Yanagi et al (1992). While Zeolites are the best adsorbent to make use of high-temperature heat sources. A maximum desorption temperatures of 300 °C has been assigned for Zeolite-13X/water which has been chosen as a working pair for the gas-fired cooling system, Dawoud (2006).

The adsorber materials are the critical components, and nearly all recent work has revolved around improving adsorber efficiency

Composite sorbents such selective water sorbents (SWSs) have been presented for sorption cooling and heating by various researchers. Typical SWS is a two-component material based on a porous host matrix and an inorganic salt impregnated inside pores. A large variety of both host matrices (such as mesoporous or microporous silica gels, aluminas, porous carbons, polymers, etc.) and salts (CaCl₂, LiBr, MgCl₂, LiCl, etc.) gives a wide possibility to change the sorbent properties in a wide range to fit the demands of particular applications. Among the different SWSs, the SWS-1L

(mesoporous silica gel impregnated with CaCl_2) have been reported showed a very high water sorption ability (up to 0.7 g of water per 1 g of dry sorbent), that results in a high heat storing capacity (up to 2000 kJ/kg) and an ability to remove most of the sorbed water at temperatures of 90–100 °C. The sorption equilibrium curves of the SWS-1L shows a combination of heterogeneous adsorption, chemical reaction with formation of solid crystalline hydrates of confined salt and liquid absorption. The complex nature of the sorption poses great difficulties for its theoretical description. Recently Restucciaa et al (2004), presented experimental and theoretical-simulation results on a lab-scale chilling module working with the composite sorbent SWS-1L (the mesoporous silica gel KSK impregnated with CaCl_2). They showed that the use of this composite material allows the module to reach a gross cooling COP up to 0.6 with desorption temperature of 90–95 °C. They also claimed that further improvement could be achieved by optimising the system and by the use of multi-bed system with internal heat recovery which would make it a promising alternative to the common Zeolite or silica gel for application in solid sorption units driven by low temperature heat ($T < 100$ °C).

SWS-2L/water compound is also another good pair which could be used for low temperature application and lower temperature heat source (e.g. solar driven adsorption systems). A maximum temperature of 130 °C has been assigned to SWS-2L/water cooling systems. Also SWS-2L/Water is more sensitive to the variation of the working temperatures compared to the Zeolite-13X/water cooling system. According to Gassel (1998), high temperature applied to SWS-2L bed are not advised due to possible degeneration of the host matrix (silica gel) as the temperature may rise locally above its stability limits.

Activated carbon –ammonia had been used as the main pair for sub-zero applications with generation temperature upto 200 °C. However, the conventional carbon-ammonia pairs have two main problems. The main technical difficulty is the poor heat transfer in the solid. Hence, the basic adsorption systems have resulted in low efficiency, cooling COP less than 0.6. In fact, Turner I and Critoph and Turner z, investigated the heat transfer properties of granular charcoals and have shown that these materials have poor thermal conductivity as a result of their high porosity, due to the absence of continuous conduction paths. This affects the cycling time which becomes long, leading to low specific cooling or heating power (kWkg⁻¹). This has lead to increased attention to cycle development and better heat management. Other drawback to the use of ammonia is that a secondary circuit would be required for its use in supermarkets. The cycle COP (based on delivered heat) for a single-stage low temperature system using a secondary refrigerant loop is in the range from 0.3 to 0.35. This would be a COP based on fuel high heating value of up to 0.29 if a burner with 82% efficiency is used. Although less efficient than the advanced absorption cycle, system costs are likely to be less.

Active Carbon- Methanol is another pair which according to Critoph (1988) and Pons and Guillemiont ((1986) and Delgado et al (1982) are less expansive than other pairs.

Li et al ((2004) have conducted many experimental test on solar driven ice maker with two different combinations Activated carbon and methanol and activated carbon and

ethanol. The results with the solar ice maker, regarding ice mass production and desorbing and adsorbing characteristics, show that the refrigeration effect with the activated carbon–methanol is superior to that of the refrigeration effect using the activated carbon–ethanol. The performance of the solar ice maker with the activated carbon–methanol working pair is about 3–4 times higher than that with the activated carbon–ethanol working pair under the condition of accepting similar radiation intensity and environment.

SYSTEM RESEARCH AND DEVELOPMENT

Commercial development of a sorption refrigerator occurred in the 1920s using silica gel and sulfur dioxide, Miller (1929). However, the availability of electrical power and development of CFC refrigerants, vapour-compression cycle became the dominant refrigeration cycle and the solid-sorption technology was abandoned until the 1970s when IGT (1972) conducted a technical feasibility study of solid adsorption cooling system. However, the modern revival of this technology did not start until the 1970s when Meunier (1978) and Tchernev (1979) began work on adsorption pairs suitable for use as solar refrigerators, either for maintaining the vaccine cold-chain or for food storage in developing countries. Interest grew rapidly in the 1980s with many researchers worldwide working on the various aspects related to adsorption. This has been complemented by the availability of adsorption cooling systems on the Market notably from Mycom and Nishiyodo in Japan and DY refrigeration from China and other products in development from companies such as Vaillant in Germany and Shuangliang in China. However, the competitiveness of these systems is limited by two main technical problems, not yet solved: (1) the lack of working pairs with good performance and low desorption temperature (80–90 °C), (2) the poor heat transfer properties of the adsorbent bed that limit the specific power of the machine. Work continues of the various. The following section presents the various novel adsorption systems and their design criteria.

Single Bed Machine

Single bed adsorption refrigerator cycle has been developed with simplicity and low initial cost in mind for applications where intermittent cooling and low cooling capacities are required, such as cooling drinks, storage of vaccine. Critoph (1993-(ISES), Hungary) reported that his group invented a solar powered refrigerator in which was recommended by the U.N. for vaccine storage in poor area; see Figure 1.3, for details.



Figure 1.3. Solar-powered cold box for vaccine preservation, Critoph (1993-(ISES), Hungary) and Critoph (2002 -ISHPC China).

Recently, Monma and Mizota (2005) patented an adsorption refrigerator. As shown in Figure 1.4, the adsorption refrigerator has a refrigeration chamber, an evaporator, an adsorbent bed. The refrigeration chamber is composed of a thermal conductive member surrounding a periphery. The evaporator is arranged in an outer side surrounding the periphery of the refrigeration chamber. The evaporator is composed of a first heat insulating layer surrounding an outer side periphery. By transferring cold generated in the evaporator into the refrigeration chamber via the thermal conductive member composing the refrigeration chamber, the cooling range by the evaporator of the refrigeration chamber can be significantly enlarged, and the initial cooling in reducing the temperature of refrigeration chamber can be carried out in a short time. A similar adsorption type cooler has been invented and patented by Hidaka et al. (2005) for cooling an object such as drinks in containers.

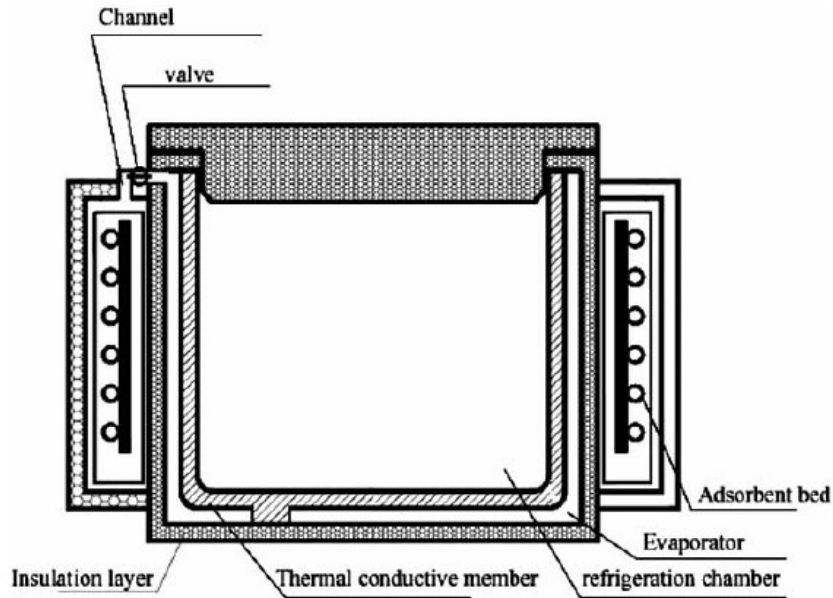


Figure 1.4. Adsorption Refrigerator invented by Monma and Mizota ((2005)-JP2005299974).

Patzner ((2001) patented disclosed a cooling method which uses at least one adsorber with Zeolite as adsorbent, water as refrigerant, with an evaporator. As illustrated in Figure 1.5, both containers are connected via at least one line containing a blocking valve. The adsorber and the evaporator each have at least one orifice and are selectively connectable to an over-pressure generator and a condenser. The selective separation and connection of individual components or component groups for carrying out regeneration and adsorption cycles take place in each in a pressure tight or vacuum-tight manner. Electrical heater can be used in this refrigerator. The capacity of this system can be extended by employing a number of identical absorbers. Endo and Komori (2005) obtained a patent for an adsorption refrigerating machine which composes of an evaporator, an adsorber, and a condenser. Water is used as the refrigerant, the adsorbent satisfying that a relative pressure is 0.14-0.2, and an adsorption swing amount is changed to be more than 0.05 kg/adsorbent (1kg) is filled. The adsorption swinging operation and the desorbing operation are performed in an area of the adsorption of 0.04 kg/adsorbent (1kg) or more. As the adsorbing/desorbing operation is performed in an area of capillary condensation, the heat of adsorption is inhibited, the heating quantity necessary for regeneration is reduced, and the freezing capacity and the energy efficiency can be improved.

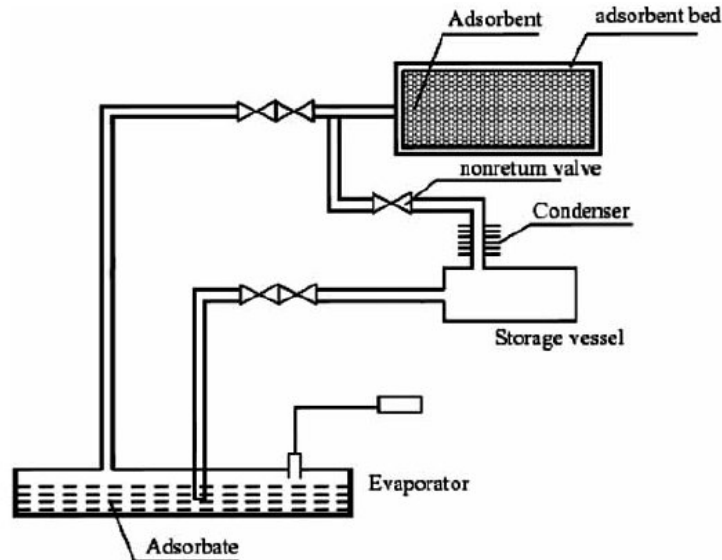


Figure 1.5. Adsorption Refrigerator invented by Patzner ((2001)- EP1154208).

When fixed adsorbent beds are employed, which is the common practice, in solar adsorption refrigeration, these cycles can be operated without any moving parts. On the one hand, the use of fixed beds results in silence, mechanical simplicity, high reliability and a very long lifetime, on the other hand, it also leads to intermittent cycle operation, with adsorbent beds changing between adsorption and desorption stages, which decreases the COP of the system. Hence, when constant flow of vapour from the evaporator is required in order to provide continuous cooling, two or more adsorbent beds must be operated out of phase

Multi-Bed System

One bed systems have low system performance in terms of SCP and COP and can only provide cooling intermittently. To solve this problem, two or more beds have been proposed by different researchers. Sato et al (1996, 1997 & 1998) have obtained four patents in the US and Japan for a multi-stage multi-bed strategy involving cooling the adsorber with refrigerant emanating from one or more evaporators see Figure 1.6 for details. The various absorbers in different stages are thermally connected in series so that the adsorbent bed of the lower stage is cooled by the flowing refrigerant which is being adsorbed by the adsorber of the higher stage. The authors reported high adsorbing and freezing capabilities.

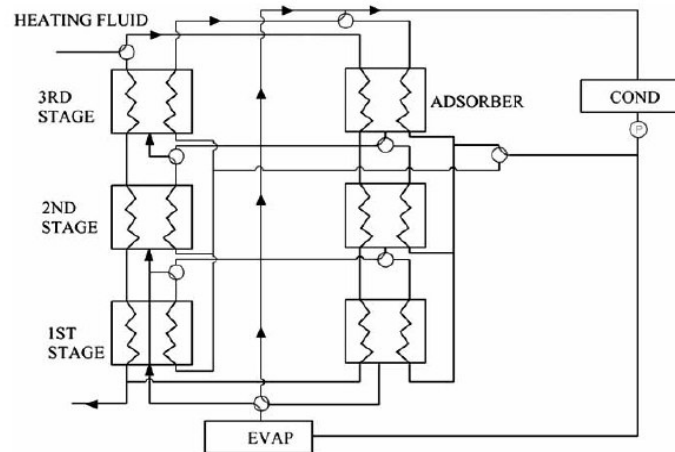


Figure 1.6. Multi-stage, Multi-bed adsorption refrigerator, Sato et al (US5775126 (1998) and JP9303900 (1997)).

Sato et al. (2001) invented an adsorption type refrigerator which has four adsorbers in the system with two adsorbers different in adsorption capacity from the others. This was done in order to cool the indoor diffused air to a satisfactory level while raising coefficient of performance of an adsorption type refrigerator, thus, coefficient of performance of an adsorption type refrigerator is raised while maintaining a sufficient cooling capacity for utilization. In addition, the sizes of the second adsorber and the fourth adsorber can be made compact. Another patent from Sato et al. (2003) mentioned an adsorption-type refrigerating apparatus to make use an adsorbent having a temperature-dependent characteristic in which the amount adsorbed in an adsorption step is larger than the amount adsorbed in a desorption step, even when a vapour pressure rate in the adsorption step is equal to or lower than a vapour pressure rate in the desorption step. Therefore, even when the cooling temperature of outside air for cooling the adsorbent increases, a sufficient cooling capacity can be obtained. In addition, a difference between the amount adsorbed in the adsorption step and the amount adsorbed in the desorption step can be made larger.

Heat and Mass Recovery

The above listed work on improved adsorption cooling system for use in various applications has not been limited to the desorption efficiency of the adsorbent bed. Other methods have been sought to provide low cost heat recovery with the adsorption cooling systems integrated in such a manner to provide an overall stable, continuous operation. Three main technologies to improve the process have been extensively researched and patented: regenerative processes with temperature front (also named thermal wave process) Shelton (1986) and Tchernev (1987) also Critoph, forced convective cycle; regenerative processes with heat and mass recovery, Chua et al- (2002), Critoph and Thorpe (1998), R.E. Critoph, Tamainot-telto (2004), Xia et al- (2005) and Akisawa et al (2005); rotating adsorber technology. Critoph (2001), Critoph (2003), Ebbeson (1999) and Liu and Fang (2005). A heat recovery cycle can shorten the cycle time and increase the SCP and COP, but if time for heat recovery is increased in order to get more heat

recovered, the performance of the system may drop, especially for SCP. In a good design of adsorption refrigeration system, the majority of the heat quantity can be recovered if the process of heat recovery lasts about 3 min. The mass recovery cycle can increase the cyclic refrigerant obviously, so the cooling power and COP of the adsorption system can be increased significantly too. In general, the mass recovery process usually arises before a heat recovery process and is practically suitable for low generation temperature.

Shelton (1986) obtained a patent for a thermal wave regenerative adsorption heat pump to improve the cycle COP. A temperature gradient is established lengthwise in the adsorbent bed in order to establish a thermal wave in the bed. The so-called thermal wave system is shown in Figure 1.7. As the heat transfer fluid is circulated through the system by a reversible pumping means, the beds are cycled between an upper and a lower operating temperature, creating the thermal wave within the bed of solid adsorbent. The heat transfer fluid always flows serially from the heater through the bed heat exchanger heating that bed while cooling the heat transfer fluid. Then the heat transfer fluid is passed through the cooling heat exchanger to further cool the heat transfer fluid, and the further cooled heat transfer fluid is passed through the other bed heat exchanger to cool that bed while heating the heat transfer fluid. Finally, the heated heat transfer fluid is returned to the heater to raise the heat transfer fluid to the original temperature. The adsorbent beds are constructed of one or more tubes through which the heat transfer fluid is passed and around which the solid adsorbent is held by a housing shell.

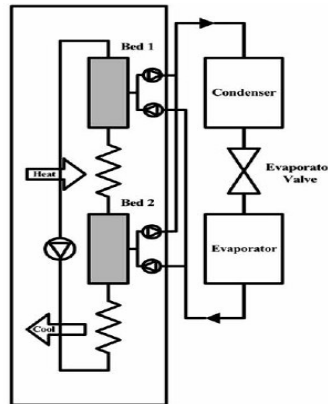


Figure 1.7. Thermal wave Adsorption system, Shelton-US4610148 (1986).

Chua et al (2002) obtained a patents for regenerative adsorption process and a multi-reactor regenerative adsorption chiller assembly. The system includes a condenser, an evaporator and a number of reactors, each being able to operate in adsorption and desorption modes and having a coolant inlet to directly or indirectly receive coolant when operating in adsorption mode before, after or simultaneous with the condenser. A waste heat inlet for directly or indirectly receiving thermal energy from a waste heat source when operating in desorption mode. Each adsorber alternately operates in adsorption and desorption modes for substantially identical time intervals. Each adsorber has an equal chance of being the first adsorber to receive the coolant when operating in adsorption mode and the waste heat from the waste heat source when operating in desorption mode.

Critoph and Thorpe (1998) obtained a patent a forced convection adsorption cycle and patented an adsorption cooling system comprising of two adsorbent beds each with an associated thermal management system. The thermal management systems are identical and consist of a circulating supply of a control fluid which passes through the adsorbent bed, a pump, a heat exchanger and an inert bed. Heat removed from the adsorbent beds by the control fluid is supplied to the inert beds and is store to be subsequently regenerated to heat the adsorbent beds in a later half of the operating cycle of the thermal compressor. The thermal compressor is energy efficient by virtue of the heat recycling (recovery) which is performed. In a recent patent granted to Critoph and Tamainot-telto (2004), another thermal driven adsorption system was described to provide energy-efficient heating or cooling by exploiting heat regeneration in an adsorption system. The enhanced heat and mass transfer resulted in an improved system COP and SCP. A COPs of upto 0.8 with their first prototype has been reported, see for Figure 1.8 details. This was obtained with evaporating temperatures down to -2°C , generating temperature of 225°C , heat rejection temperature 40°C and Condensing temperature 35°C . Granular carbon was used as the adsorbent and ammonia as the refrigerant which is forced via a gas circulator through the granular carbon bed.

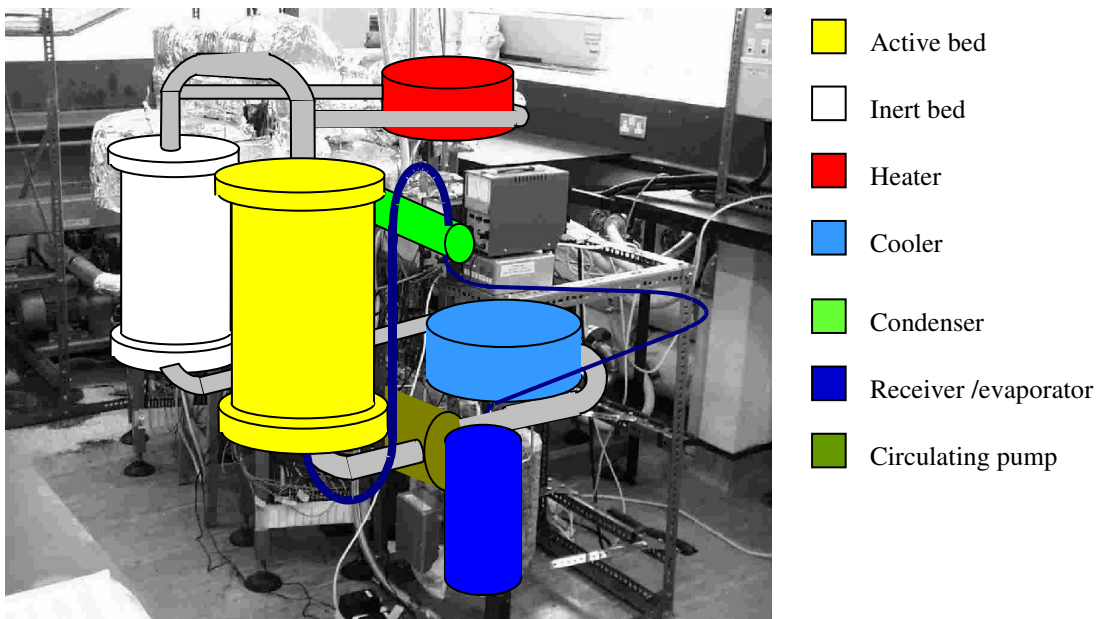


Figure 1.8. Forced convection adsorption cycle (Proto-type 1) at Warwick University, Critoph (2007)

Their second prototype was based on 12 kW cooling output and 17 kW heating power with 4 kg of ammonia charge, Figure 1.9. They have reported cooling COP of 0.9 and heating COP = 1.8 with driving temperatures ranging between $175^{\circ} - 225^{\circ}\text{C}$. The Parasitic pumping power was 200 W +200 W ancillaries. A total cost of €400-600 / kW was reported. Both these systems have been proven to give a high efficiency.

However, the team have moved away from these systems due to the complication in manufacturing and design problems with the soluble that have lead to poor performance.

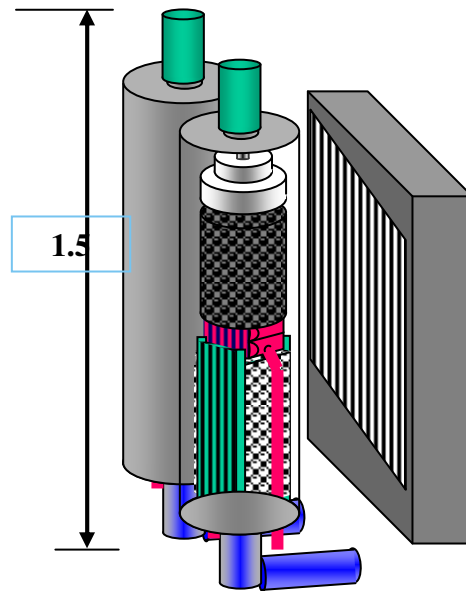


Figure 1.9.Characteristics of #2 prototype machine at Warwick University, Critoph (2007)

Xia et al. (2005), obtained a patent for a mass recovery method applied in the two bed system. This done by opening valves so that the refrigerant vapour transfers from the desorption adsorber to the adsorption adsorber due to the differential pressure. The improvements were in the order of 7-22% for the SCP and 20–30% for the COP, depending on the application and operation conditions. Temperatures or low evaporation temperatures is also possible with this method.

Rotary structure has been used for heat regeneration in adsorption system and providing continuous cooling effect. Critoph (2001) and Critoph, (2003) obtained patents for a rotary thermal regenerative adsorption system, which has a number of adsorbent module circumferentially about a rotational axis partly within a toroidal conduit (Figure 1.10). A heat transfer fluid flows from an inlet of the conduit to the outlet in counter-flow with respect to the rotational movement of the adsorbent modules. Separate fluid channels encase the evaporation/condensation zones of the vessels to enable transfer of heat between the vessels and the fluid flowing in channels. In this system, heat is regenerated in a particularly simple and convenient manner. As a result the compressive device is capable of achieving higher efficiencies than existing adsorption devices. However, the mechanical complexity of this system outweighed the benefits of the system.

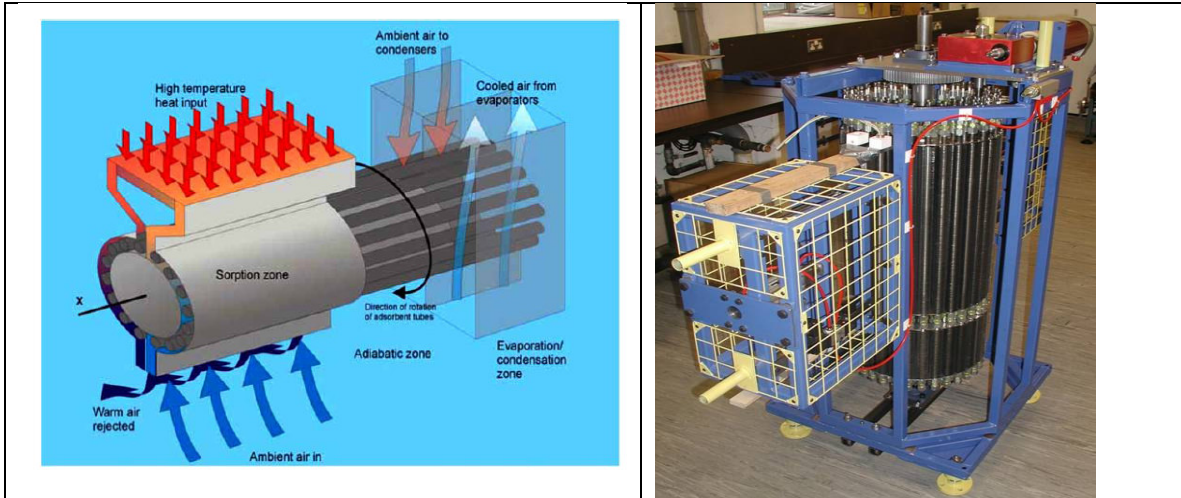


Figure 1.10. Rotary thermal regenerative sorption device, Critoph-WO200122010 (2001) and Critoph (2007).

Kim et al (2006) conducted an experimental study on the efficacy of a four-bed adsorption chiller with passive heat and mass recovery schemes. The findings of the investigation revealed substantial improvement of the adsorption chiller performance. The COP increased by as much as 30% over a broad range of cycle time with a wide heat source, coolant and chilled water temperatures. Two schemes were been considered: Firstly, only the mass recovery achieved by pressure equalization between the concomitantly cooled adsorber and heated desorber. Secondly, when both the heat and mass recovery schemes are employed at a rating point of maximum cooling capacity, the chiller COP could increase further to as much as 48%. These improvements are performed without additional hardware changes to the adsorption chiller. For two sets of supplied hot water temperatures, namely 85 °C and 75 °C, the maximum reported cooling capacities attained are 4.7 Rtons and 3.8 Rtons at 85 °C and 75 °C, respectively. They also observed that that the cooling capacity drops while the COP increases with increasing half-cycle duration. This behaviour was attributed to the high vapour-uptake potential of the adsorbent at early period of exposure from the unsaturated state.

Wang et al (2003) developed an adsorption refrigeration system (Ice Maker) by combining the mass and heat recovery processes, Figure 1.11. They presented experimental results of the system operating with an intermittent cycle and a cycle time of 35 minutes. The thermal conditions used to test the cycle are: 115°C heat source, 22°C heat sink, the evaporator temperature corresponding to the chilled ethylene glycol temperature is -7°C. At this evaporating pressure, the mass transfer resistance controls the adsorption process. Their test results showed that the COP reaches 0.07 whereas the SCP (specific cooling power) is 11 W kg⁻¹ activated carbon. Description of a two-bed adsorptive prototype ice-making machine operating with a heat and mass recovery cycle for onboard adsorption refrigeration in fishing boats was presented. The group claimed good performances due to improved mass transfer producing 18–20 kg h⁻¹ of flake ice at mean temperature of -7°C. The adsorber

configuration was designed as a shell and tube arrangement in which the shell side with highly internally finned is adsorbent and the tubes contain pressurized heat transfer fluid. Each adsorber in the shape of cuboid contains about 56 kg of carbon. The main components are two adsorber, an evaporator, a condenser, a gas–water heat exchanger, a hot-water tank and a flake icemaker (the COLDISC icemaker made by North Star Ice Equipment Co.). An oil burner is used as the simulated heat source from the engine exhaust gas for desorption. The fume gas from the burner heats the water in the hot-water tank through the gas–water heat exchanger. For a detailed description of its working process, see Wang (2001). Following initial experiments, the cycling time chosen was 40 min including the heat and mass recovery time of 1.5 min. It allows heating and desorption time of 20 min, which corresponds to the optimum heat input for maximum cooling power. That time corresponds to the maximum of the rate of concentration change averaged over time. The results of this system show that a SCP (Specific Cooling Power) of 27 W/kg carbon and a COP of 0.18 have been achieved to produce 18–20 kg/h of flake ice at temperature -7°C around.

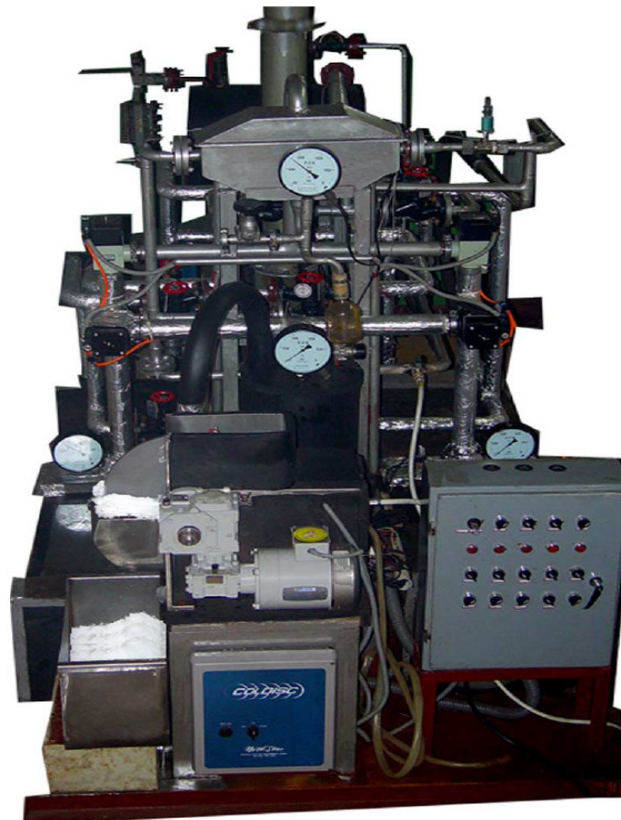


Figure 1.11. Adsorption Ice Maker Prototype Wang et al (2003).

Application of Heat Pipe Technology

The high initial costs of the machines and the low heat transfer rates of the adsorber are among the limitations to the commercialize adsorption systems. Based on the principle of heat pipe a novel silica gel-water adsorption chiller has been patented by Xia et al (2005)

and built and by Shanghai Jiao Tong University (SJTU) in China to solve these problems, see Figure 1.12 for details. There are two vacuum chambers inside this chiller; each of them encloses one adsorber, one condenser, and one evaporator. Mass recovery piping is installed between the two chambers. Cooling power of this adsorption chiller is 6–10 kW. The 6 kW cooling power and a COP of about 0.35 are obtained when the system is powered by hot water at 65 °C, which is the lowest working temperature of hot water, while 10 kW cooling power and a COP of about 0.4 are obtained when the temperature of hot water is 85 °C. This adsorption chiller could be used for solar powered air conditioner and also as the chiller for CCHP system. An adsorption system could provide 10–15 °C chilled water for normal air conditioning systems, or 15–20 °C chilled water for the cooling of dry fan coils, according to the requirements in which a COP of about 0.5 could be reached.

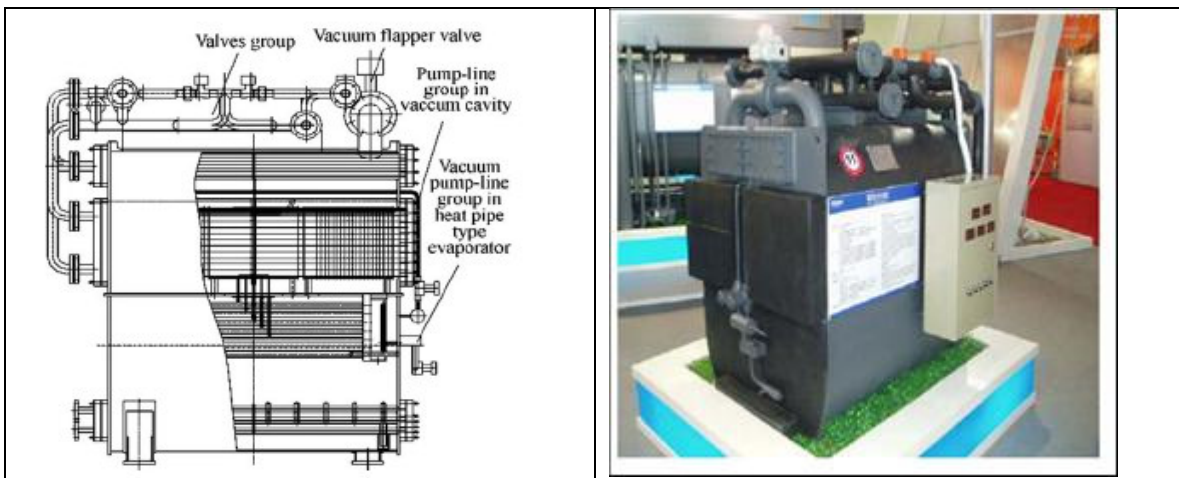


Figure 1.12. Silica gel Adsorption chiller with heat and mass recovery and heat pipes to output cooling, in the Shanghai Jiao Tong University, Wang (2006).

The second system has three vacuum chambers in the adsorption chiller: two adsorption/desorption (or evaporation/condensation) vacuum chambers and one heat pipe working vacuum chamber as the evaporator. One adsorber, one condenser and one evaporator are housed in the same chamber to constitute an adsorption/desorption unit. The evaporators of two adsorption/desorption units are combined together by a heat pipe heat exchanger, Figure 1.13. Schematic diagram of the heat pipe type silica gel-water adsorption chiller invented by SJTU, Xia, et al -CN1595017 (2005) to obtain continuous cooling effect. Since heat pipe can achieve a high heat flux, and no moving parts are used to drive the heat transfer fluid, the whole system can be made inexpensive and more reliable. In this chiller, a vacuum valve is installed between the two adsorption/desorption vacuum chambers to increase its performance especially when the chiller is driven by a low temperature heat source. The reliability of the chiller has been enhanced significantly due to using fewer valves.

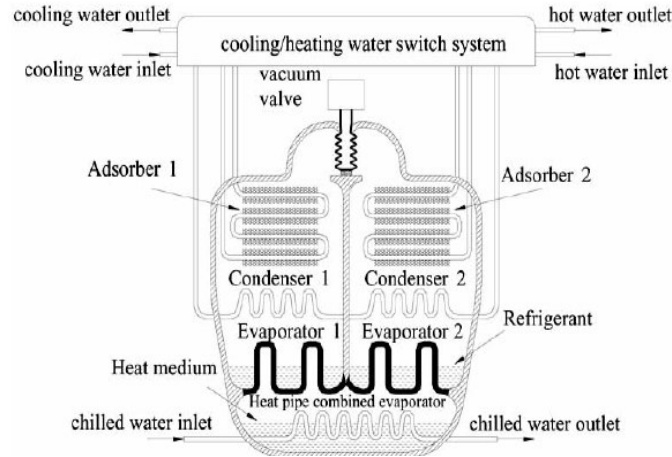


Figure 1.13. Schematic diagram of the heat pipe type silica gel-water adsorption chiller invented by SJTU, Xia, et al -CN1595017 (2005).

Wang et al. (2005), obtained another recent patent which employed a similar evaporator heat pipe device in a compact adsorption air conditioner (CAAC). This chiller was designed for combined utilization with a fuel cell for home use, and which could be considered as a mini Combined Cooling Heating and Power (CCHP) system. There are two vacuum chambers in the chiller, and each one encloses one adsorber (using silica gel as adsorbent), one condenser and one evaporator. As these equipments are inside the same chamber, there is no need of vacuum valves among them.

Besides the application of gravity heat pipes in adsorption chillers powered by low temperature heat sources, recent research in the SJTU also used heat pipes in the development of adsorption ice makers for fishing boats Wang et al. (2004) and Xia et al (2005). The utilization of this technology increased the heat transfer inside the adsorber and allowed direct use of exhaust gases as heat source and seawater as heat sink without producing corrosion in the adsorber.

Li et al (2006), presented results on the performance a multifunction heat pipe type adsorption ice making system with novel mass and heat recovery processes. The schematic diagram of multifunction heat pipe type adsorption ice maker test unit is shown in Figure 1.14, and the main components are an electric heating boiler, two adsorbent beds (Figure 1.15), a water cooler, a refrigerant condenser, a refrigerant evaporator (ice maker), a refrigerant storage vessel and heat pipes. The compound adsorbent used in the system is activated carbon-CaCl₂, which has higher adsorption performance than CaCl₂. Ammonia was as the refrigerant. The water liquid in boiler is heated by electric heater to produce water vapour, and the pressure meter and temperature sensors are installed to measure the corresponding pressures and temperatures. Water is used as the heat pipe working substance. For the test unit, the heating, cooling and heat recovery processes between two adsorbent beds are performed by multifunction heat pipes.

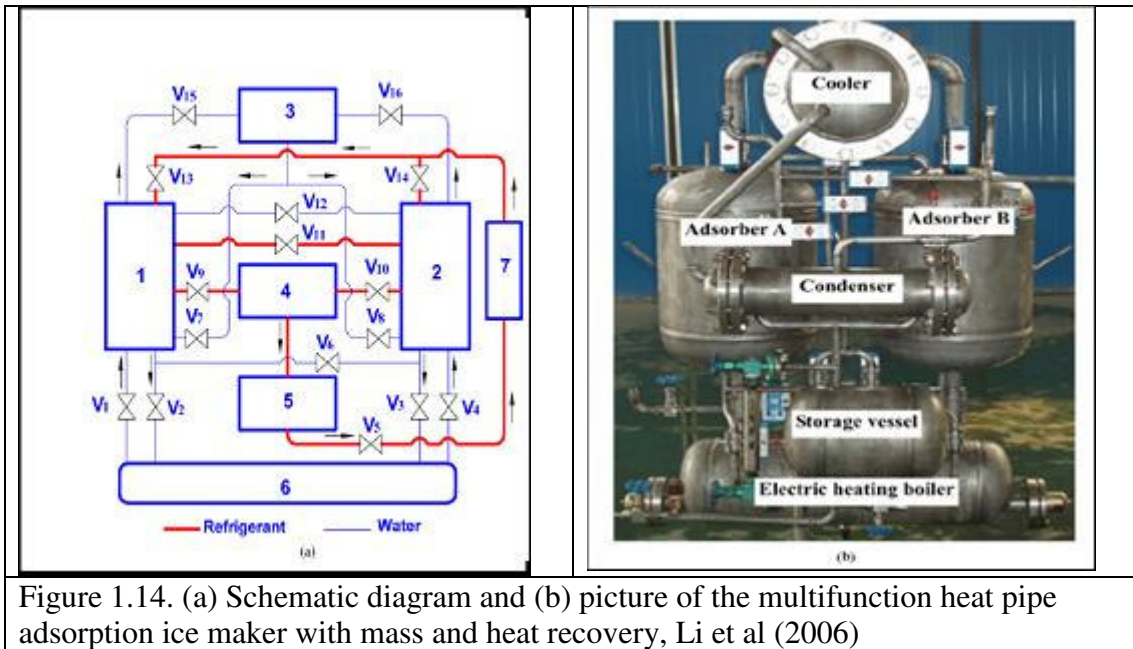


Figure 1.14. (a) Schematic diagram and (b) picture of the multifunction heat pipe adsorption ice maker with mass and heat recovery, Li et al (2006)

The evaporation of ammonia inside evaporator (component 7) provided refrigeration effect which according to the group was then transported to the flake ice maker to make ice. The group also reported that the mass recover was performed during the switch phase between desorption and adsorption by opening the valve V11 between the desorber and adsorber. This was claimed to cause a rapid transfer of the desorbed gas refrigerant from the desorber to adsorber due to the high pressure difference between two beds, thus improving the refrigerant mass circulation.

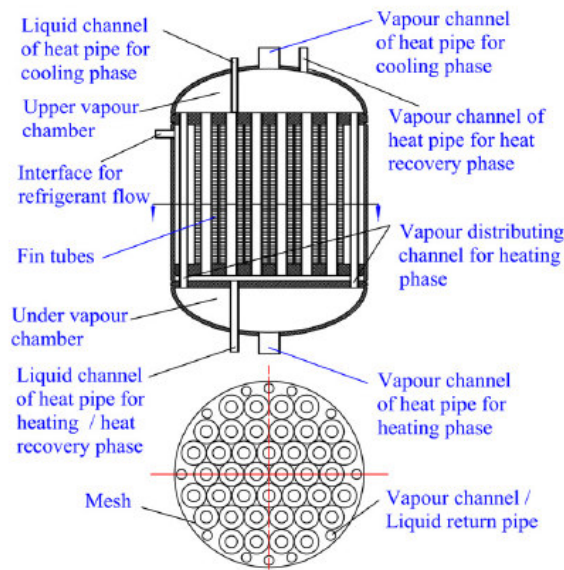


Figure 1.15. Structure of the compound adsorbent bed, Li et al (2006).

In heat recovery phase, the water vapour from the high temperature DHE flows into the lower temperature AHE and condenses there to provide latent heat, then the liquid water returns to high temperature DHE due to the gravitation of water. In this phase, low temperature bed is heated and high temperature bed is cooled by a split heat pipe in which the high temperature DHE serves as evaporator and low temperature AHE serves as condenser.

Critoph (2007) reported a study on a high efficient multifunction heat pipe type adsorption ice making system with novel mass and heat recovery processes in which the mass recovery process is carried out before the heat recovery process, and the desorber is heated and adsorber is cooled during the mass recovery phase.

Adsorption System with Heat Storage

Efforts have been made to improve refrigerating capacity and relax a temperature change of cooling liquid circulating by including energy storage in the adsorption refrigeration system. Endo and Nishikawa (2003) at Denso invented an adsorption refrigeration machine which uses a tank for cooling liquid storage Figure 1.16. Adsorption refrigerating machine with energy storage invented, The temperature variation of cooling liquid, during switch over between desorption and adsorption, is relaxed by mixing together cooling liquid circulating the absorbers and cooling liquid stored in the snubber.

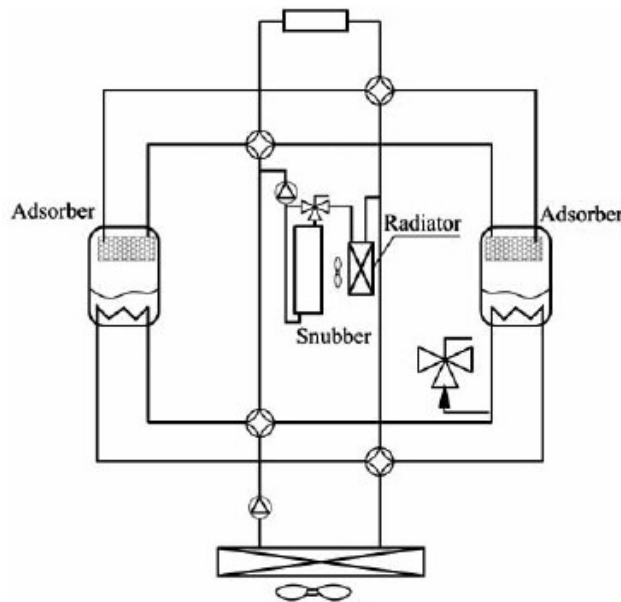


Figure 1.16. Adsorption refrigerating machine with energy storage invented, Endo and Nishikawa (2003).

Maier-Laxhuber et al. (2004) at Zeolith Tech suggested an adsorption cooling apparatus with buffer reservoir. This adsorption cooling device is so formed that a liquefaction device is connected to a buffer material storage device, and the buffer material storage

device buffers a part of liquefied heat of vapour of an operating means and guides the stored heat again to the circumference during adsorption. The liquefaction device is connected to the buffer material storage device to enable quickly desorption and high desorption capacity derived there from.

Hybrid System

In some patents, adsorptions cycles are combined with other type of refrigeration system to obtain a higher cooling efficiency. Inoue and Honda (1999) at Denso disclosed a refrigeration system which combined adsorption cycle with vapour compression cycle. As illustrated in Figure 1.17, the refrigerating unit is provided with a compressor, a condenser, an evaporator to cool the refrigerant and an adsorbent bed which has an adsorbent that generates heat during the adsorption of moisture and absorbs heat during the releasing of moisture. During the cooling, the refrigerant discharged from the compressor flows to the adsorbent bed instead of the condenser, where the adsorbate is released from the adsorbent to be condensed. During the non-cooling, the adsorbent bed is cooled by the refrigerant condensed by condenser to make the adsorbent adsorb refrigerant. By efficiently combining a steam compression type refrigeration cycle with the adsorption cycle, a higher cooling capacity can be obtained with a limited power. At the same year, Honda et al. (1999) suggested another hybrid system by compression refrigerating cycle and an adsorption type refrigerating cycle in a different form. This system is used to cool a heat generating apparatus. The heat of adsorption is absorbed by a low-temperature refrigerant of a vapour compression type refrigerating cycle.

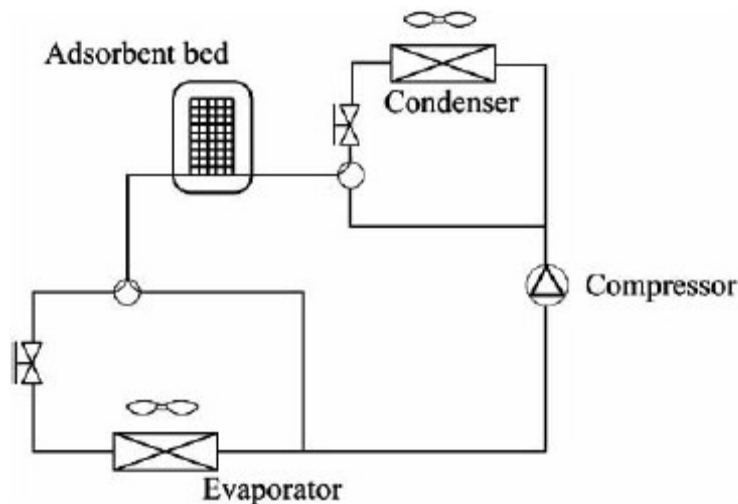


Figure 1.17. A Combined adsorption and vapour compression cycle, Inoue and Honda (1999)

Zhu (1999) invented an adsorption-absorption coupled refrigerating device which is composed of adsorber, condenser and evaporator. A valve is mounted to pipeline between adsorber and condenser. The adsorber and evaporator were jacketed unit in the form of casing. The heat exchanger is installed in the jacket of adsorber. Cooling medium is in the jacket of evaporator. Its advantages are simple structure. There is no need for

rectifying unit. Furthermore, the working pressure is close to atmospheric pressure which leads to low initial cost and high energy performance.

Ng et al. (2002) disclosed a novel modular and miniature chiller that symbiotically combines absorption and thermoelectric cooling devices. The seemingly low efficiency of each cycle individually is overcome by an amalgamation of the two technologies, Figure 1.18. From evaporator 1, heat is transferred from the heat spreader or substrate 1a where the latter is in direct contact with a surface to be cooled. Boiling refrigerant flows into adsorbent bed 5 via the pipe and valve 3. Accordingly, the other end of adsorbent bed 5 is shut to the condenser 9 by valve 7. The adsorbent bed is operated in adsorption process, and heat generated by the exothermic process is rejected via the finned surfaces 4. The temperature of the finned surfaces is maintained at a temperature below that of the ambient environment by the cold junctions of the thermoelectric device 6, which is powered by an electric current (DC) from a power source or battery 10. The direction of the DC current can be reversed should adsorbent bed 5 be operated in desorption process, while the other adsorbent bed 9 operates in adsorption process. This electroadsorption chiller incorporates solely existing technologies. It can attain large cooling densities at high efficiency, yet is free from moving parts and comprises harmless materials. This insensitivity to scale creates promising applications in areas ranging from cooling personal computers and other micro-electronic appliances, to automotive and room air-conditioning.

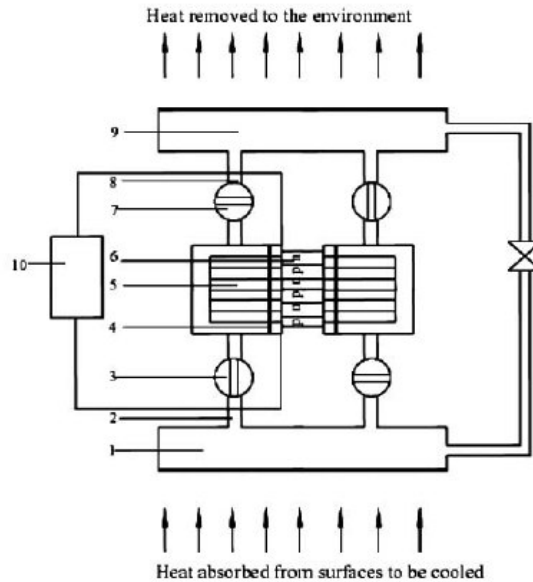


Figure 1.18. Electro adsorption Chiller, Ng et al. (2002)

Solar Refrigeration

Many researchers have worked on the development of solar adsorption refrigerators. This include Headley et al. (1994) ; Liu et al. (1998) ; Niemann et al. (1997); Boubakri et al.(1992a,b); Critoph (1994); Critoph et al. (1997); Grenier et al.(1988); Marmottant et al.

ambient temperature between 14 and 18 °C and lowest temperature achieved by the evaporator between -5 and 8 °C.

Critoph (1994) built a small solid adsorption solar refrigerator in 1994. The collector is 1.4m² in area and contains 17 kg of active carbon. The cold box is remote from the collector, being linked to it by a flexible steel hose. It is possible to produce up to 4 kg of ice per day in a diurnal cycle.

Sumathy and Li (199) operated a solar-powered ice-maker with the solid adsorption pair of activated carbon and methanol, using a flat-plate collector with an exposed area of 0.92m². This system could produce ice of about 4–5 kg/day with a solar COP of about 0.1–0.12.

Khattab (2004) developed a solar-powered adsorption refrigeration module with the solid adsorption pair of local domestic type charcoal and methanol. The module consists of a modified glass tube having a generator (sorption bed) at one end, a combined evaporator and condenser at the other end and simple arrangement of plane reflectors to heat the generator. Test results show that, the daily ice production is 6.9 and 9.4 kg/m² and net solar COP is 0.136 and 0.159 for cold and hot climate, respectively.

Hildbrand et al. (2004) built and tested a new high-efficiency adsorptive solar refrigerator in Yverdon-les-Bains, Switzerland. The adsorption pair is silica gel–water. Cylindrical tubes function as both the adsorber system and the solar collector (flat-plate, 2m² double glazed); the condenser is air-cooled (natural convection) and the evaporator contains 40 l of water that can freeze. This ice functions as a cold storage for the cabinet. This system has presented interesting performances, with a solar COP of 0.16.

A lot of research work on adsorption refrigeration has been done in Shanghai Jiao Tong University since 1993. Several prototype adsorption icemakers have been developed and tested in the past years. The research group Li et al (2002). built a flat-plate solid-adsorption refrigeration ice maker with activated carbon–methanol as working pair for demonstration purposes. The experimental results show that the thermal COP is about 0.45 and solar COP is about 0.12–0.14, with approximately 5–6 kg of ice produced per m² collector. After some improvements, a similar no valve solar icemaker was built by Li et al (2004). For this system, there are no any reservoirs, connecting valves or throttling valve, and the structure of the system is very simple. Figure 1.20, gives the outline and the sketch structure of this prototype.

Experimental results showed that 6.0–7.0 kg ice can be obtained under indoor conditions when radiation energy was about 17–20 MJ/m², for these conditions, the solar COP of this system was about 0.13–0.15. In out door conditions, the system could produce 4.0 kg ice and the solar COP was about 0.12 when the total insolation energy was about 16–18 MJ/m². And then, a new solar ice maker developed can produce about ice of 4–5 kg each sunny day under the condition of about 18–22 MJ/m² solar insolation, with the price of no more than US \$250 for per solar ice maker with 1m² collector. These improved economic solar icemakers are now fabricated for mass application in China.

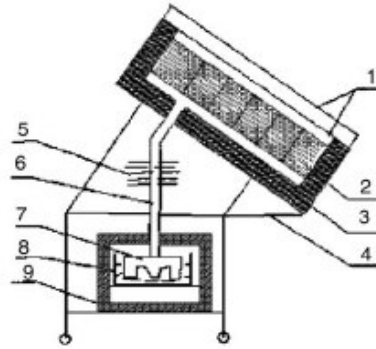


Figure 1.20., No Valve Solar Adsorption Ice Maker: (1) Cover Plate, (2) Adsorbent Bed, (3) Insulation Material, (4) Ice Frame, (5) Condenser, (6) Connecting Pipe, (7) Evaporator, (8) Water Tank, (9) Insulation Box.

Li et al (2002 and 2004) conducted a study on the effects of collector and environment parameters on the performance of a solar powered solid adsorption refrigerator. They found the performance of solar refrigerator to be affected by the condensation and evaporation temperatures, see Figure 1.21 and Figure 1.22. As could be seen from the figures, increasing the condensation temperature result in decrease in the system COP and the amount of ice produced (COPs reduced to below 0.15 when the condensation temperature increased above 20 °C. and as in the summer conditions the environmental temperatures are higher than 20 °C, this makes condensing temperature exceed 30 °C and hence results in low COP. Adiabatic cooling is recommended.

The COP and ice mass variation with evaporating temperature is shown in Figs. 15 and 16. For solar refrigerator, because the energy of solar radiation is limited by weather condition, the evaporating temperature is in the range of -10 °C_to_0 °C. If evaporating temperature is above 0 °C, zeolite– water working pair can be used, this will cause a good refrigeration effect because the latent heat of water is large than that of methanol.

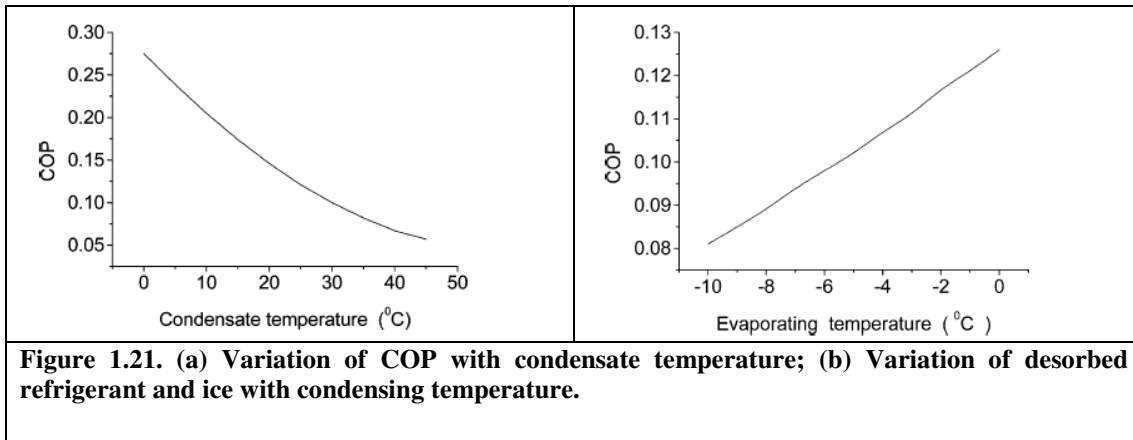


Figure 1.21. (a) Variation of COP with condensate temperature; (b) Variation of desorbed refrigerant and ice with condensing temperature.

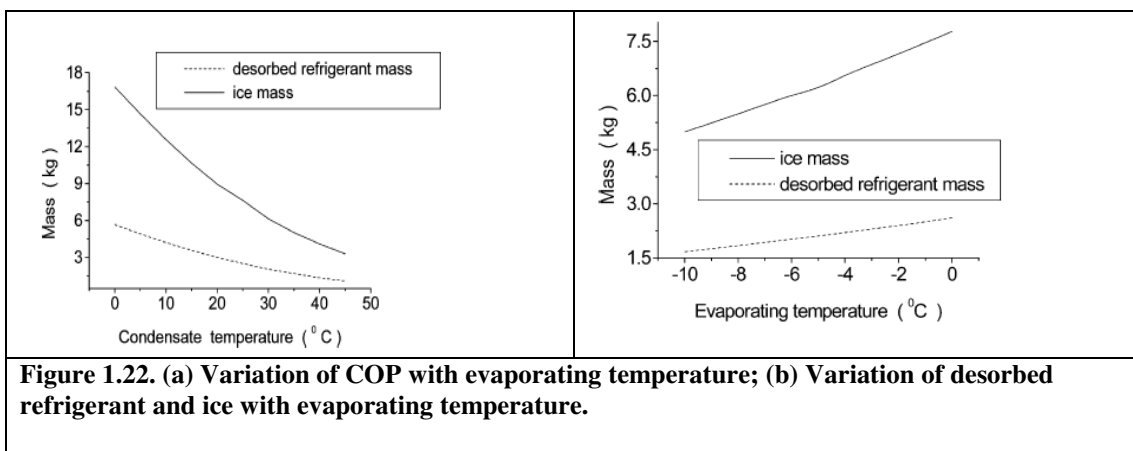


Figure 1.22. (a) Variation of COP with evaporating temperature; (b) Variation of desorbed refrigerant and ice with evaporating temperature.

A prototype of a solid–gas adsorption processes with BaCl₂–ammonia chemical reaction and transformation liquid–gas of ammonia for congelation purpose has been constructed and tested in the laboratory PROMES in Perpignan, France. The experimental results proved that it is possible to produce cold with the temperatures less than -20 °C and a minimal temperature of -30.5 °C can be reached. The solar COP obtained is 0.061.

Adsorption systems for Transport Refrigeration

Christy and Toossi (2004) designed, modelled, built and tested trailer refrigeration and bus air-conditioning ambient-air cooled adsorption system. The design employed four activated carbon sorbent beds and ammonia (R717) as a refrigerant. The adsorption system was then theoretically characterized (size, weight, heat input, operational modes and layout configurations) for the purpose of being capable of maintaining temperatures in the range -18°C to 4.5°C for transport refrigeration. The diesel engine available heat rates for powers between 225 hp and 525 hp were identified to be in the range 40 kW to 60 kW for the coolant circuit and 40 kW-140 kW for the exhaust gases.

The cooling requirements of large refrigerated semi-trailers were considered to be equal to the cooling capacities of the units usually installed on these vehicles, that is to say about 15 kW. It should be noted that those units are usually 200 to 300 % oversized. Practical COP values used for system design were in the range 0.6 to 1 and specific

cooling power rates (measure of the evaporator cooling load per mass of sorbent material) were considered to be around 614 W per kilogram of carbon for ammonia refrigerant and 198 W per kilogram of carbon for R134A refrigerant. Following these assumptions, a feasibility analysis of refrigeration systems using either R717 or R134A with cooling capacities of 9 kW, 19 kW and 35 kW (bus air-conditioning) was carried out.

Another very interesting aspect of the study was the investigation of the layout of such a system to identify the best way of installing it on a conventional articulated vehicle. First, the weight of adsorption systems using either R717 or R134A as a refrigerant was estimated for different cooling capacities and compared to a vapour compression. As shown in Figure 1.23, adsorption systems were found to be potentially lighter than a conventional system when a diesel fuel tank of around 300 kg weight was considered for the conventional system.

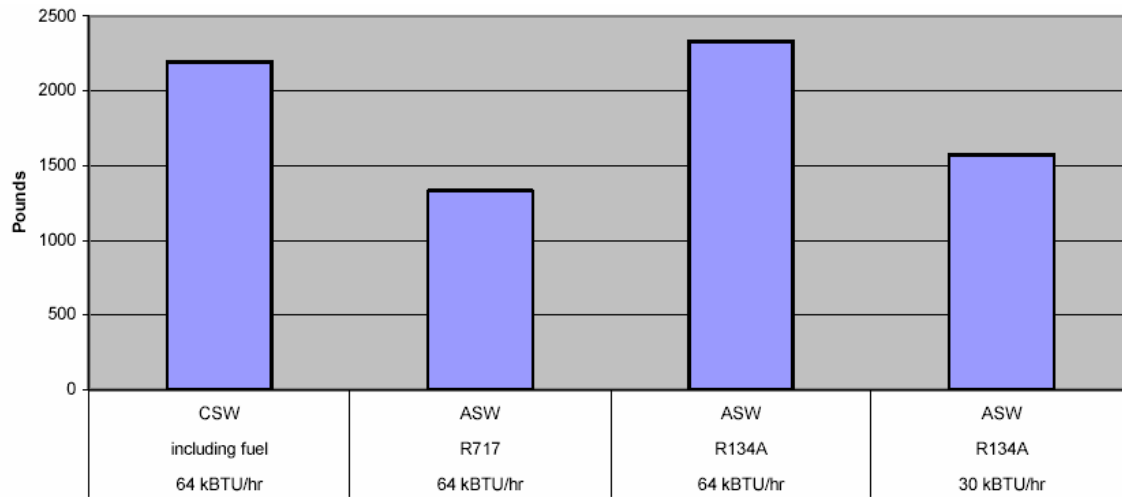


Figure 1.23. Comparison of weight of conventional vapour compression and adsorption refrigeration systems, Christy and Toossi (2004).

The most attractive location for the adsorption system was found to be the tractor, transferring the cooling effect to the trailer with a secondary fluid.

Industrial Adsorption systems

The potential for the two-bed silica-gel–water adsorption chiller was evaluated by a number of researchers; Wang et al (2002), Sakoda and Suzuki (1984), Cho and Kim (1992), Saha et al (1995), Boelman et al (1995), Boelman et al (1997), and has already been commercialized in two Japanese adsorption chillers currently on the market for air-conditioning (Mycom, Nishiyodo and GBU) in which low driving temperatures as low as 70 °C are used.

system and in special agricultural projects. However, the manufacturer did not find the development of this chiller to be cost competitive. They paid more in copper tube, silicon dioxide and manufacturing cost but COP is lower compared with other technology and hence, they stopped marketing this chiller from last year. They are currently working on the development of a new ammonia chiller, 3-5 kW. However, this is not on the market yet.

Hunan DY Refrigeration Co. Ltd, in China, used the DY adsorption refrigeration system linked to micro-gas turbine to get cooling from waste heat.

Professor Dingyu Li is the inventor of DY Adsorption Refrigeration technology with the ability to be directly added to exhaust flues of a CHP plant. The adsorption system consists of a DY Generator, one ammonia tank, one condenser. DY are marketing the DY-HWS Refrigeration System powered by 90 °C heat energy (hot water, steam, oil, surplus heat and waste water in industry). System refrigeration capacities of 14 kW, 20 kW and 30 kW have been advertised with ability to give temperatures between -25 and 18 °C with heating temperature over 120 to 270 °C with COPs of 0.3 to 0.5.

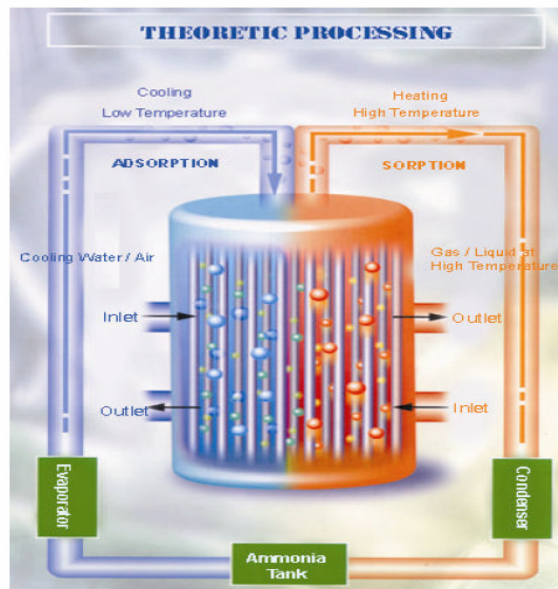


Figure 1.25. Principle of the DY refrigeration System.

Wang and Wang (2005) presented an assessment of the DY chemical reaction icemaker driven with the exhausted gas from a fishing vessel diesel engine exhaust. The ice maker is the refrigeration equipment mainly designed for fishing vessels with tonnage about 100

tons. It takes DY double salt as absorbent and ammonia as refrigerant. Based on chemical affinity, chemical reaction is monovariant and chemical changes occur which induce modification of the solid itself. It is powered by exhaust heat of diesel engine to make flake ice and there is no any increase in consumption of oil.

The whole set of DY fishing vessel diesel engine exhaust icemaker includes one icemaker, one condenser and one DY generator system (see Figure 1.26). One DY generator system contains one DY generator, one ammonia tank. The method of chilling uses fresh water or seawater. Ice-making capacity with thickness about 1.5–2 mm is 33–38 kg/h with the ice temperature of -15 °C.

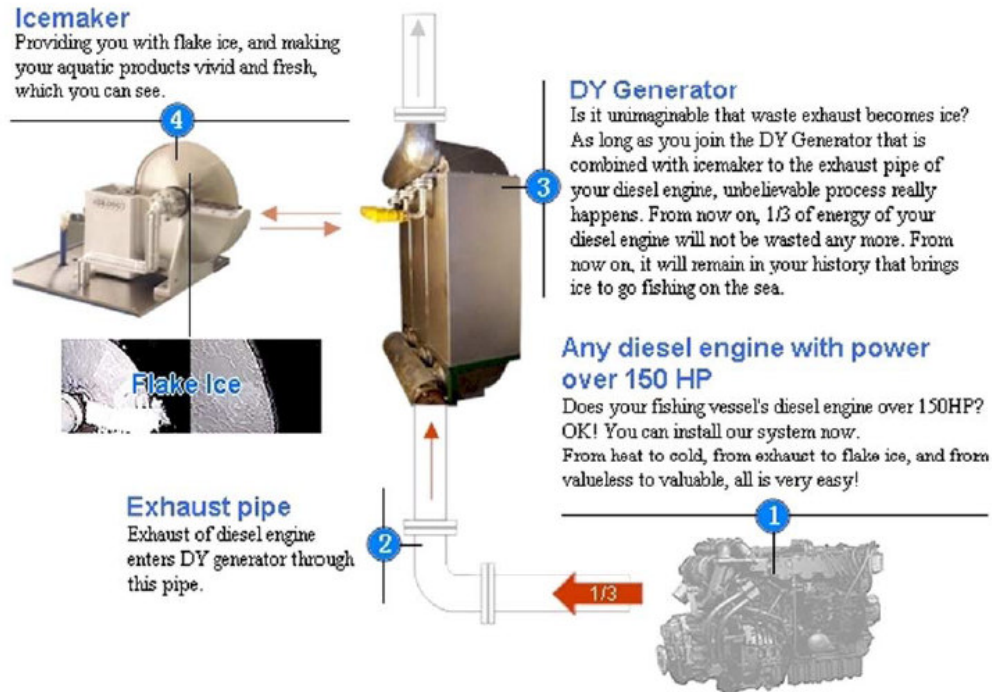


Figure 1.26. DY fishing vessel diesel engine exhaust icemaker.

ENC have designed a solid sorption based heat pump both for cooling and heat purposes. The former are based on solid/water sorption by either Na₂S (the so called SWEAT system) of Silica, the latter are based on solid ammonia sorption in metal halides e.g. LiCl or MgCl₂. the working principles is based on the reversible desorption (endothermic) and the absorption (exothermic) of vapours in solids. Typical cooling efficiency is approximately 55% for cooling (W. Haije, R. de Boer, E. Bevers, P. van Ekeren, Solid Sorbents in Heat Pump Applications, Report presented at the international Symposium of Inorganic and Environmental Materials, (ISIEM 2004), Eindhoven. ECN-RX-04-104. The current SWEAT unit is a batch system. For continuous cooling system it is necessary to use two or more sweet units. The unit is capable of producing 35 kW of cooling in 130 Minutes and 69 kW of heating in 130 minutes. This system limitation is that it would require low cooling temperature of 15 oC for charging the system.

Refrigeration Classification

Three typical refrigeration applications within the food manufacturing and food retail sectors have been identified; Medium temperature cooling (+ 10 to -10 °C), Low temperature cooling (-10 to -40 °C) and very low temperature cooling (- 40 °C). Applicability of the technology in each of these temperature ranges was assessed based on the system that could be used with the food retail and food manufacturing application. This included, integral cabinets, remote cabinets, cold storage, transport and food production, see table 1 for details

Table 1.1 Assessment of adsorption refrigeration technology in food application.

Evaporating Temperature Ranges	Food Application					State of Development	Capacities (kW)	COP	Summary
	Integral Cabinets	Remote Cabinets	Cold Storage	Transport	Food Production				
MTC (+ 10 to -10 °C)	X	✓	✓	✓	✓	Commercially Available ($T_e \geq 3$ °C)	35 - 1300	0.4-0.6	Advantages: Use of reject or solar heat low environmental impact, Low Noise Low Maintenance Cost, upto 30 year Life Disadvantages: Complex large size Cost compared to VC Higher Capital Cost Research and development needs Control COP
						Commercially Available ($T_e = -25$ to 18 °C)	14, 20& 30	0.3-0.5	
						Prototype ($T_e \geq 3$ °C).	10	0.4-0.6	
LTC (-10 to -40 °C)	X	✓	✓	✓	✓	Commercially Available ($T_e = -25$ to 18 °C)	14, 20 &30	0.3-0.5	
						Commercial Prototype.	3 & 5	N/A	
VLTC (FP) (< -40 °C)					✓	Theoretical Research			

Table 2.2, presents a summary of the various adsorption studies for evaporation temperatures below -8 °C.

Table 2.2 Comparison of several typical adsorption studies

<u>Te</u>	<u>Working Par</u>	<u>Cooling Water Temp</u>	<u>SCP</u>	<u>COP</u>	<u>State of Research</u>	<u>Ref</u>
- 10	SrCL2-NH3	40	250	0.3	Test	Pons et al (1999 -int Ref)
- 25	MnCl2/NiCl2-NH3	40	140	0.4	Simulation	Pons et al (1999int Ref)
- 10	Metal hydride-hydrogen	35	50	0.4	Test	Willers and Groll 1999
- 8	Activated	32	45.1	0.1	Test	Li et al .

	Carbon-methanol					(2004)
- 19	Activated Carbon and CaCl ₂ - NH ₃	30	528	0.3	Test	Lu et al (2006)
-21		20	770.4	0.4	Test	Lu et al (2006)
-15		30	161.2	0.12	Test	Lu et al (2006)

Technical Disadvantages

Adsorption refrigeration is an inherently cyclical process and multiple adsorbent beds are necessary to provide approximately continuous capacity. Adsorption systems inherently require large heat transfer surfaces to transfer heat to and from the adsorbent materials which automatically makes cost an issue. High efficiency systems require that heat of adsorption be recovered to provide part of the heat needed to regenerate the adsorbent. These regenerative cycles consequently need multiples of two-bed heat exchangers and complex heat transfer loops and controls to recover and use waste heat as the heat exchangers cycle between adsorbing and desorbing refrigerant. This exacerbates issues concerning first cost and also adds an electric parasitic load. Performance can deteriorate over numerous adsorption cycles because of decrepitation and surface contamination. Ammonia-carbon: materials compatibility issues with ammonia, stainless steel heat exchanger tubes and pipes. Ammonia is not universally accepted as a refrigerant in residential and confined applications because it is toxic and flammable in some concentrations; precautions must be made to isolate ammonia from the occupied space and to contain it within a machine room or disperse it in the atmosphere safely if a leak occurs.

Water-Zeolite Adsorption: size and cost are both factors working against Zeolite adsorption heat pumps. ADL estimated a three ton adsorption heat pump would require 240 kg of Zeolite and large amounts of copper. The cost of materials and components alone for a three ton system would cost \$2500 exclusive of labour, overheads, dealer mark-ups, and installation costs (DOE 1993).

Metal-Hydride Adsorption: flammability of the refrigerant (i.e. hydrogen).

Organic salts or complex compounds: materials compatibility issues with ammonia, stainless steel heat exchanger tubes and pipes. Rocky research has reported that absorbent salts have shown no change in properties over thousands of cycles (DOE 1993, p. A-28).

Economic Analysis

The absence of efficiency data for all of the adsorption systems makes it impossible to perform any kind of analysis for annual energy use or any economic comparisons. A figure of \$250 per kW has been presented on the NISHIYODO KUCHOUKI CO web site for 481 kW chiller.

Conclusions

Classical vapour-compression technologies have reached a significant state of maturity up to now with wide use for this technology in the food retail and food production sectors. All of these systems consume precious fuel or electricity to achieve refrigeration. Along with a consideration for energy efficiency, increasing attention is being given also to the use of waste heat. Adsorption systems are heat-operated units that need little electricity, so they can utilize waste heat or renewable energies. Other advantages of solid sorption machines (noiseless, safety).

In comparison with the vapour compression refrigeration and absorption refrigeration systems, the adsorption refrigeration system has its drawbacks, such as low mass and heat transfer performance, expansion and agglomeration phenomenon for chemical adsorbent, low coefficient of performance (COP) and low specific cooling power. Besides the simple intermittent cycle and in order to provide steady refrigeration and improve the performance of adsorption refrigeration system. Some advanced cycles have been proposed and investigated, such as the multi-bed cycles, the thermal wave cycle, the forced convection cycle, the heat and mass recovery based on different adsorbent bed and different control strategies, heat pipe technologies hybrid.

Research has shown that solid-adsorption technology has a promising potential for competing with conventional absorption technology but not vapour compression systems. Commercial solid adsorption systems are still limited for air-conditioning applications with only one commercially available system for sub zero temperatures. To this date, lower temperature adsorption refrigeration systems are still under laboratory testing stages. So we find only laboratory experiments of adsorption machines in the open literature.

References

A. D. Little, Energy Savings Potential for Commercial Refrigeration Equipment, Final Report Prepared by, Inc. For Building Equipment Division Office of Building Technologies, U.S. Department of Energy, June 1996, Reference 46230-00.

A. Gassel, Die Adsorptionska" lteanlage—Betriebserfahrungen und thermodynamische Berechnung. Klima Luft- und Ka" ltechnik 1998;8:380–4.

B. B. Saha, E.C. Boelman, T. Kashiwagi, Computer simulation of a silica gel–water adsorption refrigeration cycle—the influence of operating conditions on cooling output and COP, ASHRAE Trans Res 101 (2) (1995) 348–357.

B. Dawoud, A hybrid solar-assisted adsorption cooling unit for vaccine storage, Renew. Energy, 2006, Volume: 32, Issue: 6, Page: 947- 964).

C. A. A. Akisawa, Y. Kan, Y. Hamamoto, T. Kashiwagi,,: JP2005061726 (2005).

Critoph 2004

D. I. Tchernev,,: US4637218 (1987).

D. I. Tchernev and D.T. Emerson, 1988. "High-Efficiency Regenerative Zeolite Heat Pump," ASHRAE Transactions, Vol 94, Pt. 2, pp. 2024-2032.

D. I. Tchernev. Solar refrigeration utilizing zeolites. In: 14th Inter. Conv. Engng Conf., Amer. Chem. Soc., p.2070, (1979).

D. I. Tchernev. Solar refrigeration utilizing zeolites. In: 14th Inter. Conv. Engng Conf., Amer. Chem. Soc., p.2070, (1979).

D. J. Miles, D. M. Sanborn, G. A. Nowakowski and S. V. Shelton. Gas @red sorption heat pump development. In: Proceedings of ``Solid Sorption Refrigeration" Symposium Paris November 18±20 1992, p. 91±96.

D. J. Miles, D. M. Sanborn, G. A. Nowakowski and S. V. Shelton. Gas @red sorption heat pump development. In: Proceedings of ``Solid Sorption Refrigeration" Symposium Paris November 18±20 1992, p. 91±96.

D. M. Ruthven, Principles of Adsorption and Adsorption, Processes, 1984 (John Wiley, London).

D. S. Zhu, : CN1232159 (1999).

D. Y. refrigeration, <http://www.dyrefrigeration.com>

D. Y. refrigeration, <http://www.dyrefrigeration.com/products/chp/index.htm#>

Delgado et al 1982

DOE 1993. "A Research Needs Assessment: Energy Efficient Alternatives to Chlorofluorocarbons (CFCs)," DOE/ER/30115-H1, June. Rockenfeller, U., Kirol, L, and Ryan, W., 1992. "Solid-gas chemisorption: Efficient HVAC&R Without CFCs," ASHRAE Journal, March 1992, pp. 54-58.

E. B. Miller, The development of silica gel refrigeration, refrigerating engineering. American Society of Refrigerating Engineers 17(4), 103-108 (1929).

E. C. Boelman, B.B. Saha, T. Kashiwagi, Experimental investigation of a silica gel–water adsorption refrigeration cycle—the influence of operating conditions on cooling output and COP, ASHRAE Trans Res 101 (2) (1995) 358–366.

E. C. Boelman, B.B. Saha, T. Kashiwagi, Parametric study of a silica gel–water adsorption refrigeration cycle—the influence of thermal capacitance and heat exchanger UA-values on cooling capacity, power density and COP, ASHRAE Trans 103 (1) (1997) 139–148.].

E. Willers, M. Groll, Evaluation of metal hydride machines for heat pumping and cooling applications. Int J Refrig 1999;22:47–58.

Ebbeson,: US5941093 (1999).

Endo, A. Komori, JP2005127614 (2005).

Exell and Korsakoo, Thailand

F. Lemmini, A. Errougani, Building and experimentation of a solar powered adsorption refrigerator. Renewable Energy 2005;30:1989–2003.

F. Meunier, Sorption contribution to climate change mitigation, in: Proceedings of the International Sorption Heat Pump Conference ISHPC 02, Shanghai, September 24–27 2002, pp. 1–9.

F. Meunier, Utilisation des cycles à sorption pour la production de froid par l'énergie solaire, Cahiers de l'AFEDDES no 5 (1978) 57±67.

F. Ziegler, State of the art in sorption heat pumping and cooling technologies, Int. J. Refrig. 25 (2002) 450–459].

G. Restucciaa, G., Frenia, A., Vastaa, S. and Yu Aristovb, Yu., "Selective water sorbent for solid sorption chiller: experimental results and modelling", International Journal of Refrigeration 27 (2004) 284–293.

Gassel. "Die Adsorptionska" lteanlage—Betriebserfahrungen und thermodynamische Berechnung. Klima Luft- und Ka" ltechnik" 1998;8:380–4.

H. Hidaka, H. Kakiuchi, Y. Iwade, T. Takewaki, M. Yamazaki, N. Watanabe: JP2005098647 (2005).

H. Sato, K. Ishii, A. Kosaka, S. Numazawa, S. Inoue, K. Inagaki, K. Yano, N. Setoyama, Y. Fukushima, Y.: US2003005721 (2003).

H. Sato,, K. Tanaka, , S. Honda, S. Inoue, M. Terao,: US5619866 (1997) and JP8240357 (1996).

H.T. Chua, K.C. Ng, A. Malek, T. Kashiwagi, A. Akisawa, B.B Saha,: US2002053217 (2002).

C. Hildbrand, P. Dind, M. Pons and F. Buchter. A new solar powered adsorption refrigerator with high performance. May 2004, *Solar Energy* 77 (2004) 311–318.

IGT, Technical feasibility of solid adsorption cooling system, Institute of Gas Technology, Project HC-4-15, December (1972).

Justin Zhu (2007), from Jiangsu Shuangliang Air-Conditioning Equipment Co.,Ltd, Personal Communication.

K. Endo, K. Nishikawa,: JP2003166770 (2003).

K. Sato, H. Ishii, Y. Nagashima, S. Tanaka, S. Inoue,: JP2001215068 (2001).

K. Sato, S. Tanaka, K. Honda, Y. Fujiwara: US5775126 (1998) and JP9303900 (1997).

K. Sumathy, Z.F. Li, Experiments with solar-powered adsorption ice-maker. *Renewable Energy* 1999;16:704–7.

K.C. Ng, J.M. Gordon, H.T. Chua, A. Chakraborty,: US20026434955 (2002).

K.C. Ng, X. Wang, Y. S. Lim, B.B. Saha, A. Chakraborty, S. Koyama, A. Akisawa, T. Kashiwagi, Experimental study on performance improvement of a four-bed adsorption chiller by using heat and mass recovery, , Available online 19 May 2006.

L.W. Wang, R.Z. Wang, J.Y. Wu,: CN1544864 (2004).

M. Li, C.J. Sun, R.Z. Wang, and W.D.Cai, Development of no valve solar ice maker, *Renewable Energy* 27 (2002) 369–382

M. Li, H.B. Huang, R.Z Wang, , L.L Wang,, W.D. Cai and W.M. Yang, Active Carbon-Ethanol “Experimental study on adsorbent of activated carbon with refrigerant of methanol and ethanol for solar ice maker, *Renewable Energy* 29 (2004) 2235–2244 2243,

M. Pons, J.J. Guillemont, Design of an experimental solar-powered, solid-adsorption ice maker, *Trans. ASME, J. Solar Energy Eng.* 108 (4) (1986) 332–337.

M. Ponsa, F. Meuniera, G. Cacciola, R.E. Critoph, M. Groll, L. Puigjanere, B. Spinner, F. Ziegler, Thermodynamic based comparison of sorption systems for cooling and heat pumping, *International Journal of Refrigeration* 22 (1999) 5±17.

M.A. Lambert, Design of solar powered adsorption heat pump with ice storage, *Applied Thermal Engineering* 27 (2007) 1612–1628.

N. Patzner, EP1154208 (2001).

N.M. Khattab, A novel solar-powered adsorption refrigeration module. *Appl Therm Eng* 2004;24: 2747–60.

P. Maier-Laxhuber, A. Becky, R. Schmitt, R. Woerz, N. Weinzierl, JP2004150792 (2004).

R. Christy, Toossi, Adsorption Air-Conditioning for Containerships and Vehicles, 2004, available online, http://www.mettrans.org/research/final/99-19_Final.pdf#search=%22C%20Christy%20R%20Toossi.%20Adsorption%20Air-Conditioning%20for%20Containerships%20and%20Vehicles%22).

R.E. Critoph, TECCS meeting, 26 April 2007.

R.E. Critoph, Performance limitations of adsorption cycles for solar cooling, Engineering Department, Available online 7 August 2003.

R.E. Critoph and Zhong (2004),

R.E. Critoph Carbon-ammonia systems-revious experience, current projects and challenges for the future. In: *Proceedings of the international sorption and heat pump conference (ISHPC 2002)*, China, (2002).

R.E. Critoph, An ammonia carbon solar refrigerator for vaccine cooling. *Renewable Energy* 1994;5:502–8.

R.E. Critoph, Performance limitations of adsorption cycles for solar cooling, *Solar Energy* 41 (1988) 21–31.

R.E. Critoph, R. Thorpe, US5845507 (1998).

R.E. Critoph, TOWARDS A ONE TONNE PER DAY SOLAR ICE MAKER, WREC 1996

R.E. Critoph, Z. Tamainot-Telto and G.N.L. Davies, A prototype of a fast cycle adsorption refrigerator utilizing a novel carbon–aluminium laminate, *Proc Instn Mech Engrs Vol 214 Part A*, A07299 Ó IMechE 2000

R.E. Critoph, Z. Tamainot-telto, Z.: WO04011859 (2004).

R.E. Critoph, WO200122010 (2001).

R.E. Critoph., Rapid cycling solar/biomass powered adsorption refrigeration system. *Renewable Energy* 1999;16:673–8.,

R.E. Critoph., Towards a one tonne per day solar ice maker. *Renewable Energy* 1996;9:626–31.

R.E. Critoph: US20036629432 (2003).

R.Z. Wang, and R.G. Oliveira, Adsorption refrigeration—An efficient way to make good use of waste heat and solar energy, *Progress in Energy and Combustion Science* 32 (2006) 424–458.

R.Z. Wang, Efficient adsorption refrigerators integrated with heat pipes, *Applied Thermal Engineering*, accepted 12 February 2006.

R.Z. Wang, J.Y. Wu, Y.J. Dai, Adsorption refrigeration, China Machine Press, Beijing, 2002.

R.Z. Wang, Performance of improvement of adsorption cooling by heat and mass recovery operation. *Int J Refrig* 2001;24(7):602–11.

R.Z. Wang, Z.Z. Xia, J.Y. Wu, : CN1614336 (2005).

RE. Critoph, Laboratory testing of an ammonia carbon, solar refrigerator. In: *Proceedings of the solar world congress (ISES)*, Hungary, 1993.

S. G. Wang, R. Z. Wang, J. Y. Wu and Y. X. Xu, Experimental results and analysis for adsorption ice-making system with consolidated adsorbent. *Adsorption* 2003;9(4):349–58.]

S. G. Wang, R. Z. Wang, Recent developments of refrigeration technology in fishing vessels, *Renewable Energy* 30 (2005) 589–600>

S. Honda, K. Ishii, K. Tomoari, T. Suzuki, : JP11083235 (1999).

S. Inoue, S. Honda, : JP11211261 (1999).

S.H. Cho, J. N. Kim, Modeling of a silica gel/water adsorption cooling systems, *Energy* 17 (9) (1992) 829–839.

Sakoda, M. Suzuki, Fundamental study on solar powered adsorption cooling system, *JChemEng Jpn* 17 (1) (1984) 52–57.

Shelton: US4610148 (1986).

T. Monma, , T. Mizota, : JP2005299974 (2005).

T. X. Li, R.Z. Wang, L.W. Wang, Z.S. Lu, C.J. Chen, Performance study of a high efficient multifunction heat pipe type adsorption ice making system with novel mass and heat recovery processes, International Journal of Thermal Sciences , December 2006.

T. X. Li, R.Z. Wang, L.W. Wang, Z.S. Lu, C.J. Chen, International Journal of Thermal Sciences, 2006.

W. Ryan, 1993. "CFC-Free Chemisorption Heat Pumps and Refrigeration," Proceedings of the 1993. Refrigeration and Air-Conditioning Technology Workshop, Breckenridge, Colorado, June 23-25.

Yanagi et al 1992

Z.B. Liu, L.N. Fang,: CN1664478 (2005).

Z.S. Lu, R.Z. Wang *, L.W. Wang, C.J. Chen. Performance analysis of an adsorption refrigerator using, Carbon 44 (2006) 747–752

Z.Z. Xia, J.Y. Wu, R.Z. Wang,: CN1614342 (2005).

Z.Z. Xia, R.Z. Wang, J.Y. Wu,: CN1595017 (2005).

2. AIR CYCLE REFRIGERATION

INTRODUCTION

Brief history

Air cycle systems produce low temperatures for refrigeration by subjecting the gaseous refrigerant (air) to a sequence of processes comprising compression, followed by constant pressure cooling, and then expansion to the original pressure to achieve a final temperature lower than at the start of compression.

The first air cycle apparatus working on the above principle was invented by Dr John Gorrie, a Florida based physician, as a means for the production of artificial ice to treat yellow fever patients. His open cycle machine was patented in 1851. Over the following 25 years or so several other refrigeration pioneers secured patents on air cycle refrigeration systems. These include a closed air cycle system developed by the Alexander Kirk in Scotland based on the Stirling engine, the single and two-cylinder cold air machines developed by Franz Windhausen of Germany, the air refrigeration machine developed by Paul Giffard of France, and the Bell-Coleman open air cycle developed by Joseph Coleman in collaboration with Henry and John Bell of Glasgow. From the early 1880s air cycle machines of Giffard and Bell-Coleman design were manufactured by J&E Hall of Dartford and the Haslam Company respectively. These so-called 'cold air machines' were used to provide direct cooling for the preservation of provisions at sea, including the shipment of frozen meat from South America, New Zealand and Australia, and were also installed in land-based cold stores. Reciprocating air cycle machines dominated the marine refrigeration sector at the end of the 19th century but were eventually displaced by more reliable, more efficient vapour compression systems using carbon dioxide.

After the decline of reciprocating air cycle machines around the start of the 20th century little interest was shown in air cycle technology until the last two decades, apart from in two specialized areas, namely (i) aircraft cabin air conditioning and cooling for avionic equipment, and (ii) gas liquefaction. The availability of efficient turbomachinery used for these two established applications together with other technological advances have, to some extent, encouraged and facilitated the development of air cycle equipment for new applications (e.g. air conditioning of high speed trains). However, the requirement to find environmentally safe alternative refrigerants and the prospect of using a natural working fluid appears to have been a main driver behind the renewed interest in air cycle refrigeration.

Basic Air Cycle

Air cycle refrigeration is based on the reversed Joule (or Brayton) cycle illustrated in Figure 2.1. The working fluid, air, flows steadily through each of the system components without changing phase, remaining as a gas throughout. The large arrows indicate the directions of energy transfer to and from the air around the closed cycle, with Q_{IN} representing heat transfer from the region at T_C (refrigeration effect), Q_{OUT} the heat transfer to the warmer region at T_H (heat rejection) and W_{IN} the net work input required

by the cycle, i.e. the difference between the compressor work input and the expander work output.

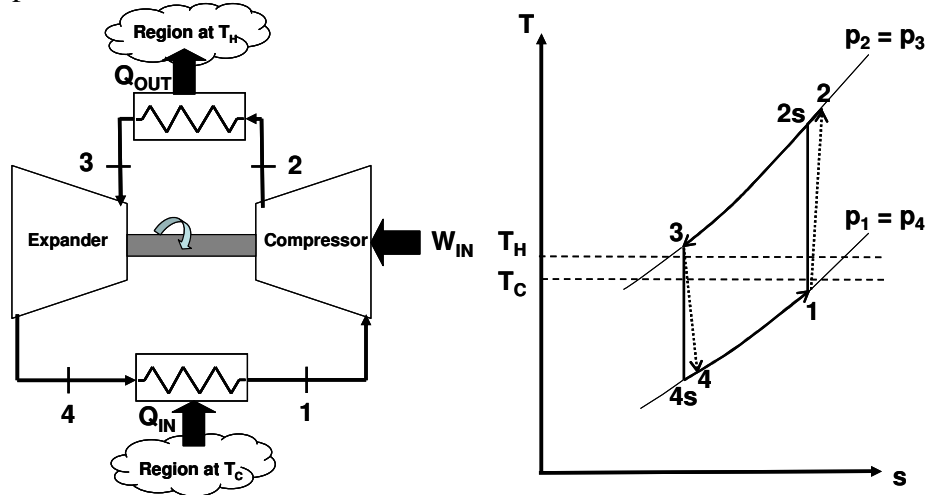


Figure 2.1 Reversed Joule cycle

The ideal reversed Joule cycle, indicated by the sequence 1-2s-3-4s-1 on the T - s diagram in Figure 2.1, comprises four internally reversible processes as follows:

- 1-2s: isentropic compression
- 2s-3: constant pressure heat rejection to region at T_H
- 3-4s: isentropic expansion
- 4s-1: constant pressure heat supply from region at T_C

In terms of areas on the T - s diagram shown in Figure 2.1, the coefficient of performance for refrigeration ($= Q_{IN}/W_{IN}$) of the ideal reversed Joule cycle is equal to the area enclosed by the cycle 1-2s-3-4s-1 divided by the area below the process line 4s-1.

In contrast to vapour compression cycles where the transfer of enthalpy of vapourization associated with evaporation and condensation occur at constant temperatures (and pressures), the air cycle works with a single-phase gas and only sensible heat transfer is involved. Consequently, the air cycle exhibits gliding temperatures during the constant pressure heat transfer processes. During the heat supply process, the air temperature increases continuously to T_1 , but remains below T_C to provide the necessary driving force for heat transfer from the cold region. Similarly, the air temperature falls continuously to T_3 during the heat rejection process, but remains above T_H to provide the necessary driving force for heat transfer to the warm region. Compared to a reversed Carnot cycle operating between constant temperatures of T_1 and T_3 , the ideal air cycle shown in Figure 2.1 operates over a much wider range of temperatures, from T_{4s} to T_{2s} , and hence has a significantly lower efficiency.

In practice the processes of compression and expansion are non isentropic and accompanied by entropy increases as illustrated by the dotted lines 1-2 and 3-4 on the T - s diagram in Figure 2.1. In addition, frictional pressure drops (not shown) occur during the

heat supply and heat rejection processes, causing a departure from the assumed constant pressure conditions. For a given pressure ratio, these internal irreversibilities are responsible for an increase in the compressor work input, a reduction in the expander work output and a reduction in refrigeration capacity. As a result the actual cycle coefficient of performance is much lower than for the corresponding ideal cycle.

Modifications of the basic air cycle

In practice a number of improvements to the basic cycle may be introduced:

Regenerative heat exchange

The use of internal heat exchange between the high pressure stream leaving the high-temperature heat exchanger and the low pressure stream leaving the low-temperature heat exchanger overcomes the basic cycle limitation that the expander inlet temperature cannot be lower than the heat sink temperature T_H for heat rejection. Removal of this restriction allows the air to be expanded to a much lower temperature for refrigeration.

According to Gigiel (1997) regenerative heat exchange has the effect of reducing the air temperature on the low pressure side and increasing the air temperature on the high pressure side, with only a small increase in the cycle work input, resulting in little change in the *COP*. Sicars and Kruse (1994) state that with a high temperature difference between the high and low pressure sides a regenerator improves the *COP* by reducing the pressure ratio, hence reducing the losses caused by non-isentropic compression and expansion.

To achieve good system performance a heat exchanger with high thermal effectiveness and low pressure drop is required. Two main types of air-to-air heat exchanger have been used for regenerative heat exchange in air cycle systems. Most systems utilize a recuperative type heat exchanger, normally of tube-fin or plate-fin construction, but fixed bed regenerators are used in one plant discussed later in this review. Use of a rotary regenerative heat exchanger wheel with an absorbent coating, permitting humidity and heat transfer, was evaluated for one application although the difficulty posed by providing an effective seal between the streams was recognized.

Multi-stage compression and intercooling

The overall pressure ratio of an air cycle may be achieved in one or more stages of compression. Two-stage compression is common with a motor driven first (or primary) stage compressor followed by a separate second stage compressor driven directly by the expansion turbine (known as a bootstrap configuration). In this arrangement the two compressors are not coupled mechanically and therefore can operate at different rotational speeds.

With two or more stages of compression intercooling may be employed to reduce the power input required. Consideration must be given to the associated capital cost and pressure drop introduced by using intercooling. Air cycle plants have been built with up to four stages of compression with intercooling.

Closed, open and semi-open/closed cycles

Air cycles can be classified as closed, as illustrated in Figure 2.1, open or semi-open/closed (Williamson and Bansal, 2003).

Closed cycles are, by definition, sealed systems and consequently there is no direct contact between the working fluid and the product being cooled. Hence, in comparison with open and semi-open/closed cycles an additional heat exchanger (with associated temperature difference) is required for transferring heat from the refrigeration load. The system can be filled with *dry* air, thus obviating problems with condensation or ice formation. One of the system pressures can be set independently of the cycle temperatures. Operation at high pressure increases air density and mass flow rate, and reduces relative pressure losses.

Open cycles can be open on either the low-pressure side or the high-pressure side of the cycle. Only the first arrangement is discussed here. Cold air leaving the expander passes through the refrigerated space coming in direct contact with the product being cooled. After leaving the refrigerated space and passing through the low-pressure side of the regenerative heat exchanger the air is discharged to atmosphere. Fresh air is drawn into the compressor from the atmosphere.

Semi-Open/Closed cycles are also open to the refrigerated space, where the cold air comes into direct contact with the product being cooled. The air is then drawn back through the low-pressure side of the regenerator to the compressor.

Figure 2.2 shows an air cycle refrigeration system operating on a semi-open/closed cycle with two-stage compression and intercooling. A recuperative heat exchanger is employed for regenerative heat exchange and the plant is also provided with an ice capture section. Further details of this plant are given in a later section on open air cycle systems.

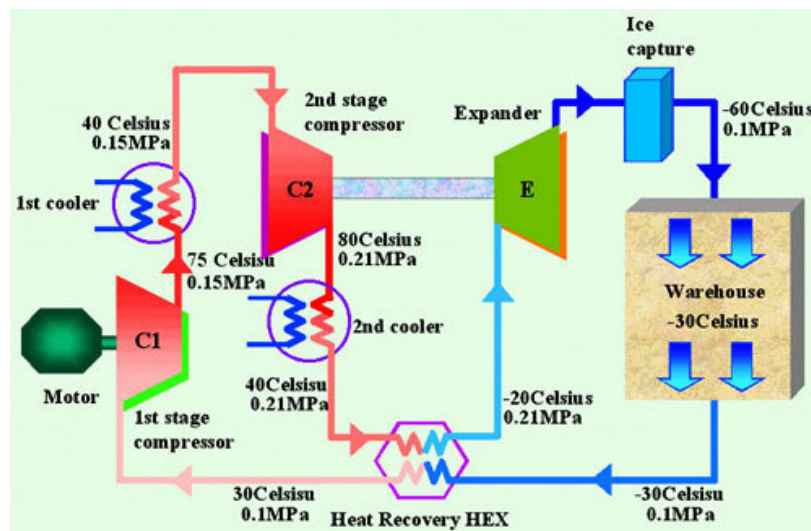


Figure 2.2 AIRS™50 air cycle refrigeration system

Williamson and Bansal (2003) considered a variety of different air cycle configurations, systematically investigating the effects of including either one or two stages of compression (with or without intercooling), a regenerator or no regenerator, and the expander driving either the first or second stage compressor. Thermodynamic analyses were made for both semi-open/closed and fully open systems. For the latter arrangement the models included a fan to draw air from the cold room via the cold side of the regenerator to atmosphere. Fully closed systems were not considered. Values of COP were calculated for refrigeration (and combined heating and refrigeration) assuming the following fixed parameters: refrigeration capacity = 3 kW, air temperature at cold room inlet = -21°C , air temperature at cold room exit = -15°C , ambient temperature = 20°C , cooling water flow rates = 150 ml/s, cooling water supply temperature = 20°C , isentropic efficiency of compressors and expander = 75%, effectiveness of heat exchangers (incl. regenerator) = 0.7, pressure loss per heat exchanger = 5 kPa.

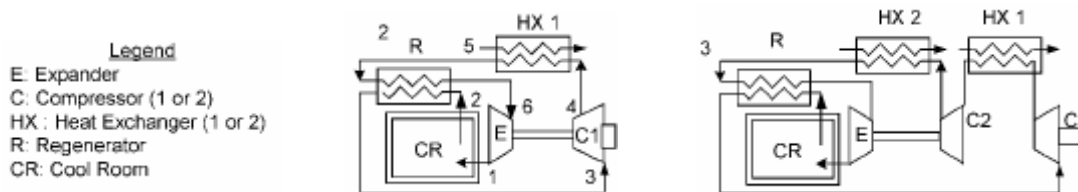


Figure 2.3 Optimal single and two-stage compression air cycles (adapted from Williamson et al, 2003)

The results illustrated the positive effect of including a regenerative heat exchanger on coefficient of performance values in general. In addition, COP_H was found to be higher for a semi-open/closed system than for the comparable open cycle system, whereas the corresponding difference in COP_R values was only marginal. For the assumed conditions, the two cycles (both semi-open/closed systems) shown in Figure 2.3 were considered optimal on the basis of the total combined COP calculated for heating and refrigeration, $COP_{TOTAL} (= COP_H + COP_R)$, which was equal to 1.3 with $COP_R = 0.15$ in both cases. It was concluded that capital cost considerations would make the single stage compression cycle the preferred option. Williamson et al (2003) also commented on the low COP values and questioned the viability of the air cycle for moderately low temperature refrigeration with heat recovery. It should be noted, however, that their calculations assume rather modest efficiency values for the turbomachinery and heat exchange components.

Advantages and disadvantages of air cycle technology

Air cycle systems offer several distinct advantages over other refrigeration technologies:

- air is free, environmentally neutral, non-flammable, safe and sterile for direct contact food processing;
- air delivery temperatures down to -100°C or lower possible;
- beyond range of mechanical vapour compression systems;
- cheaper than or competitive with cryogenics;
- more rapid freezing, increased throughput, less evaporative loss, better quality products;
- integrated cooling and heating possible;
- performance is tolerant of off-design or part-load operation;

- plant is light, robust and reliable, reducing breakdowns and maintenance intervals, and improving availability;
- flexibility to easily re-route air pipe runs in low-pressure plants without refrigerant leakage concerns.

The following disadvantages and concerns regarding air cycle systems have been raised:

- low cycle coefficient of performance;
- effects of water droplets and ice on system and performance;
- possibility of lubricating oil contamination of air in open cycle systems.

Applications

Air cycle technology has been used, evaluated or proposed for a wide range of applications which are categorized in two groups in Table 2.1 below.

Table 2.1 Applications of air cycle technology

Food industry related applications	Other applications
<ul style="list-style-type: none"> • rapid chilling and/or freezing (including air blast, tunnel, spiral, fluidised bed and rotary tumble equipment); • cold storage facilities; • chilled or frozen retail display cabinets; • refrigerated transport (trucks, containers, rail freight, ships, air cargo); • grocery delivery centres; • integrated rapid heating and cooling (cook-chill-freeze or hot water/steam raising and refrigeration); • thermal and refrigerated processing of yogurt and fermented milks. 	<ul style="list-style-type: none"> • aircraft cabin air conditioning and avionic cooling (Rogers, 1995); • railway carriage air conditioning (Engelking & Kruse, 1996; Haller, 2003); • automotive and truck air conditioning (Bhatti, 1998; Halm et al, 2000); • integrated heating and cooling in buildings (Butler et al, 2001); • cooling of mines; • pharmaceutical production (freeze drying); • laboratories, clean rooms and environmental chambers; • volatile organic compound recovery; • natural gas liquefaction.

- Food industry related applications: Published literature relevant to the application of closed and open air cycle systems to freezing, chilling, storage, retail display and transport of food is reviewed in the following sections.
- Other applications: References to published literature are given in Table 2 for some of the non-food industry related applications of air cycle technology listed.

CLOSED AIR CYCLE SYSTEMS

VIC closed cycle turbo refrigerating machine

The NPO ‘VIC’ company of Moscow developed and manufactured a closed air cycle refrigeration system, a so-called turbo refrigeration machine (TRM), using centrifugal compressor and radial turbo-expander technology (Verechchaguine and Kolontchine, 1998). A ‘monorotor’ TRM design is shown diagrammatically in Figure 2.4 with the single-stage compressor (C) and turbine (T) mounted on the same shaft as the high-frequency, water cooled, electric drive motor (M). Other components in Figure 2.4 are labelled as follows: HX – recuperator; RC – refrigerating chamber; W – water cooler.

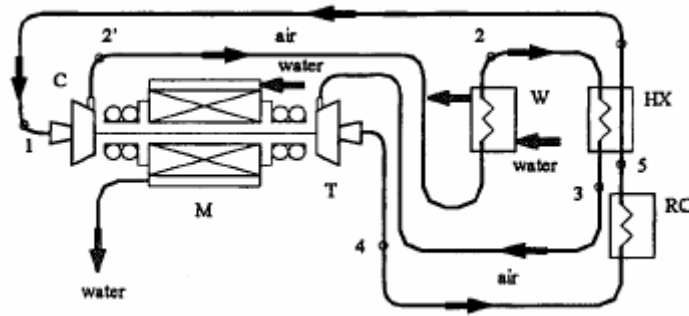


Figure 2.4 VIC 'monorotor' turbo refrigerating machine with single-stage compression
(from Verechtchaguine and Kolontchine, 1998)

Verechtchaguine and Kolontchine (1998) presented results of design calculations for the above 'monorotor' bootstrap arrangement, for a compression ratio of 1.6, and two more complex two-rotor designs with two and three separate compression stages (without intercooling) operating at overall compression ratios of 2.4 and 3.2 respectively. The three designs were evaluated for a range of compressor inlet pressure p_1 from 2 to 8 bar and the following fixed parameter values: electric power input = 30 kW, refrigerating chamber outlet temperature = -75°C and cooling water temperature = 20°C . Refrigeration capacity and COP values calculated for the simpler single-stage compression design equalled or exceeded those for the other designs at higher compressor inlet pressures. For the range of parameters given above the highest COP value computed for the 'monorotor' design was 0.38, at $p_1 = 8$ bar, with a corresponding refrigeration capacity of 11.4 kW, an air mass flow rate of 0.84 kg/s and a cold air temperature at turbine exit of -90°C . Furthermore, it was predicted for this condition that a rotational speed of 38 000 rev/min would be required, with a compressor impeller diameter of 146 mm and a turbine rotor diameter of 73 mm.

Air Products' closed cycle air refrigeration technology CCAR

Closed cycle air refrigeration (CCAR) technology was developed in the USA during the late-1990s by Air Products & Chemicals and Toromont Process Systems in a joint venture project partly funded by the NIST Advanced Technology Program (Pelsoci, 2001). In comparison to the COLDBLAST™ open air cycle refrigeration system (see next section), where fresh air must be continuously compressed and dehumidified to make up for the cold air exhausted to atmosphere, it was anticipated that an improvement in efficiency could be achieved with a closed cycle configuration using dry air at high pressure as the working fluid. The layout of the main CCAR components is illustrated in Figure 2.5. The cycle was designed to produce cold air delivery temperatures down to -150°F ($\approx -100^\circ\text{C}$) with a maximum cycle pressure of 1200 lbf/in² (≈ 83 bar) and a cycle pressure ratio of 1.6 with the single shaft compressor/expander assembly (or Compander) running at 30 000 rev/min. Special dry gas shaft seals were employed to minimise air leakage under the severe combination of pressure, temperature and rotational speed. A high effectiveness aluminium plate fin heat exchanger was specified for the recuperator (or Core Heat Exchanger).

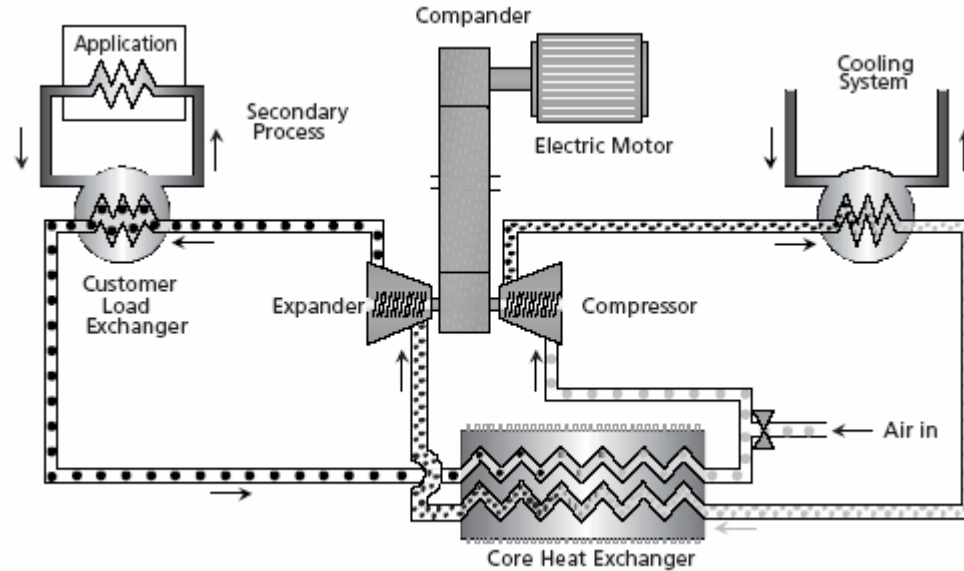


Figure 2.5 Air Products closed cycle air refrigeration system (from Pelsoci, 2001)

In pilot tests a CCAR demonstration unit achieved a refrigeration capacity of 60 ton (≈ 211 kW), 20% greater than the design rating. The unit ran for 6000 hours with 98% reliability maintaining the refrigeration temperature within approximately one kelvin of the -100°F ($\approx -73^{\circ}\text{C}$) design value. The corresponding *COP* value measured for the demonstration unit was 0.66. At a higher temperature of -70°F ($\approx -57^{\circ}\text{C}$) a *COP* of 0.75 was achieved. At 60% part load the *COP* was found to be only 3% less than the full load value.

Pelsoci (2001) analysed potential end markets for the application of CCAR technology. The food processing industry was identified as the most promising area, particularly the rapid chilling and freezing of precooked processed products, as a cost effective alternative to the use of cryogenics. Air Products has developed a standard skid mounted 200 ton (≈ 703 kW) refrigeration capacity CCAR unit for food industry applications.

OPEN AIR CYCLE SYSTEMS

Air Products' COLDBLAST™ air cycle freezing system

The COLDBLAST™ open air cycle refrigeration system developed in the USA by Air Products & Chemicals for high volume in-line food freezing operations is described by Shaw et al (1995). The figures quoted here are for a system with a nominal refrigeration capacity of 10^6 BTU/h (≈ 300 kW) although design capacities between one half and five times this value are claimed to be feasible. A flow diagram of the process, which employs turbomachine components of the type used in air separation plants, is shown in Figure 2.6.

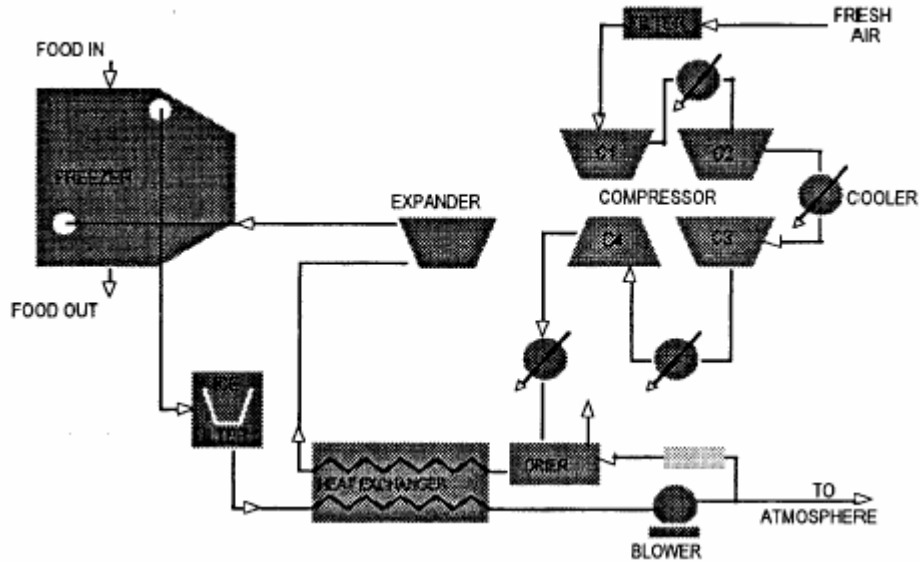


Figure 2.6 COLDBLAST™ air cycle freezing system flow diagram (from Shaw et al, 1994)

Following filtration of the incoming air to remove dust and particulate a four-stage centrifugal compressor raises the pressure to around $200 \text{ lb}_f/\text{in}^2$ ($\approx 14 \text{ bar}$). The pressurized air is cooled after each stage before passing through a pressure swing adsorption dryer where water is removed to prevent ice formation and erosion damage downstream. Two adsorption beds are used cyclically; with one on-line while the other is off-line being regenerated by purging with air supplied from the exhaust blower. After further cooling in the recuperative heat exchanger, against the cold exhaust stream, the air is expanded to approximately atmospheric pressure and -250°F ($\approx -157^\circ\text{C}$) at inlet to the freezer. Air is drawn out of the freezer, at about -100°F ($\approx -73^\circ\text{C}$), and exhausted to atmosphere via an ice particle filter and the low-pressure side of the recuperator. The compressor and exhaust blower are driven by an electric motor (not shown), and power generated by the turbo-expander is returned to the system.

Spiral and tunnel freezers have been designed to interface with the COLDBLAST™ system. Shaw et al (1995) estimated the installed cost of a COLDBLAST™ air cycle freezing system, including a spiral freezer, for a refrigeration capacity of 10^6 BTU/h ($\approx 300 \text{ kW}$) to be $1.8 \times 10^6 \text{ USD}$ (in 1994). The corresponding electrical power consumption, including the power to drive the refrigeration plant, the freezer fans and the conveyer is given as 1200 kW . A coefficient of system performance is not quoted but the above nominal figures imply a value around 0.25.

The low freezer temperatures produced by the COLDBLAST™ air cycle refrigeration system result in very fast freezing rates, reported to be two to four times faster than for ammonia cycles at around -40°C and almost as rapid as with liquid nitrogen. Rapid freezing has associated benefits for the food producer in terms of improved product yield, enhanced product quality and value, and faster processing occupying less floor space for a given production rate. Shaw et al (1995) present freezing times for various food products, (including hamburgers, raw chicken and cooked chicken) based on laboratory

simulations and COLDBLAST™ pilot plant trials, and estimated freezing costs per unit weight for these foods assuming plant operation of 4000 hours per year.

According to Pelsoci (2001) the technical and economic potential of the open cycle COLDBLAST™ system was not completely realised. Air Products subsequently developed the high pressure, closed cycle air refrigeration (CCAR) technology described in the next section.

TNO air cycle pilot plant

The air cycle pilot plant built at the Apeldoorn site of TNO in the Netherlands was developed to provide ‘proof of concept’ for an industrial blast freezing system for the food industry. The project was funded by the Commission of the European Community under the Joule programme and involved the participation of partners from four member states. A layout diagram of the TNO air cycle plant is shown in Figure 2.7 with typical temperatures and pressures around the cycle. The plant was designed for relatively small refrigeration capacities (less than 3 kW) but air temperatures down to -55°C can be attained. Details of the plant and its performance are given by Fleming et al (1998a, 1998b).

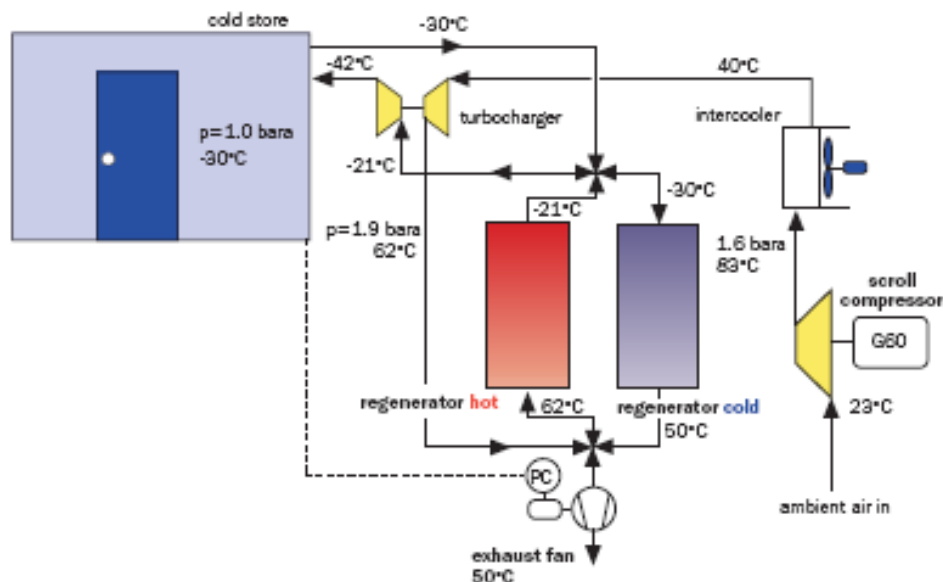


Figure 2.7 TNO air cycle pilot plant for industrial freezing (from TNO, 2003)

Ambient air is drawn into the open cycle system and undergoes two stages of compression with intercooling and a maximum overall pressure ratio of about 1.9. The first stage is provided by an electrically driven positive displacement scroll compressor and the second stage by a turbo-compressor directly driven by the turbo-expander in a bootstrap arrangement. The speed of the first stage compressor and the refrigeration load in the cold room determine the operating condition of the plant.

The TNO plant features a pair of fixed bed regenerators fitted with valves to periodically (every 60 s) and simultaneously reverse the flow direction in each bed. Before being expanded in the turbo-expander to atmospheric pressure, the pressurized air is cooled as it

flows through, and warms, the regenerator bed cooled during the previous half cycle. In addition to sensible heat, latent heat is also transferred from the hot and humid air by condensation and frost formation on the colder bed material. During the next half cycle, after reversal of the flow direction, the low-pressure cold air stream drawn through the bed from the cold room by the exhaust fan removes the deposited moisture and frost. Fleming et al (1998a) reported that monitoring of the regenerator pressure drops showed no sign of problems with ice accumulation, indicating satisfactory functioning of the dehumidification and defrosting mechanisms described above. A very slight deposition of fine powdery snow particles, from the remnant moisture content of the air, was observed in the cold room and could be removed by brushing. A mathematical model has been developed describing the transient behaviour and heat and mass transfer processes in the fixed bed regenerators (Fleming et al, 1998b).

Performance results for the TNO pilot plant are presented by Fleming et al (1998a), for cold room temperatures from 0°C down to -45°C and first stage compressor speeds from 3000 rev/min to 5500 rev/min. The values obtained for the internal *COP* of the cycle (taken as the ratio of the air temperature rise across the cold room to that across the first stage compressor) ranged from about 0.1 to 0.4, with the lowest values corresponding to the highest temperature lifts and vice versa. The corresponding overall plant *COPs* (taking into account mechanical drive losses and fan power) were lower, ranging from approximately 0.075 to 0.24. The poor energy efficiency was attributed to low isentropic efficiencies associated with the small size of machines, particularly for the turbo-expander. In contrast, recent TNO documentation (TNO, 2003) states that with 'currently available technology' an air cycle plant of the type shown in Figure 2.7 can produce cold air at -50°C with a *COP* value of 0.72 (including the energy required to compress and transport air to and from the cold room).

Kajima and AIRSTM50 air cycle refrigeration systems

The AIRSTM50 system, illustrated in Figure 2.8 and claimed to be the first commercially available packaged air cycle refrigeration system, is produced by the Earthship Company who acquired the IPR for this technology from Kajima Inc. in 2001. Kajima developed the original system and installed several prototypes in Japan as well as the one in Ancona, Italy discussed below. Two models are available, both rated at 5 ton (≈ 17.6 kW) refrigeration capacity, for application temperatures of -30°C and -60°C respectively, as detailed in Table 2.2.

Figure 2.2 shows the layout of an AIRSTM50 system operating in semi-open/closed cycle mode delivering cold air at -60°C to a warehouse operating at -30°C. In this arrangement, the cold air is delivered directly into the warehouse space and the low-pressure side of the cycle is atmospheric (≈ 0.1 MPa). The maximum pressure in the cycle, shown as 0.21 MPa corresponds to an overall cycle pressure ratio of 2.1. An ice capture section is incorporated between the turbine exit and the refrigerated warehouse. The AIRSTM50 brochure states that defrosting inside the storage space is not necessary.



Figure 2.8 AIRSTM50 packaged air cycle refrigeration system

Table 2.2 AIRSTM50 product specifications *

Model	AIRS50-30	AIRS50-60
Application temperature	-30°C	-60°C
Outside temperature	32°C	32°C
Supply air temperature	-54°C	-84°C
Air discharge pressure (guage)	150 Pa	150 Pa
Supply air flowrate	0.29 m ³ /s	0.29 m ³ /s
Coefficient of Performance	0.69	0.69
Dimensions	2 m W x 2 m D x 2.2 m H	2 m W x 2.5 m D x 2.2 m H
Weight	3.0 tonne	3.3 tonne

*nominal SI unit values converted from Imperial unit values given on Earthship USA website at url: <http://www.earthshipusa.com>.

Gigiel et al (2004) describes tests on a 15 kW Kajima air cycle refrigeration system installed at the Ancoopesca factory in Italy (see above) for supplying cold air axially into the drum of a tumble freezer which rotates at between 6 and 30 rev/min. The freezer is employed for rapid freezing of pieces of seafood in a batch process. The cycle operates in semi-open/closed mode with atmospheric pressure in the freezer. The pressure ratios across the primary compressor and for the overall cycle are 1.4 and 1.85 respectively. In the experimental set-up mains water at approximately 15°C was used to cool the intercooler and aftercooler, and the hot and cold sides of the recuperator were connected by an oil run-around coil (not shown in Figure 2.9).

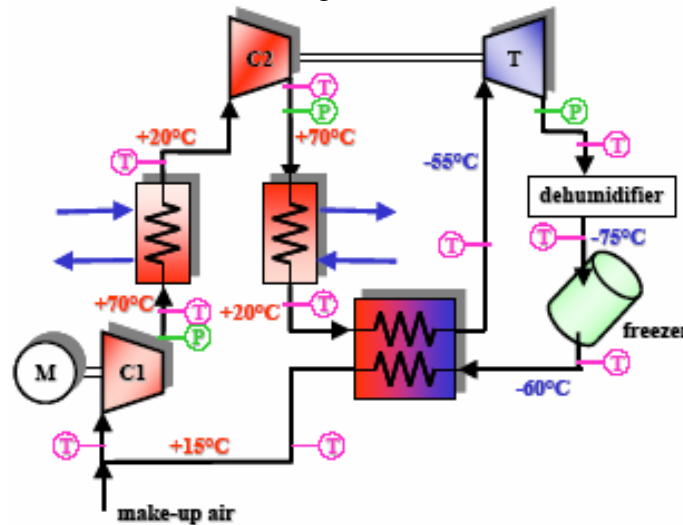


Figure 2.9 Kajima air cycle refrigeration system used to supply cold air to a rotary tumble freezer (from Gigiel et al, 2004)

Periodic defrosting of the ice capture section (labelled dehumidifier in Figure 2.9) was required at intervals in excess of 8 hours to remove frozen moisture from the system caused by evaporation from the food. In general, the air temperature achieved within, and at exit from, the freezer is governed by the primary compressor speed, the cooling water temperature and the freezer load. Figure 2.9 shows air temperatures around the cycle corresponding to a cold air supply temperature into the tumble freezer of -75°C . Measurements were made of the freezing times and weight loss of surimi sticks for freezing in air at temperatures around -75°C . The average weight loss measured was about 2%, and the average of the measured freezing times was in reasonable agreement with the freezing times predicted by a combination of mathematical modelling and empirical data. Furthermore, the paper emphasizes the reduction in freezing times, and consequent increase in freezer throughput, achievable as a result of the lower air temperatures available in the air cycle compared to conventional freezers.

Mitsubishi Heavy Industries system

Details of the air cycle refrigeration system developed by Mitsubishi Heavy Industries (MHI), shown in Figure 2.10, are given by Kikuchi et al (2005). At the heart of the system is a single shaft compressor/turbine assembly mounted vertically in oil-free, non-contact, active magnetic bearings. This turbomachine is driven by an integrated 100 kW synchronous permanent magnet electric motor with a rated speed of 21 000 rev/min at full load. Inverter control provides for speed adjustment to accommodate variation of refrigeration load and temperature. The operating temperature range of the MHI system is given as -100°C to -20°C .

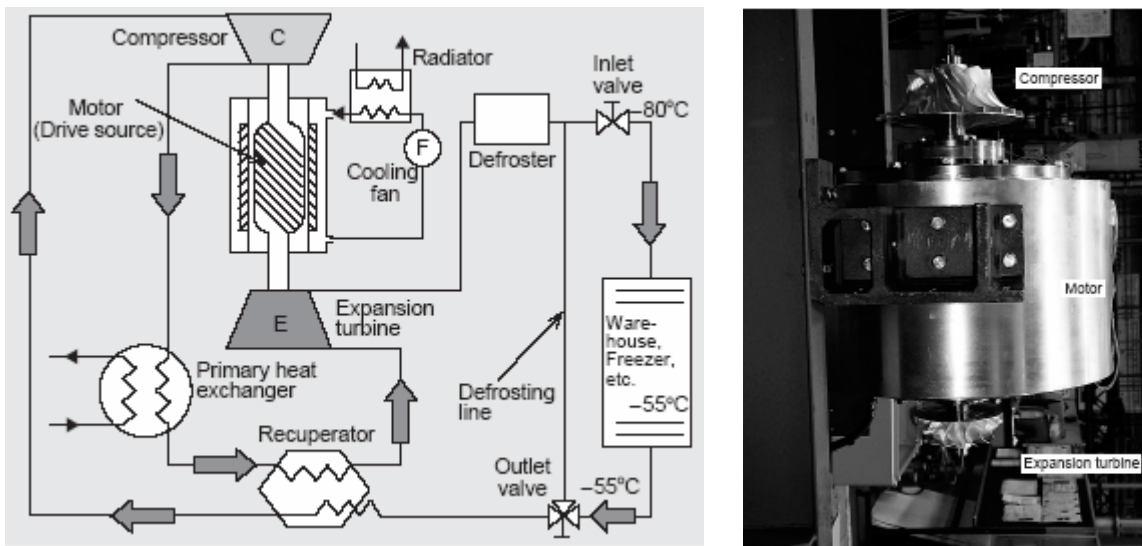


Figure 2.10 Mitsubishi Heavy Industries air cycle system and photograph of turbomachine (from Kikuchi et al, 2005)

The warehouse/freezer inlet and exit air temperatures shown in Figure 2.10 are for an application with a refrigeration capacity of 42 kW. The corresponding value of overall system COP_R (including auxiliaries) is 0.44 and the maximum values of the (guage) pressure and temperature for the air in the cycle are 0.1 MPa and 125°C at compressor delivery.

Kikuchi et al (2005) present comparisons, for power consumption and life cycle cost (LCC), between the MHI air cycle system and three other methods of refrigeration: (i) two-stage R22 vapour compression at -30°C , (ii) dual $\text{NH}_3/\text{R23}$ compressor at -55°C and (iii) liquid N_2 at -80°C . The power consumed by the air cycle is about twice that for the R22 system at -30°C , almost equal to the $\text{NH}_3/\text{R23}$ system at -55°C and less than one-eighth of the liquid N_2 system at -80°C . The LCC (comprising initial cost and 15 years operating costs, including power and maintenance) for the air cycle is approximately twice that for the R22 system at -30°C , about 75% of the $\text{NH}_3/\text{R23}$ system at -55°C and less than 25% of the liquid N_2 system at -80°C .

Air cycle spiral freezer

Pearson (2006) used MHI performance figures (Andou and Okuda, 2004) in making a comparison between using an air cycle system and conventional air blast to freeze 450 kg/h of uncooked burgers in a continuous spiral freezer. The proposed air cycle spiral freezing chamber, which does not require an air cooling coil or circulating fans and is designed to produce counterflow between the cold air and the product, is shown on the right in Figure 2.11. Mean freezer air temperatures of -28°C for the conventional system and -67°C for the air cycle system were assumed, giving freezing times of 15 minutes and 7 minutes respectively. As a consequence it was calculated that, for the same throughput of product, the air cycle freezer would require only 3 spiral tiers compared to 13 spiral tiers for the conventional freezer, which was reflected by a lower estimated capital cost for the spiral freezing chamber (not including the refrigeration equipment). However, the total power consumption required by the air cycle freezing system, calculated to be 71 kW, was about 25% higher than for the conventional system. The corresponding hourly running costs were calculated as £2.85 for the conventional freezer and £3.55 for the air cycle freezer, assuming an electrical energy cost of 5 p/kWh. In comparison, the hourly cost of freezing using liquid N_2 was estimated to be £27.25, assuming a cost for LN_2 of £60/tonne and a usage of 1 kg/kg of product frozen.

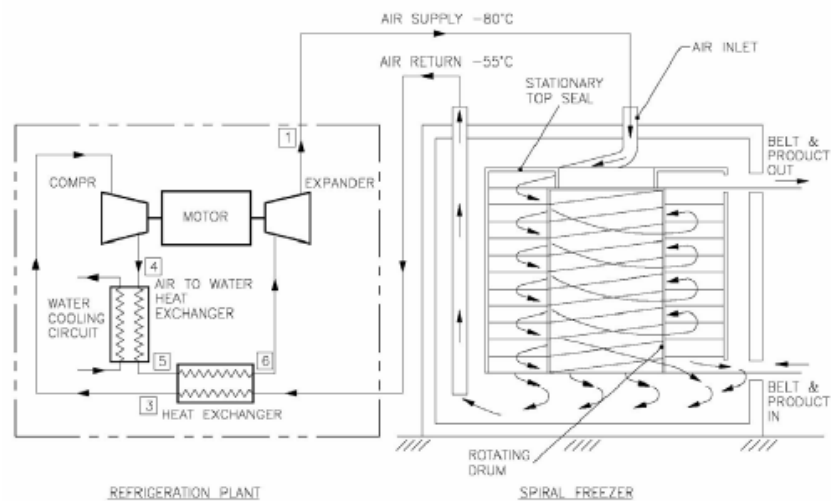


Figure 2.11 Continuous spiral freezer with air cycle refrigeration system (from Pearson, 2006)

Fluidised bed food freezing

Russell et al (2000) identified fluidised bed freezing of particulate foods as a promising application for air cycle refrigeration. This combination of technologies offers the following advantages for the production of individual quick frozen (IQF) foods of high quality and value: (i) more rapid freezing as a result of the low air temperatures provided by the air cycle and the high heat transfer coefficients associated with fluidised beds, (ii) use of the flow delivered by the air cycle to fluidise the bed without the need for additional fans, and (iii) physical separation of individual food particles.

Experiments were performed to establish minimum and maximum fluidisation velocities and to measure surface heat transfer coefficients for a range of small particulate foods (petit pois, peas, carrots, squid, surimi and prawns) in a 300 mm diameter bed. Both frozen and unfrozen food items, and a range of different bed depths. The temperature of the fluidising air supplied in the tests is not given.

The experimental data obtained was used to produce information for the design of belt-fed fluidised bed freezers. For chosen belt dimensions, the information given includes the depth of product required on the belt, the belt speed, and the minimum and maximum fluidisation air velocities and air flow rates. An example is presented for a final design based on a nominal product refrigeration load of 2 kW and belt dimensions of 1000 mm x 350 mm.

Retail food display cabinets

The application of air cycle refrigeration technology to chilled and frozen food display cabinets was investigated by Russell et al (2001). Two prototype cabinets were developed: (i) a chilled multi-deck type for a specified product temperature of 0 to 5°C, and (ii) a frozen well type for specified product temperature of -18°C (-15°C max.). Direct injection of cold air into the cabinet from an open air cycle was adopted as this system is known to reduce infiltration loss. An open system also obviates the need for an air-to-air heat exchanger, providing more space and flexibility for air distribution. Cold air entering the cabinet was directed through a number of ejector nozzles which entrained air from the cold space, thereby creating internal recirculation without the use of a fan. The resulting mixing of the cold air supply with recirculated air promoted temperature and flow uniformity in the cabinet.

Russell et al (2001) proposed a layout for the use of air cycle cooled display cabinets in supermarket installations locating the primary compressor and intercooler remotely in a central plant room delivering a single supply of compressed dry air to a distribution pipe network in the store. Removal of moisture from the ambient air entering the primary compressor would be achieved by a rotary wheel desiccant dehumidifier, with the hot counterflow air stream exhausting from the intercooler used to regenerate the desiccant. Each run of display cabinets connected to the compressed air network would have a separate bootstrap unit and an adjacent recuperator cooled by return air from the cabinets. The suggested scheme would allow greater flexibility with regard to placement of cabinets in the store.

Tests on the prototype air cycle cooled display cabinets demonstrated that the specified product temperatures could be achieved, although air cycle energy consumption figures were predicted to be slightly greater than for typical vapour compression units. However, optimising the air cycle performance and taking into account the additional energy for defrost and internal fans required in the case of vapour compression cabinets would result in more comparable energy consumption values.

Combined heating and cooling systems for the food and dairy industries

Utilization of both the low temperature cooling and high temperature heat rejection produced by an air cycle system can provide an integrated and energy efficient solution where a refrigeration load and a heating duty must be satisfied simultaneously.

The following relevant projects are being prosecuted currently:

- A novel environmentally friendly and cost effective technology for thermal and refrigerated processing of yoghurt and fermented milks by air cycle based heat pumps.

This project, known by the acronym YOGHURTAIR, is funded by the European Commission under the 6th Framework Programme (FP6) and coordinated by the National University of Ireland, Dublin with participants from 10 other organisations. A major objective is to develop and optimise an alternative air-cycle based pasteurisation-fermentation-chilling process for the production of safe yoghurts and associated fermented dairy products with improved nutritional and sensory quality.

- Development of integrated, rapid heating and cooling systems for the food industry.

This project is funded by the Defra LINK programme and coordinated by the Food Refrigeration and Process Engineering Research Centre at the University of Bristol with partners from 13 other organisations. The aims of the project are to (i) develop and demonstrate the use of air cycle with impingement heat transfer to produce a totally integrated process for food heating followed by immediate rapid refrigeration, (ii) demonstrate a combined hot water generation/rapid freezing system based on air cycle, and (iii) prove to potential users and system suppliers that air cycle heating/cooling systems have considerable commercial potential for food manufacturing applications (Evans, 2005).

Evans et al (2006) examined the feasibility of using air cycle technology to integrate the cooking and subsequent cooling (chilling or freezing) processes in the manufacture of a typical pre-cooked convenience food. The study was based on the calculated energy requirements to cook (at 80°C), chill (to 5°C) and freeze (to -18°C) Bolognese sauce at a throughput of 900 kg/h.

The air cycle configuration considered by Evans et al (2006) is shown schematically in

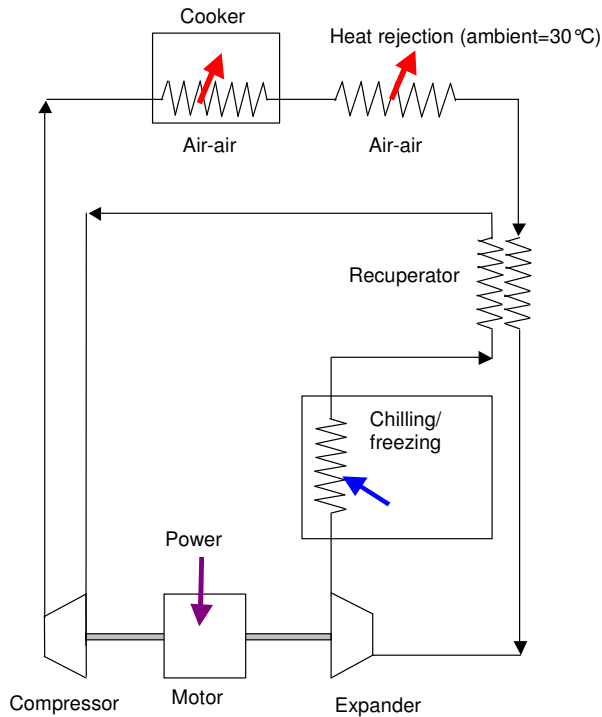


Figure 2.12. Isentropic efficiencies of 85% and 80% were used for the compressor and turbine respectively, and the recuperator effectiveness was taken as 0.85. Open cycle operation was assumed with the air expanding to ambient in the chiller/freezer, where counterflow heat exchange with the product was simulated, utilising the air temperature 'glide' characteristic of the air cycle. Spreadsheet calculations, linking the air cycle thermodynamics with a model for heat transfer between the product and the air, were performed to determine values of bootstrap driving power, excess heat rejection rate (available to heat water or raise steam), chilling and freezing times, and the cost to cook and cool for a range of cycle pressure ratio from 2.2 to 5.0.

Figure 2.12 Air cycle with integrated cooker and chiller/freezer (from Evans et al, 2006)

The chilling and freezing times, and hourly energy consumption costs, predicted for integrated cooking and cooling using air cycle technology were compared with corresponding values calculated for conventional food industry processing using gas cooking followed by either spiral chilling/freezing or liquid nitrogen freezing. Air temperatures assumed for the conventional chilling/freezing methods were as follows: 5°C (spiral chiller), -30°C (spiral freezer) and -100°C (LN₂ freezer). In general, the operating cost of the air cycle was found to increase with pressure ratio, but the required chilling and freezing times decreased. In comparison with conventional processing, with spiral chilling/freezing, the air cycle was less expensive to run for pressure ratios up to 3.0. However, the air cycle pressure ratio needed to be in excess of 3.0 to achieve a freezing time equivalent to the spiral freezer, and above 2.5 to achieve a chilling time equivalent to the spiral chiller. The use of LN₂ gave the shortest freezing time but at a significantly higher cost.

Refrigerated Transport

Sicars and Kruse (1994) reviewed the requirements for refrigeration systems used for transporting frozen and chilled products by road, rail and sea. System size (weight and volume), reliability, low maintenance, satisfactory refrigeration performance under a wide range of ambient conditions and tolerance of extremely rough working conditions, including vibration, shock and movement, were identified as important criteria. Refrigerant loss is a common problem associated with mobile vapour compression systems. James (1996) states that, in comparison, the performance of air cycle packages is much less affected by leaks, and they are also lighter and more reliable. Furthermore, Sicars and Kruse (1994) pointed out that a transport refrigeration system based on a cycle

using a natural working fluid (e.g. air), instead of a conventional vapour compression unit prone to leakage of refrigerant with high global warming potential, can lead to a reduction in total equivalent warming impact (TEWI), albeit with increased energy consumption. Fleming et al (1998) listed air cycle refrigeration for containers in transport as an application with large market potential.

Sicars and Kruse (1994) calculated the performance of various open air cycles for transport refrigeration. Their preferred configuration, for which the highest *COP* of 0.55 was predicted, was a cycle open to atmosphere on the high pressure side (i.e. a low pressure cycle) incorporating a rotary regenerative heat exchanger wheel with an absorbent coating. A refrigeration load of 10 kW and a cold storage room temperature of 0°C, simulating transport conditions for fruit, were assumed. The regenerator calculations accounted for transfer of mass (humidity) as well as heat transfer from the incoming air stream to the cold stream downstream of the storage space. Ambient conditions were taken as 32°C and 60% relative humidity, and an isentropic efficiency of 0.8 was used for both compression and expansion. For the above conditions the air mass flow rate and the corresponding compressor pressure ratio were found to be 0.15 kg/s and 4.85 respectively, the latter value indicating that two-stage compression would be necessary. The high compression ratio was due in part to the large pressure drop introduced by the air-to-air heat exchanger required in the cold storage space, giving a turbine expansion ratio of only 3.71. It was recognized that the large pressure differential between the streams would result in air leakage due to imperfect sealing in the rotary regenerator.

Engelking and Kruse (1996) focussed on the influence of component isentropic efficiencies on the coefficient of performance and the selection of suitable compressor and expander machines for open air cycle systems to be used in small transport refrigeration applications. Performance simulations were conducted for a system featuring a compact turbo-compressor and turbine unit with an integrated electric motor capable of rotational speeds up to 100000 rev/min. All system components were treated in the simulation program. Polynomial functions were used to represent turbomachinery characteristics obtained from the manufacturer and measured performance data for the heat exchangers. *COP* values calculated for a wide range of speed, assuming an ambient temperature of 30°C and cold room temperatures of 5°C and -30°C, exhibited peak values of approximately 0.5 and 0.25 respectively. Simulated results were also obtained using assumed isentropic efficiencies which demonstrated that: (a) efficiencies of about 0.8, the best that can be expected for small capacity turbomachines, are necessary to achieve a reasonable *COP*, and (b) *COP* is more sensitive to a change in the expander efficiency than the compressor efficiency. Engelking and Kruse (1996) also advocated use of the pressure wave machine as a compressor – expander, working with an additional compressor, instead of turbomachines to achieve high efficiencies for small capacity air cycle systems. Pressure wave machine test results presented illustrate the achievement of isentropic efficiencies between 0.7 and 0.8 for expansion and up to 0.7 for compression, for a pressure ratio of 1.4.

Spence et al (2004) reported on the design, construction and testing of an air cycle demonstrator plant for refrigerated road transport. The project objectives were to

accommodate the system within the physical envelope of an existing R404A vapour compression refrigeration trailer unit (Thermo King model SL200) and to achieve an equivalent refrigeration capacity (specified as 12 kW at 0°C trailer temperature and 7.2 kW at -20°C trailer temperature, both at 30°C ambient). Due to project resource limitations production of custom components was not an option. The demonstrator unit was constructed, where possible, utilizing commercially available or existing parts, including the diesel engine prime mover and air circulation fans from the SL200 unit. Standard exhaust turbocharger components were selected for the two compressor stages and the turbine, the latter requiring modification to suit the significantly different conditions of the air cycle. The choice of heat exchangers was also compromised by cost considerations as well as packaging constraints imposed by the restricted layout inside the SL200 space envelope. A schematic of the air cycle demonstrator plant, taken from a later paper (Spence et al, 2005), is shown in Figure 2.13. On the basis of their design analysis Spence et al (2004) decided not to provide intercooling between the compressor stages, but to compensate by fitting a larger aftercooler with a reduction in pressure loss and an improvement in effectiveness. An overall system *COP* of around 0.41 was predicted with a system pressure ratio of 2.14 with an air mass flow rate of 0.278 kg/s.

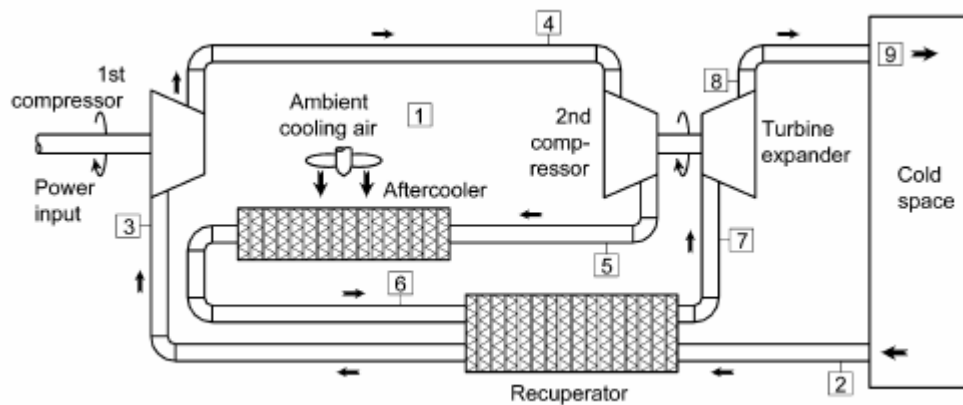


Figure 2.13 Air cycle demonstrator plant for refrigerated transport (from Spence et al, 2005)

Performance of the demonstrator plant depicted in Figure 2.13 was measured on a Thermo King calorimeter test facility at two operating conditions, 0°C and -20°C. A full-load capacity of 7.8 kW was achieved at -20°C (8% higher than the SL200 unit), but at 0°C the cooling capacity was only 9.5 kW (21% less than the SL200 unit). However, the fuel consumption of the air cycle plant was approximately 200% higher than for the vapour compression unit at both conditions. At a part load test condition of 3.4 kW refrigeration capacity (44% of the full load capacity), at -20°C, the air cycle plant fuel consumption reduced by approximately the same percentage, indicating that the overall plant *COP* remained almost constant for this load change. In contrast, at an equivalent part load condition the SL200 vapour compression unit would require 73% of its full load fuel consumption. It follows that the air cycle plant used only 80% more fuel than the vapour compression unit at the part load condition, compared to approximately 200% more at full load.

In a follow-up paper Spence et al (2005) presented a detailed performance analysis for their air cycle unit based on the demonstrator plant test results and a thermodynamic model incorporating previously determined characteristics for individual components. Comparison with values assumed in the original design predictions, for the full load condition at -20°C , revealed that underperformance of the demonstrator could be attributed mainly to low heat exchanger effectiveness (aftercooler and recuperator), high recuperator pressure loss and unaccounted heat gains by the cold air stream from adjacent hotter parts. The thermodynamic model was further used to assess the potential performance of an optimised air cycle unit employing state of the art technology, including specifically designed turbomachinery components, higher performance heat exchangers and air bearings. The predicted overall *COP* (allowing for all cooling and circulating fan power) for the optimised unit was 0.526 at the -20°C , 7.8 kW refrigeration capacity full load condition; only 7% less than the corresponding value estimated for the SL200 unit. Moreover, based on the demonstrator test results, it was anticipated that under part-load conditions, which represent a large proportion of refrigerated transport long haul operations, the optimised air cycle would maintain its full-load *COP* and require significantly less driving power than the vapour compression unit.

CONCLUDING REMARKS

- An up-to-date review has been conducted of published literature and other sources of information on air cycle technology from the mid-1990s to the present, with particular reference to food industry applications.
- The work carried out by industrial, academic and research organisations covers both the development of air cycle systems and food-related applications of the technology, including rapid chilling and freezing, integrated cooking and cooling, storage, display and transport.
- Air cycle refrigeration can deliver air temperatures down to -100°C , giving it a niche position in the -50°C to -100°C range beyond the capability of vapour compression plant, and is a cost-effective alternative to the use of cryogenics for low temperature food freezing operations. More rapid chilling and freezing benefits food safety, product yield, product quality and value, and allows an increase in production rate or a saving in floor space.
- Air cycles also generate high air temperatures, typically of over 200°C , that can be used in combination with the low temperatures to integrate cooking and refrigeration processes.
- Closed and open air cycle systems have been developed by industrial companies with refrigeration capacities ranging from 11 to 700 kW for closed systems and from 15 to 300 kW for open systems.

- Information on coefficient of performance for refrigeration is sparse but most values quoted are in the range 0.4 to 0.7. It is also noted that the efficiency of air cycle systems is relatively unaffected under part load conditions.
- Air cycle is a reasonably well established technology. Plant operating characteristics are understood and issues such as condensation and icing have been addressed and solutions developed. Very little information was found on costs and the position on take-up of this technology is unclear.
- Further development work to improve air cycle systems for refrigeration applications would benefit from the ready availability of suitable high efficiency small turbo-machines and high-effectiveness heat exchangers at reasonable cost.

REFERENCES

- K. Andou and S. Okuda, Development of air refrigerating system, 6th IIR Gustav Lorentzen Conference on Natural Working Fluids, Glasgow, 2004.
- M.S. Bhatti, Open air cycle air-conditioning system for motor vehicles, Paper 980289, SAE International Congress & Exposition, February 1998, Detroit, MI, USA, Session: Climate Control.
- D.J.G. Butler, A. Gigiel and S. Russell, Using air for cooling, Building Research Establishment, BRE Publication Draft number 202296, January 2001.
- S. Engelking and H. Kruse, Development of air cycle technology for transport refrigeration, Proc. 1996 International Congress of Refrigeration, Purdue University, Indiana, USA, 23-26 July, 1996, 349-356.
- J. Evans, Integrated, rapid heating and cooling systems, FoodLINK News, Issue 53, 10, December 2005, Defra.
- J. Evans, A. Gigiel and T. Brown, Development of integrated, rapid heating and cooling systems for the food industry using air cycle technologies, 7th IIR Gustav Lorentzen Conference on Natural Working Fluids, Trondheim, May 28-31, 2006.
- J.S. Fleming, B.J.C. van der Wekken, J.A. McGovern and R.J.M. van Gerwen, Air cycle cooling and heating – Part 1: A realistic appraisal and a chosen application, *International Journal of Energy Research*, 22, (1998), 639-655.
- J.S. Fleming, L. Li and B.J.C. van der Wekken, Air cycle cooling and heating – Part 2: A mathematical model for the transient behaviour of fixed matrix regenerators, *International Journal of Energy Research*, 22, (1998), 463-476.
- A. Gigiel, Air cycle refrigeration - a brief review, Seventh Congress on Engineering and Food (ICEF7), F21-F24, 1997.
- A. Gigiel, F. Polonara and G. Di Nicola, Rapid freezing of food in an open cycle freezer, Proc. 6th IIR Gustav Lorentzen Conference on Natural Working Fluids, Glasgow, 2004.
- N.P. Halm, M. Scmitz and M. Pratsch, Air-cycle technology used for truck air conditioning, Proc. 4th IIR Gustav Lorentzen Conference on Natural Working Fluids, Purdue University, West Lafayette, USA, 25-28 July, 2000, 499-507.
- G. Haller, Railway vehicle air conditioning developments, Paper ICR0620, International Congress of Refrigeration 2003, Washington.

- D.M. Holder, T. Brown & A.J. Gigiel, The effects of water and icing on the performance of open air cycle systems - Problems and solutions, IIR The Hague, Holland August 1995.
- S. James, New technology in food cooling, *International Journal of Refrigeration*, 19, (1996), 76-77.
- S. Kikuchi, S. Okuda, H. Igawa, S. Morii, M. Mitsuhashi and H. Higashimori, Development of air cycle system for refrigeration, *Mitsubishi Heavy Industries Technical Review*, Vol. 42, No. 4, 1-4, November 2005.
- S.F. Pearson, Air cycle refrigerating system for continuous freezer, IIR Conference, Palmerston North, New Zealand, 2006.
- T. Pelsoci, Closed-cycle air refrigeration technology for cross-cutting applications in food processing, volatile organic compound recovery, and liquid natural gas industries: Economic case study of an ATP-funded program, National Institute of Standards and Technology, Gaithersburg, Report NIST GCR 01-819, December 2001.
- B.H. Rogers, Cooling in aircraft, paper presented before the Institute of Refrigeration, London, 5 January 1995, 40-44.
- S.L. Russell, A.J. Gigiel, S.J. James, Progress in the use of air cycle technology in food refrigeration and especially retail display, Australian Refrigeration Air Conditioning and Heating (AIRAH) Journal, Volume 55, No. 11, 20 -23, November 2001.
- S.L. Russell, A.J. Gigiel, S.J. James, Development of a fluidised bed food freezing system that can use air cycle technology, IChemE Food and Drink 2000, Birmingham, 78-81, 2000.
- R.J. Shaw, E.F. Kiczek and J.C. Rossman, Coldbast™ air cycle freezing system, Vol IIIa, Proc. 19th International Congress of Refrigeration, The Hague, Netherlands, 20-25 August, 1995, 684-691.
- S. Sicars and H. Kruse, Air cycle systems for transport refrigeration, IIR conference, Hannover, Germany, 10-13 May, 1994.
- S.W.T. Spence, W.J. Doran and D.W. Artt, Design, construction and testing of an air-cycle refrigeration system for road transport, *International Journal of Refrigeration*, 27, (2004), 503-510.
- S.W.T. Spence, W.J. Doran, D.W. Artt and G. McCullough, Performance analysis of a feasible air-cycle refrigeration system for road transport, *International Journal of Refrigeration*, 27, (2005), 381-388.

TNO, Cooling, freezing and heating with the air cycle, TNO Environment, Energy and Process Innovation, Refrigeration and Heat Pump Technology, Documentation Sheet, 2003/09/26/002e, 2003.

N.J. Williamson and P.K. Bansal, Feasibility of air cycle systems for low-temperature refrigeration applications with heat recovery, Proc. Inst. Mech. Engrs. Part E: *Journal of Process Mechanical Engineering*, 217, (2003), 267-273.

3. MAGNETIC REFRIGERATION

INTRODUCTION

Magnetocaloric effect

A magnetic refrigeration cycle employs a solid-state magnetic material as the working substance, or refrigerant, and exploits the magnetocaloric effect (MCE), or the ability of a material to warm up in the presence of a magnetic field and cool down when the field is removed, to produce a cooling effect. Heat absorption and heat rejection are facilitated by thermally linking the magnetic material with the cold source and hot sink respectively, using a harmless heat transfer fluid such as water, anti-freeze mixture or a gas, depending on the operating temperature range. The forces involved in applying and removing the magnetic field provide the necessary net work input to the cycle for heat pumping from the source to the sink.

Magnetization and demagnetization of a magnetic refrigerant can be viewed as analogous to compression and expansion in a vapour compression refrigeration cycle, but in contrast these magnetic processes are virtually loss-free and reversible for soft ferromagnetic materials. Further advantages associated with the solid-state nature of magnetic refrigerants are the absence of vapour pressure, resulting in zero ODP and zero GWP, and a large magnetic entropy density which is the key thermodynamic property determining the magnitude of the MCE. Magnetic refrigeration therefore offers the prospect of efficient, environmentally friendly and compact cooling. The reviews contributed by Pecharsky and Gschneidner (1999, 2006), Yu et al (2003), Brück (2005), Gschneidner et al (2005) and Kitanovski and Egolf (2006) provide a comprehensive introduction to the magnetocaloric effect and its history, relevant thermodynamics, and developments in magnetocaloric materials and magnetic refrigeration.

The magnetocaloric effect was first observed in 1881 during experiments with iron. The phenomenon was explained early in the 20th century and proposals were made in the 1920s to use adiabatic demagnetization refrigeration to cool to temperatures below 1 K. Since its first use in the early 1930s, ADR has been developed as a standard technique for low temperature experiments and commercial equipment is now available for reaching temperatures in the milli-kelvin range. Low-temperature magnetic refrigeration has also been investigated for the liquefaction of gases such as hydrogen, helium and natural gas.

The feasibility of near room temperature magnetic refrigeration was first demonstrated by Brown (1976) using a regenerative apparatus incorporating a bundle of 1 mm thick gadolinium plates. This assembly was cycled up and down in a vertical tube of fluid (80% water/20% ethyl alcohol) under applied magnetic fields of zero and 7 T respectively. After 50 cycles a no-load temperature difference of 47 K was achieved between the top (46°C) and bottom (-1°C) of the tube.

Magnetic refrigeration technology for operating temperatures near to room temperature, including both magnetic materials and systems design, is under active development in North America, the Far East, Europe and Russia. In excess of 20 prototype magnetic

refrigeration systems have been built since the late 1990s (Gschneidner and Pecharsky, 2007).

The MCE is an intrinsic property of all magnetic materials and originates from coupling of the magnetic moments of electrons with an external magnetic field, which produces a change in the magnetic part of the total entropy of a solid when the field strength is increased or decreased. In the case of magnetization, application of a magnetic field aligns the magnetic moments, thereby reducing magnetic disorder with a corresponding decrease in magnetic entropy. Removal of the magnetic field constraint (demagnetization) allows the magnetic moments to randomize, restoring the magnetic entropy to its original level.

Two different measures of the MCE are defined:

(i) Isothermal magnetic entropy change, $(\Delta S_M)_T$

When the magnetic field strength is changed from an initial value H_i to a final value H_f with the temperature held constant it can be shown that the corresponding change in the magnetic entropy (in $\text{J/m}^3 \text{K}$) can be expressed as

$$(\Delta S_M)_T = \mu_o \int_{H_i}^{H_f} \left(\frac{\partial M}{\partial T} \right)_H dH$$

3.1

where μ_o is the permeability of vacuum (in N A^{-2}), M is the magnetization (in A m^{-1}) and H is the magnetic field strength (in A m^{-1}). Equation 3.1 shows that $(\Delta S_M)_T$ depends on the rate of change of magnetization with temperature at constant field $(\partial M/\partial T)_H$ and the change of magnetic field $\Delta H = H_f - H_i$. Since $(\partial M/\partial T)_H < 0$ for ferromagnetic materials it follows for an isothermal increase in the magnetic field ($H_f > H_i$) that the magnetic entropy S_M decreases and heat is rejected. Conversely, S_M increases and heat is absorbed for an isothermal decrease in the magnetic field ($H_f < H_i$).

(ii) Adiabatic temperature change, ΔT_{ad}

If the magnetic field is changed adiabatically and reversibly (i.e. isentropically) the total entropy of the magnetic material remains constant. In this case the change in the magnetic entropy is balanced by an equal and opposite change in the lattice and electronic entropy contributions. The resulting adiabatic temperature change is given by

$$\Delta T_{ad} = -\mu_o \int_{H_i}^{H_f} \frac{T}{c_H} \left(\frac{\partial M}{\partial T} \right)_H dH$$

3.2

where T is absolute temperature (in K), c_H is volumetric heat capacity at constant field (in $\text{J/m}^3 \text{K}$) and other symbols are as previously defined. It follows from Equation 3.2 that ΔT_{ad} is positive (i.e. a temperature rise) for an increase in the magnetic field strength and vice versa.

Examination of Equation 3.1 and Equation 3.2 show that both $(\Delta S_M)_T$ and ΔT_{ad} depend on the magnitude of the magnetic field change ΔH , which is limited for permanent magnets, and $(\partial M/\partial T)_H$, which depends on the composition of the magnetic material.

The isothermal magnetic entropy change $(\Delta S_M)_T$ and the adiabatic temperature change ΔT_{ad} for a typical second order magnetic phase transition material undergoing an increase in magnetic field from $H_i = H_0 = 0$ to $H_f = H_1 > 0$ are shown on the entropy-temperature diagram in Figure 3.1. The inset graph in Figure 3.1 shows how both $(\Delta S_M)_T$ and ΔT_{ad} peak around the magnetic ordering (or Curie) temperature of the magnetic material, where $|\partial M/\partial T|_H$ is maximised, and fall off at higher and lower temperatures. It should be noted that most magnetic phase transitions are of the continuous second order type.

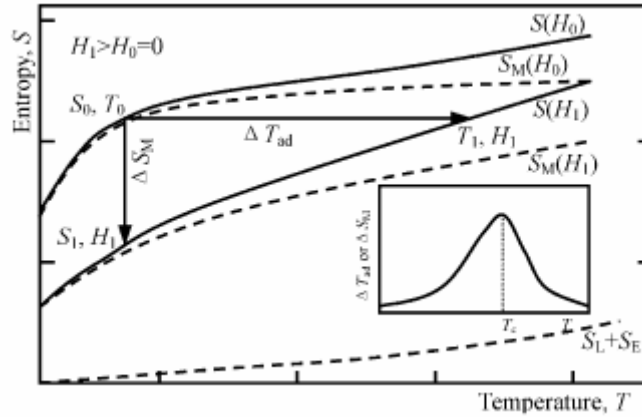


Figure 3.1 $S - T$ diagram for a second-order magnetic phase transition material (from Yu et al, 2003)

Magnetocaloric materials

The lanthanide metal gadolinium (Gd) has been used in many research studies on near room temperature magnetic refrigeration and is regarded as a benchmark against which other magnetocaloric materials can be compared. Gadolinium is ferromagnetic and undergoes a second order phase transition at its magnetic ordering temperature (or Curie temperature), $T_C = 294$ K. For an applied magnetic field increase from 0 to 2 T, representing the approximate maximum field that can be generated using permanent magnets, Gd experiences a peak adiabatic temperature rise ΔT_{ad} (at T_C) of about 6 K.

Several gadolinium based intermetallic compounds, including Gd-R alloys where R denotes another lanthanide metal such as dysprosium (Dy), erbium (Er), holmium (Ho) or terbium (Tb), have been investigated to find improved materials. Compared with Gd the Gd-R alloys were found not to enhance the MCE but shifted T_C downwards.

A major advance in magnetic refrigerants for near room temperature applications was achieved with the discovery by Pecharsky and Gschneidner (1997) of a giant magnetocaloric effect (GMCE) in the $Gd_5(Si_xGe_{1-x})_4$ pseudobinary alloys, where $x \leq 0.5$. It was established that the GMCE, reflected by a magnetic entropy change 2-10 times larger than previously known best materials at the same Curie temperature, is associated with a first order phase transition which is reversible with respect to alternating magnetic field. Furthermore, by altering the Si/Ge ratio, the ordering temperature is tunable from ~ 30 K to ~ 276 K, the upper limit of this range corresponding to T_C for the alloy $Gd_5Si_2Ge_2$.

The major distinction between the behaviours of MCE and GMCE materials is that in the latter the magnetocaloric effect is usually accompanied by a simultaneous structural change.

At present, Gd and $Gd_5Si_2Ge_2$ are regarded as leaders in the second order phase transition (MCE) and first order phase transition (GMCE) materials, respectively, for near room temperature magnetic refrigeration applications (Pecharsky and Gschneidner, 2006). A comparison of ΔS_M for Gd and $Gd_5Si_2Ge_2$ for a magnetic field increase $\Delta H = 5$ T is shown in Figure 3.2 (Gschneidner and Pecharsky, 2007).

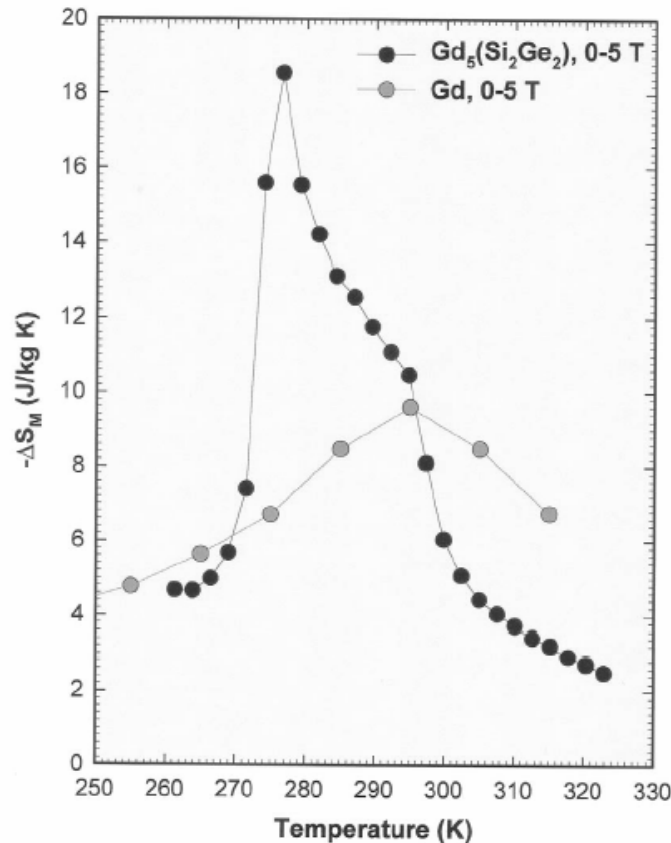


Figure 3.2 Magnetic entropy change ΔS_M versus temperature for Gd and $Gd_5Si_2Ge_2$ for a magnetic field increase of 5 T (from Gschneidner and Pecharsky, 2007)

Other types of magnetic material demonstrating GMCE behaviour are listed by Gschneidner and Pecharsky (2007) as follows:

- manganites $(R_{1-x}M_x)MnO_3$
(R = lanthanide, M = alkali, alkaline earth)
- lanthanum-iron-silicon $R(Fe_{1-x}Si_x)_{13}$
- manganese-antimony arsenide $MnAs_{1-x}Sb_x$
- iron-manganese-arsenic phosphides $(FeMn)(P_{1-x}As_x)$
- Heusler alloys $Ni_{2+x}Mn_{1-x}Ga$

Research efforts are continuing to identify new magnetic materials exhibiting strong MCEs that can be produced on a large scale and fabricated into suitable forms for application at reasonable cost and are compatible with heat transfer fluids.

Active magnetic regeneration cycle

The use of regeneration is a key feature in the efficient operation of a room temperature magnetic refrigerator as the small temperature rise produced by the magnetocaloric effect at a single temperature is insufficient by itself for practical refrigeration applications. Fortunately, this limitation can be overcome using a regenerative cycle that utilizes ΔT_{ad} of the magnetic refrigerant (or better still a series of magnetic materials with different Curie temperatures) over a range of temperature to produce a useful source-to-sink temperature span. The majority of magnetic refrigerator prototypes developed in the last decade operate on the active magnetic regeneration cycle.

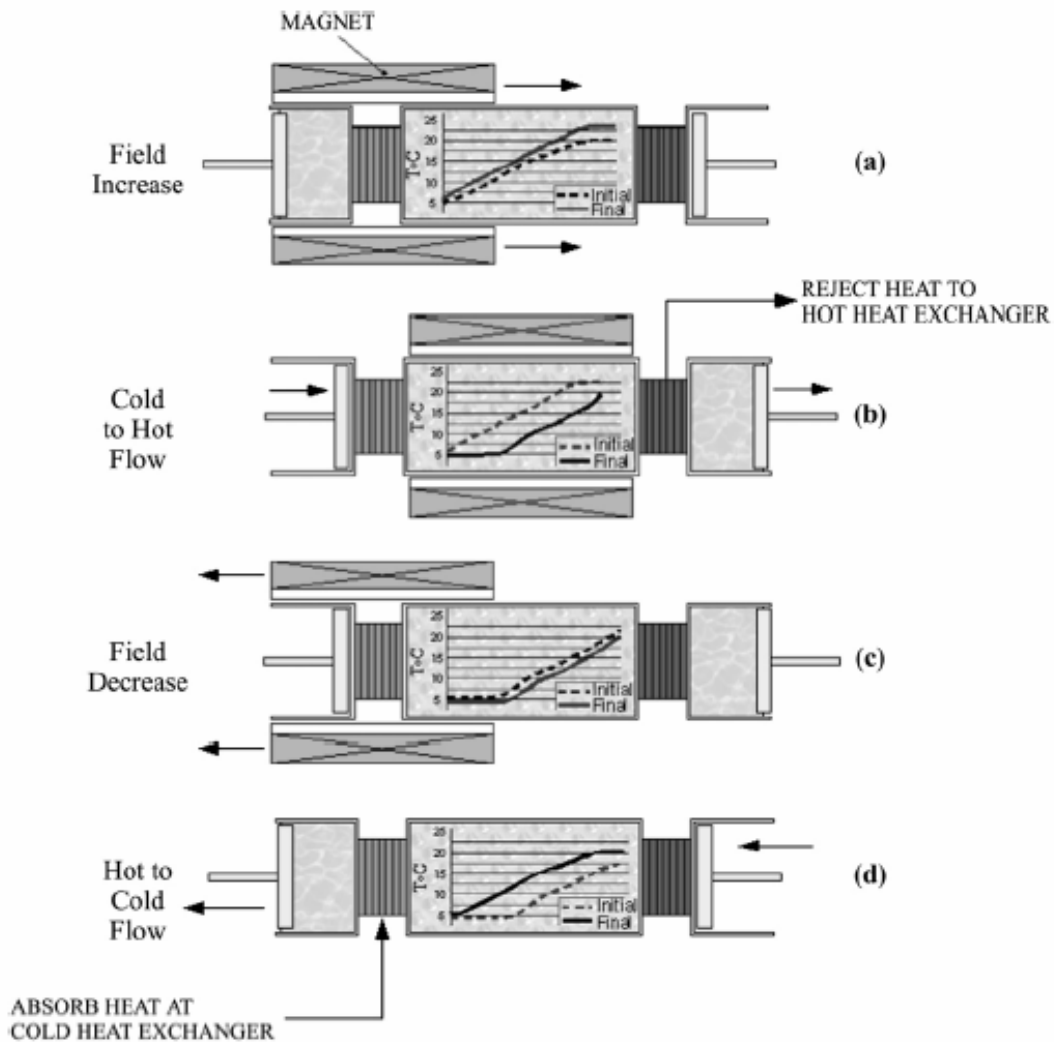


Figure 3.3 Active magnetic regeneration cycle (from Russek and Zimm, 2006)

In the active magnetic regeneration cycle (AMR), developed at Los Alamos in the late 1970s and early 1980s (Barclay and Steyert, 1982), the magnetocaloric material combines the functions of both a solid-state magnetic refrigerant and a thermal regenerator bed, or matrix. Heat transfer fluid is forced through the porous regenerator in alternate directions carrying heat to or from the hot and cold heat exchangers in sequence with periodic magnetization and demagnetization of the magnetocaloric material.

During one AMR cycle the magnetic refrigerant undergoes the following four processes, as illustrated in Figure 3.3 (a)-(d) where the broken and solid lines indicate the initial and final temperature profiles along the regenerator for each process:

- (a) Adiabatic magnetization: As a magnetic field is imposed, each element along the regenerator experiences a temperature rise equal to the local magnetocaloric value ΔT_{ad} less the effect of the heat capacity of the fluid in the regenerator pores.
- (b) Cooling at constant magnetic field: Heat transfer fluid (at T_c) enters the magnetized regenerator from the cold end and flows through to the hot end, cooling the regenerator and warming the fluid. The fluid emerges at a temperature above T_h and rejects heat through the hot heat exchanger.
- (c) Adiabatic demagnetization: The magnetic field is removed, causing a temperature decrease throughout the regenerator due to the local magnetocaloric effect.
- (d) Heating at constant magnetic field: Heat transfer fluid (at T_h) enters the demagnetized regenerator from the hot end and flows through to the cold end, warming the regenerator and cooling the fluid. The fluid emerges at a temperature below T_c and absorbs the refrigeration load through the cold heat exchanger.

Hence, each particle in the regenerator undergoes its own Brayton cycle. The effect of the heat transfer fluid flowing back and forth is to establish a temperature gradient along the regenerator between the source and sink heat exchanger temperatures.

Water, aqueous mixtures and helium have been employed as heat transfer fluids. Li et al (2006) numerically modelled the performance and efficiency of a reciprocating AMR system incorporating regenerator beds packed with Gd particles (300 μm particle size, 0.37 porosity) with various fluids, including water, water/glycol, helium and nitrogen. The results indicated that liquid is preferable to gas as a heat transfer fluid, due to its higher thermal conductivity and higher volumetric specific heat capacity, despite having a higher dynamic viscosity. An anti-freeze mixture would obviously be necessary for operation at or below 0°C. For lower temperatures a gas such as helium may be used.

Different structural forms of the solid refrigerant have been adopted for regenerator construction in near-room temperature magnetic refrigerators. Prototype AMR refrigerators often use porous beds of spherical or irregular magnetic refrigerant particles, typical size 250-600 μm . Regenerator designs where the active magnetocaloric material is fabricated into various forms (microchannels, corrugated sheets, fins) have been reported.

NEAR ROOM TEMPERATURE MAGNETIC REFRIGERATORS

Prototypes (including both reciprocating and rotary designs) are under development by groups in America, Japan, Canada, China, Russia and several European countries, including the UK (Wilson et al, 2007). Two of the leading 'state of the art' AMR systems are described below, illustrating different rotary designs for producing relative movement between the magnetic material and the magnetic field source.

Astronautics Corporation of America

The design and performance of the rotary magnetic refrigerator developed by Astronautics, shown in Figure 3.4, are described by Zimm et al (2006). The system operates on an active magnetic regenerator (AMR) cycle and features a wheel partitioned into three sectors packed with magnetocaloric material in particulate form. Each sector in turn is subjected to a magnetic field of 1.5 T as the wheel is continuously rotated through a Nd₂Fe₁₄B permanent magnet with steel flux concentration poles extending over 120° of the wheel circumference. The system can be operated at rotational speeds between 30 and 240 rev/min.

Radial pipes carrying the aqueous heat transfer fluid connect the two ends and the middle of each sector via disk valves to the hot and cold heat exchangers respectively. The valves, each comprising a fixed part and a rotating part with appropriate porting, switch the direction of flow in the radial pipes as the wheel rotates. When a sector is in the magnetic field, fluid from the cold heat exchanger enters at the middle position and exits from both ends of the sector to the hot heat exchanger. Conversely, when the sector is outside the magnet, the flow direction is reversed, entering the sector at both ends from the hot heat exchanger and exiting to the cold heat exchanger from the middle position. Thus, circumferential reciprocating flow and a temperature gradient are generated in the magnetocaloric material between each (hot) end and the (cold) middle of the sector, establishing two AMR beds per sector. The flow directions in the heat exchangers remain unidirectional as indicated by the arrows in Figure 3.4.

Zimm et al (2006) obtained results for the temperature span versus cooling power characteristics of the above system with the AMR beds packed with different magnetocaloric materials. With gadolinium particles (spherical, 425-500 µm diameter) the maximum temperature span was approximately 18.5 K at zero cooling power and a maximum cooling power of about 44 W was achieved as the temperature span approached zero. The corresponding rotational speed, fluid flow rate and heat rejection temperature were 240 rev/min, 0.67 litre/min and 25°C respectively. For the same conditions, layered beds packed with equal masses of Gd particles and 94% Gd-6% Er alloy particles (spherical, 250-355 µm diameter) in succession produced a greater maximum temperature span of about 25 K at zero cooling power, but slightly less cooling (~ 41 W) at the lowest temperature span. However, for temperature spans greater than 4 K the cooling power achieved with the two-layer beds surpassed that for Gd alone, demonstrating the increasing influence of the lower Curie point of the Gr-Er alloy. Coefficients of performance were not stated.

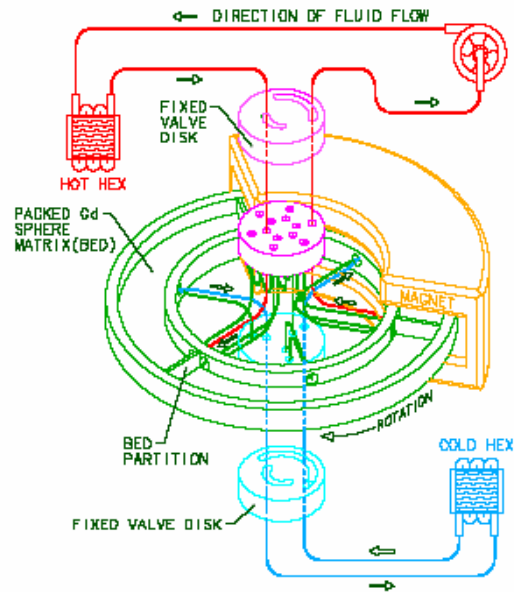


Figure 3.4 Schematic of the Astronautics rotary magnetic refrigerator (from Zimm et al, 2006)

Tests were also performed using $\text{La}(\text{Fe}_{1-x}\text{Si}_x)_{13}\text{H}_y$ particles (irregular, 250-500 μm size). This first order phase transition material was compared with the second order phase transition materials, Gd and the Gd-Er alloy, on the basis of the cooling load sustained at a small temperature span. The LaFeSiH exhibited a characteristic sharp peak in cooling capacity over a narrow temperature range, comparable in magnitude to values obtained for Gd over a broader operating range. It was concluded that use of LaFeSiH in an AMR bed would require a layered bed with materials with different Curie temperatures to ensure a significant temperature span.

Chubu Electric Power Co. Inc., Japan

In contrast to the Astronautics rotary magnetic refrigerator system described above the Chubu Electric design features fixed active magnetic regenerator beds and rotating magnets as illustrated in Figure 3.5 and Figure 3.6 (Okamura et al, 2006).

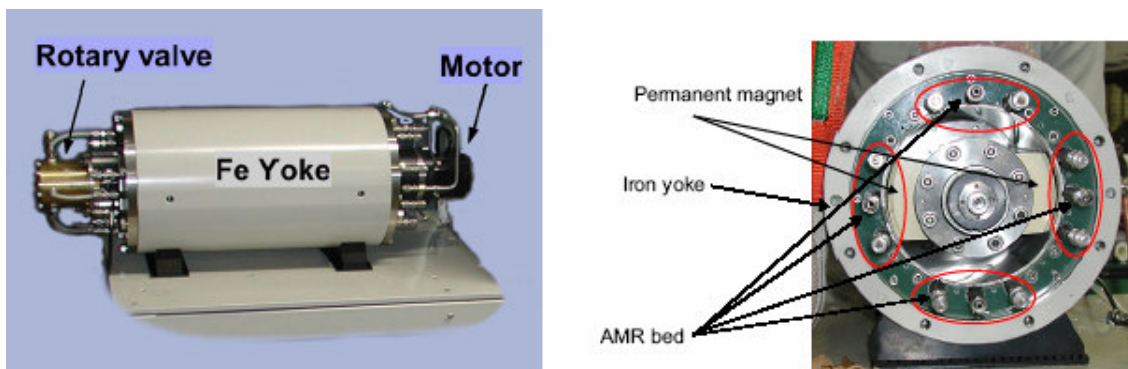


Figure 3.5 External and cross sectional views of the Chubu Electric rotary magnetic refrigerator system (from Okamura et al, 2006)

The main body of the refrigerator consists of an iron yoke housing four equally spaced AMR beds. Two neodymium permanent magnets are rotated inside the main body by an electric motor, alternately magnetizing and demagnetizing each pair of diametrically opposite AMR beds. The magnets apply a magnetic field of 0.77 T and the maximum magnetic torque is given as 52 Nm. Each AMR bed contains 1 kg of magnetocaloric material, comprising four gadolinium-based alloys ($Gd_{0.92}Y_{0.08}$, $Gd_{0.84}Dy_{0.16}$, $Gd_{0.87}Dy_{0.13}$ and $Gd_{0.89}Dy_{0.11}$) alloy spheres of 600 μm diameter. The alloys exhibit a peak in ΔT_{ad} over slightly different temperature ranges and, accordingly, occupy different sections along the beds in the direction of increasing temperature from T_L to T_H , to take advantage of this. Water is used as the heat transfer fluid and is pumped from the hot end through the demagnetized AMR beds, where it is cooled, before passing through the cold stage where it absorbs the refrigeration load (simulated by an electrical heater). The circuit is completed as water returns to the hot end through the magnetized AMR beds, where it is heated, before rejecting heat from the system via a heat exchanger. A rotary valve switches the flow direction through the AMR beds in sequence with the rotation of the magnets. One complete cycle comprises two equal periods when the magnet is being rotated through 90° plus two stopping periods. Flow through the beds takes place mainly during the stopping periods but with some overlap into the rotation periods.

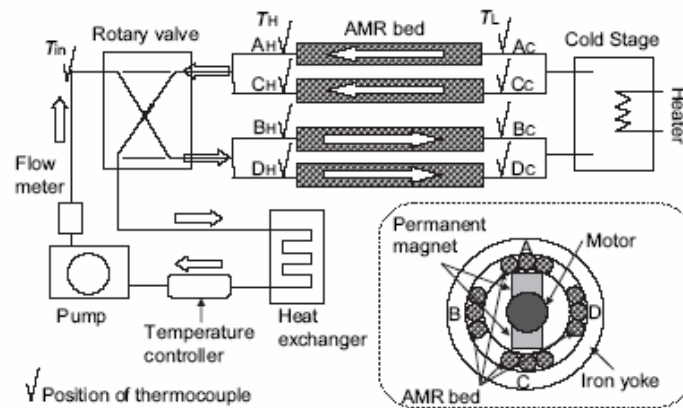


Figure 3.6 Schematic of Chubu Electric rotary magnetic refrigerator system (from Okamura et al, 2006)

Okamura et al (2006) performed experiments to investigate the effects of varying the water flow rate, the inlet temperature and the cycle time on the cooling performance. The magnet rotation periods were held constant at 0.5 s each. The highest cooling rate obtained at the cold end was 60 W, with a temperature span of 1.1 K and $T_H = 10.8^\circ\text{C}$. The water flow rate and cycle time were 4 litre/min and 2.4 s respectively. The corresponding coefficient of performance was just over 0.15. As the temperature span was increased the rate of cooling (and the COP) steadily decreased, reaching zero when $(T_H - T_L)$ was approximately 8.5 K.

A recent press release from Chubu Electric (dated 7 November 2006) announces performance improvements of the above system by optimising the magnet positioning enabling a larger magnetic field change (1.1 T compared to 0.77 T previously), improving heat exchange efficiency and reducing heat infiltration. A nearly ten-fold increase in the refrigeration capacity, from 60 W to 540 W, and a coefficient of performance of 1.8 (compared to the COP value of about 0.15 quoted above for the

earlier version) are reported. Unfortunately, the corresponding temperature span is not stated but it is likely to be at the lowest end of the operating characteristic.

A recent paper (Okamura et al, 2007) reporting on the improved Chubu Electric prototype reports a maximum *COP* of 2.4 with a corresponding maximum cooling capacity of 560 W at $T_H = 20^\circ\text{C}$ and zero temperature span. For a 5 K temperature span and $T_H = 20^\circ\text{C}$ the *COP* and cooling capacity are given as 0.6 and 159 W respectively.

CONCLUDING REMARKS

- The application of magnetic refrigeration for near room temperature uses is an emerging technology which offers the prospect of efficient, environmentally friendly and compact cooling for wide field of applications. A review of relevant published literature and other sources has been conducted covering the magnetocaloric effect, magnetocaloric materials, the active magnetic regenerator cycle and prototype systems.
- Near room temperature magnetic refrigeration is being actively developed in industrial, university and research organisation laboratories worldwide, including groups in America, Japan, Canada, China, Russia and several European countries, including the UK. More than 20 prototype systems (including both reciprocating and rotary designs) have been announced since the late 1990s.
- The highest *COP* reported for permanent magnet, near room temperature AMR refrigerator is 2.4 with a corresponding maximum cooling capacity of 560 W at zero temperature span (Chubu Electric, Japan).
- The following requirements have been identified for successful commercialization: (i) magnetic refrigerants (higher MCEs, large quantity production), (ii) permanent magnets (higher strength, smaller volume and lower cost), (iii) thermodynamic cycles (improvement of AMR cycle, new cycles), (iv) improved engineering designs.

REFERENCES

- J.A. Barclay and W.A. Steyert, Active magnetic regenerator, US Patent 4,332,135, June 1, 1982.
- G.V. Brown, Magnetic heat pumping near room temperature, *Journal of Applied Physics*, 47, 3673-3680, 1976.
- E. Brück, Developments in magnetocaloric refrigeration, *Journal of Physics D: Applied Physics*, 38, R381-R391, 2005.
- Chubu Electric Power Co. Inc., Development of room temperature magnetic refrigeration system – world leading performance a big step forward in achieving practical systems, Press Release, 7 November 2006.
(available at http://www.chuden.co.jp/english/corporate/press2006/1107_1.html)
- K.A. Gschneidner, Jr and V.K. Pecharsky, 30 years of near room temperature magnetic cooling, Keynote Lecture, 2nd International Conference on Magnetic Refrigeration at Room Temperature, Portoroz, Slovenia, 11-13 April, 2007.
- K.A. Gschneidner, Jr, V.K. Pecharsky and A.O. Tsokol, Recent developments in magnetocaloric materials, *Reports on Progress in Physics*, 68, 1479–1539, 2005.
- A. Kitanovski and P.W. Egolf, Thermodynamics of magnetic refrigeration, *International Journal of Refrigeration*, 29, 3-21, 2006.
- P. Li, M. Gong, G. Yao and J. Wu, A practical model for analysis of active magnetic regenerative refrigerators for room temperature applications, *International Journal of Refrigeration*, 29, 1259-1266, 2006.
- T. Okamura, K. Yamada, N. Hirano and S. Nagaya, Performance of room-temperature rotary magnetic refrigerator, *International Journal of Refrigeration*, 29, 1326-1331, 2006.
- T. Okamura, R. Rachi, N. Hirano and S. Nagaya, Improvement of 100 W class room temperature refrigerator, 2nd International Conference on Magnetic Refrigeration at Room Temperature, Portoroz, Slovenia, 11-13 April, 2007.
- V.K. Pecharsky and K.A. Gschneidner, Jr, Tunable magnetic regenerator alloys with a giant magnetocaloric effect for magnetic refrigeration from ~20 to ~290 K, *Applied Physics Letters*, 70 (24), 3299-3301, 16 June 1997.
- V.K. Pecharsky and K.A. Gschneidner, Jr, Magnetocaloric effect and magnetic refrigeration, *Journal of Magnetism and Magnetic Materials*, 200, 44-56, 1999.
- V.K. Pecharsky and K.A. Gschneidner, Jr, Advanced magnetocaloric materials: What does the future hold? *International Journal of Refrigeration*, 29, 1239-1249, 2006.

S.L. Russek and C.B. Zimm, Potential for cost effective magnetocaloric air conditioning systems, *International Journal of Refrigeration*, 29, 1366-1373, 2006.

B.F. Yu, Q. Gao, B. Zhang, X.Z. Meng and Z. Chen, Review on research of room temperature magnetic refrigeration, *International Journal of Refrigeration*, 26, 622-636, 2003.

N. Wilson, S. Ozcan, K. Sandeman and P. Burdett, Overview of magnetic refrigeration, Advance Proof, Presented before the Institute of Refrigeration, 11 January 2007.

C. Zimm, A. Boeder, J. Chell, A. Sterberg, A. Fujita, S. Fujieda and K. Fukamichi, Design and performance of a permanent-magnet rotary refrigerator, *International Journal of Refrigeration*, 29, 1302-1306, 2006.

4. STIRLING CYCLE REFRIGERATION

INTRODUCTION

Stirling cycle machines

The Stirling cycle cooler is a member of a family of closed-cycle regenerative thermal machines, including prime movers as well as heat pumps and refrigerators, known collectively as Stirling cycle machines. The Stirling cycle machine genus is named after Robert Stirling, a Scottish clergyman and the inventor of the Stirling engine, an improved hot air engine incorporating an “economiser” (now known as a regenerator) which he patented in 1816. John Herschel is attributed with making the proposal, in 1834, that a refrigerator could be operated on a reversed Stirling cycle. However, such a system was not practically realised until 1862 when Alexander Kirk built and patented a closed cycle refrigerator based on Stirling’s engine. His first machine reportedly ran for 10 years producing a temperature of -13°C . These early Stirling cycle machines used air as the working fluid.

Numerous designs of Stirling cycle machine exist but the following common elements can be identified:

- a closed system containing a fixed mass of gas. The enclosed working fluid flows in alternate directions between two interconnected gas spaces, at different temperatures, controlled by cyclic volume changes of the spaces.
- cyclic compression and expansion of the system by a piston-cylinder arrangement.
- a displacement arrangement to shuttle working fluid back and forth between the hot end and cold end gas spaces.
- a regenerator connecting the hot end and cold end gas spaces. The regenerator consists of a porous metal or fine wire matrix (e.g. woven wire gauze) and provides temporary thermal storage from one part of the cycle to another, substantially enhancing efficiency, by alternately absorbing and releasing heat as gas passes through it from the hot end and the cold end respectively.
- heat exchangers for transferring heat to and from the cycle.

Modern high-performance Stirling cycle machines use helium, or sometimes hydrogen, as the working gas because of their superior heat transfer properties (compared with air or nitrogen). Due to the normally low densities of these gases, power density is improved by charging the system gas spaces to high pressure, which in combination with the small molecule size of He and H_2 requires designs with special attention to leakage prevention. Although hydrogen is better from a thermodynamic efficiency viewpoint, helium is non-flammable and presents fewer material compatibility issues.

The various piston-cylinder and displacement arrangements employed in Stirling cycle machines fall into three types:

Alpha-type: The α -type has two pistons in separate cylinders connected by the hot and cold heat exchangers and the regenerator. The cylinders can be directly opposed, parallel or arranged in a V-formation. The pistons compress and expand the gas in the system as well as displacing it between the cylinders. There is no separate displacer.

Beta-type: The β -type has one piston and a separate displacer which operate in-line within the same cylinder. The displacer is a long, loosely fitting plug separating the hot end from the cold end of the cylinder and is normally hollow. Its function is to move (displace) gas between these two spaces via the regenerator and the heat exchangers – not to compress and expand the gas in the system. Consequently, there is just sufficient pressure difference across the displacer to overcome the loss in the regenerator and only minimal force is required to move it.

Gamma-type: The γ -type is also a piston-displacer type, similar to the β -type, but with the piston and displacer in separate cylinders.

Correct operation of a Stirling cycle machine relies on the movements of the piston and displacer (β -type and γ -type machines), or the two pistons (α -type machines), maintaining the proper phase relationship between the pressure oscillation in the system and the cyclical volume variations of the gas spaces. In this connection, Stirling cycle machines can be broadly categorized according to the means by which the reciprocating elements are moved, as follows:

Kinematic machines: The piston (or pistons) and the displacer (if used) are connected to the crankshaft of the machine by connecting rods and hence move in a fixed relationship creating the necessary variations in the gas space volumes. Mechanisms such as crossheads, the scotch yoke and the rhombic drive may be incorporated to eliminate piston side forces and hence reduce friction and wear.

Free-piston machines: The piston and displacer are not mechanically connected to a crankshaft, but supported by planar springs or gas springs. Work transfer at the piston is achieved by employing a linear alternator (in the case of a prime mover), or a linear motor (for a refrigerator or heat pump). The resulting motions of the piston and displacer and the thermodynamics of the system are strongly interrelated. The free-piston Stirling engine was invented in 1964 by William Beale at Ohio University who founded the Sunpower company in 1974. Subsequent development of free-piston technology has resulted in free-piston Stirling cryocoolers and refrigerators, and linear compressors.

Stirling cycle refrigeration

In any refrigeration cycle, including the reversed Stirling cycle, net work input is necessary in-line with the second law of thermodynamics. This is achieved by shuttling the gas in the system backwards and forwards between the hot end and cold end spaces so that the temperature of the system during compression is, on average, higher than during expansion. As a result the work done on the gas during compression is greater than the work done by the gas during expansion. Accordingly, the hot end and cold end gas spaces are also referred to as the compression space and the expansion space respectively.

Furthermore, for operation as a refrigerator, heat must be rejected via a heat exchanger at the hot end, and heat must be absorbed from the space to be cooled via a heat exchanger at the cold end.

The sequence of piston and displacer movements implemented in a Stirling refrigeration cycle is illustrated in Figure 4.1 for a β -type piston-displacer configuration. It must be emphasized that a practical Stirling cycle refrigerator does not follow the ideal reversed Stirling cycle, which comprises two isothermal processes, namely compression at T_h and

expansion at T_c , joined by two constant volume processes, and consequently its coefficient of performance must be less than for a reversed Carnot cycle operating between the same temperatures, given by $T_c/(T_h - T_c)$.

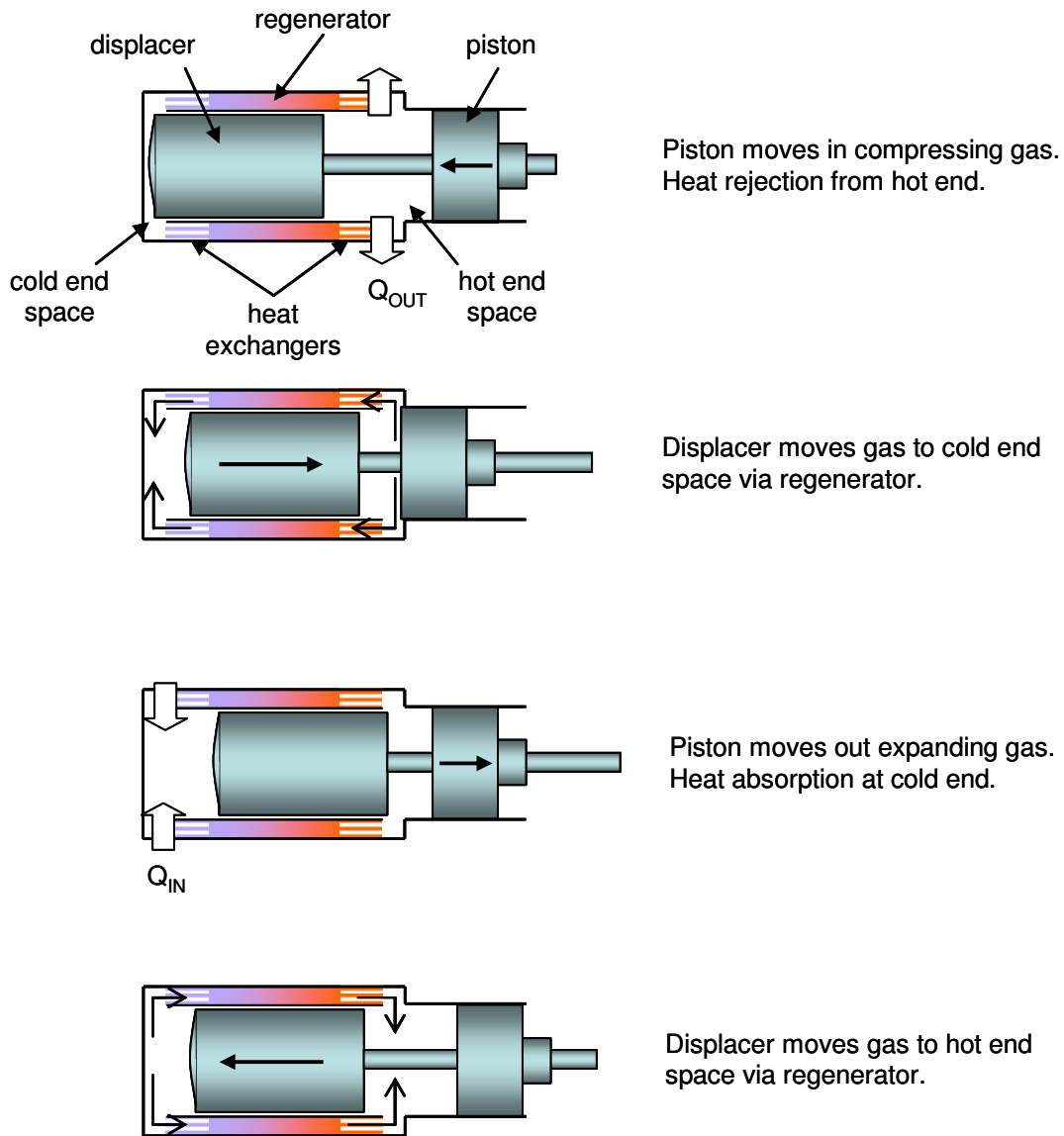


Figure 4.1 Piston and displacer movements during Stirling refrigeration cycle.

In the 20th century, advances in the exploitation of Stirling cycle technology for cooling effectively began in the 1940s when the Philips Company in Eindhoven commenced a separate research and development programme to produce cryogenic cooling machines for the liquefaction of air and other gases, based initially on their experience in the Stirling engine field. Philips introduced their first commercial Stirling cycle air liquefier in the mid-1950s and subsequently developed cryogenic equipment with a wide range of cooling capacities, establishing a leading position in the manufacture of Stirling cycle machines for cryogenic cooling and liquefied gas production.

As indicated above, the use of Stirling cycle cooling at cryogenic temperatures ($< 150\text{K}$) has been established for more than 50 years. However, at the higher temperatures encountered in conventional refrigeration applications very little attention was paid to Stirling cycle cooling until the 1990s. That position is now changing, principally because of the development of free-piston Stirling coolers as reflected by the coverage in the next section.

STIRLING CYCLE BASED REFRIGERATION SYSTEMS

Large cryogenerators

In 1990, the Philips cryogenics business was split off to form Stirling Cryogenics & Refrigeration BV, an independent company specializing in systems based on Stirling cycle cryogenerator technology for low temperature refrigeration and liquefaction, including fully-automatic stand-alone liquid gas production plants. The StirLIN range of liquid nitrogen plants, with production capacities ranging from 7 up to 150 litres per hour, is available for food industry applications where LN_2 is used in freezing tunnels to conserve high value products with high quality requirements. Figure 4.2 shows a basic plant flow diagram of the liquid nitrogen production process. The single-stage, closed-cycle Stirling process cryogenerators employed are shaft driven by an electric motor and of the piston-displacer type with either one or four cylinders. They are normally used for cooling in the range from 65 K to 200 K. The SPC-4 four-cylinder Stirling process cryogenerator is illustrated in Figure 4.3.

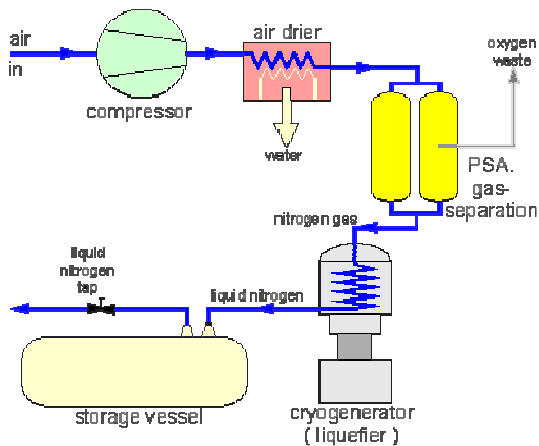


Figure 4.2 Liquid nitrogen production using a Stirling process cryogenerator (*Stirling Cryogenics & Refrigeration BV*)



Figure 4.3 SPC-4 four-cylinder Stirling process cryogenerator (*Stirling Cryogenics & Refrigeration BV*)

The variations of cooling capacity and electrical power consumption with cold head temperature for the SPC-4 unit given by the manufacturer are reproduced in Figure 4.4 and Figure 4.5 respectively. It can be deduced from these two graphs that the *COP* of the SPC-4 unit falls from approximately 0.72 at a cold head temperature of 250 K to about one-tenth of that value at 70 K. Similar values are obtained for the 1-cylinder unit.



Figure 4.4 Cooling capacity of SPC-4 Stirling process cryogenerator vs cold head temperature (*Stirling Cryogenics & Refrigeration BV*)



Figure 4.5 Power consumed by SPC-4 Stirling process cryogenerator vs cold head temperature (*Stirling Cryogenics & Refrigeration BV*)

Small cryocoolers

In addition to gas liquefaction, Stirling cycle cryogenic coolers are used for cooling sensors, instruments and specimens in a variety of research, industrial, commercial, military, aerospace, medical and pharmaceutical applications. Companies involved in the development and manufacture of small size Stirling cycle cryocoolers of free-piston-displacer design include Sunpower and Infinia (previously the Stirling Technology Company). For example, cryocoolers in Sunpower's CryoTel standard range have nominal cooling capacities ranging from 5 W to 15 W at 77 K for a heat rejection temperature of 35°C. The corresponding input powers range from 80 W to 240 W. Lane (2005) recently reported that, in sufficient volumes, Sunpower expect the unit price of these coolers to be lower than \$2000.

The modified Stirling cycle cryocoolers produced by the Cryomite company use both a compressor piston and an expander piston rather than a piston-displacer configuration. Cryomite lists transport refrigeration (for truck and container cargo preservation), supermarket food refrigeration, domestic refrigeration and food processing as examples of commercial applications. The most powerful cooler developed by Cryomite is the YODY transport trailer refrigeration system. This was demonstrated on a commercial unit and is claimed to be adaptable to refrigerated containers and railway freight wagons.

Free-piston Stirling cycle coolers

Global Cooling, a licensee of Sunpower, was set up in the mid-1990s to commercialize the free-piston Stirling cooler (FPSC) for applications above 150K, based on the technology originally developed by Sunpower. The company has a base in the Netherlands (Global Cooling BV) and development and manufacturing facilities in the USA (Global Cooling Manufacturing Co). Global Cooling licenses the technology to appliance manufacturers to commercialize and extend the range of FPSC based products. Applications listed by Global Cooling for the FPSC include small domestic and portable

refrigerators, mini-bars, ice cream makers, low-temperature food storage (below -50°C), vaccine storage and recreational vehicle use.

Global Cooling has developed FPSC units with nominal maximum cooling capacities of 40 W (model TB40) and 100 W (model M100). According to the company website models with higher cooling capacities, up to 300 W, are under development. Figure 4.6 shows a M100B unit that has a mass of 2.25 kg and an overall length of approximately 240 mm. The model illustrated has corrugated fins fitted to the hot end to assist forced convection heat rejection to air flowing through the surrounding casing. The cold head end of the cooler is at the extreme left hand side of Figure 4.6 where the copper band is located. For integration into a refrigeration application, an external heat exchanger, usually a thermosyphon or a pumped fluid loop, must be attached to the cold end of the cooler to enable heat to be transferred from the space or object being cooled.

Global Cooling FPSCs use helium as the working fluid which is pressurized, typically to 20 to 30 times atmospheric pressure, before the system is hermetically sealed. The high pressure helium also acts as a gas bearing between the piston and the cylinder wall ensuring non-contact operation, thus eliminating wear, extending component life and obviating the need for lubrication. In the FPSC the piston is driven by a moving magnet linear motor requiring an AC input. For portable applications, where only DC sources such as batteries or solar power may be available, conversion is necessary to provide the required AC input. It is a characteristic of FPSC operation that the piston amplitude, which determines the cooling capacity, is approximately proportional to the applied RMS voltage applied to the linear motor (see for example Kwon and Berchowitz, 2003). This allows for simple modulation of cooling capacity by stroke control in response to the error signal between the set and measured temperatures.

Furthermore, the current required to start a FPSC at very low amplitude is minimal due to the inherently low friction associated with the gas bearing feature. Figure 4.7 shows the performance map for the M100B unit with at a fixed heat rejection temperature of 30°C and cold head temperatures between 5°C and -50°C .

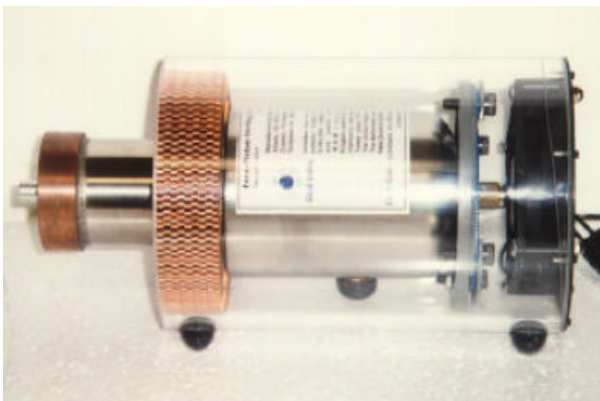


Figure 4.6 M100B free piston-Stirling cooler
(Global Cooling)

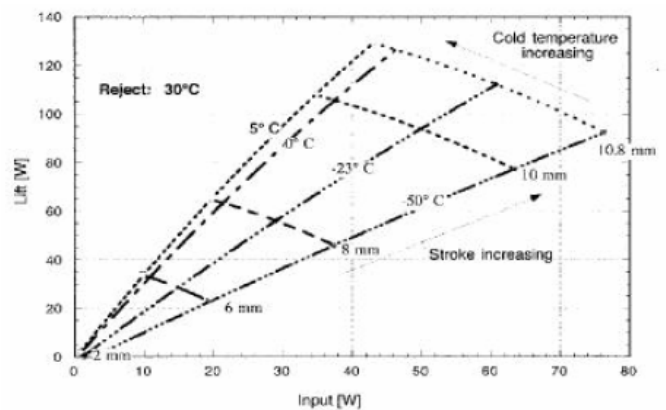


Figure 4.7 Performance map of the M100B at a fixed heat rejection temperature of 30°C and cold head temperatures between 5°C and -50°C .
(Global Cooling)

Kim et al (1997) of LG Electronics integrated a free-piston Stirling cooler (Global Cooling M100A) into a commercial 60 litre, single temperature, domestic chest freezer following removal of the compressor and condenser of the original vapour compression circuit. The tube-and-plate evaporator in the freezer cabinet was retained and connected to the cold end heat exchanger on the FPSC to form a secondary coolant circuit. This loop was filled with ethanol and fitted with a recirculation pump. Heat was rejected to ambient via a fan-cooled heat sink with corrugated copper fins brazed on the warm end of the FPSC. Testing was carried out for a cabinet interior temperature of -20°C at an ambient temperature of 20°C . In comparison with the vapour compression system the FPSC freezer required slightly longer to pull down the freezer temperature and generated a higher noise level (60 dBA compared with 55 dBA). At steady-state, however, the FPSC set up consumed over 20% less energy (including the pump and fan requirements): $0.689\text{ kWh}/24\text{ h}$ compared to $0.869\text{ kWh}/24\text{ h}$. Furthermore, a coefficient of performance of 1.04 was determined for the FPSC, significantly below the value of 1.4 quoted by the manufacturer for the same cold end and warm end temperatures.

Kim et al (1997) concluded that the free-piston Stirling cycle cooler has good potential for the refrigeration applications and the development of increased cooling capacity, more effective secondary heat transfer systems and better insulation would assist earlier commercialization. The authors highlighted freezer applications as an application area where the FPSC would have several advantages over the vapour compression cycle, including its large range of temperature, good efficiency and ability to modulate the cooling capacity over a wide range.

Berchowitz (1998) reported measured values of *COP* for a 100 W free-piston Stirling cooler of between 2.61 (with cold and warm head temperatures of -2.1°C and 32.1°C respectively) and 3.06 (with cold and warm head temperatures of 2.4°C and 30.3°C respectively).

Figure 4.8 shows a small free-piston Stirling cooler of 40 W capacity, developed by Global Cooling for use in portable refrigerators (Berchowitz et al,1999).

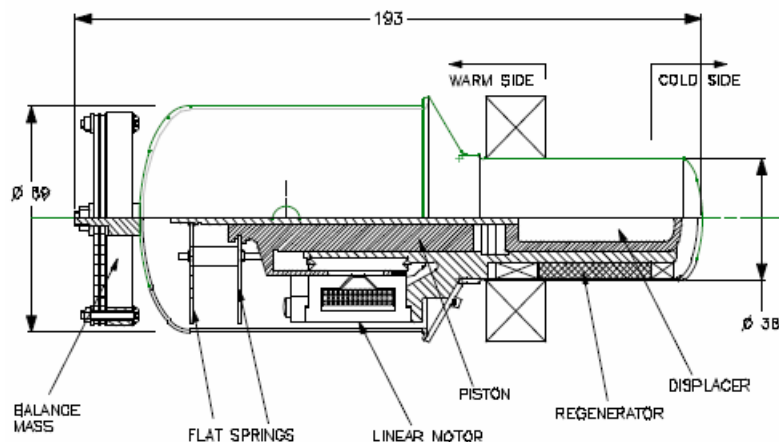


Figure 4.8 40 W free-piston Stirling cooler prototype (from Berchowitz et al, 1999)

For testing, the prototype FPSC was integrated with a 40 litre cabinet. A simple two-phase thermosyphon loop, constructed from 3 mm bore copper tubing, incorporated an evaporator section around the cabinet walls and a condenser section wrapped around the cold head of the FPSC, as depicted in Figure 4.9. Carbon dioxide was used as the heat exchange fluid. Fins were fitted on the warm side surface of the FPSC for heat rejection.

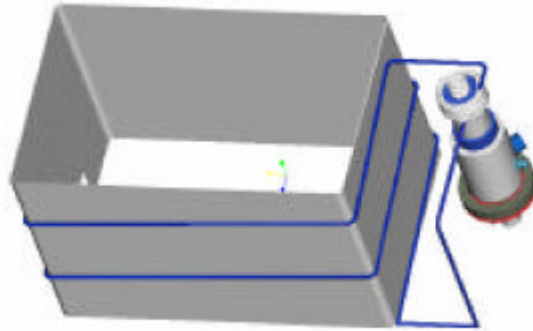


Figure 4.9 Integration of 40 W free-piston Stirling cooler prototype with small refrigerator cabinet using thermosyphon (from Berchowitz *et al*, 1999)

The tests covered both frozen food and fresh food conditions. Initial results presented by Berchowitz *et al* (1999) show coefficients of performance ranging from 0.939, with temperatures of -22°C and 35.6°C on the cold and warm sides of the FPSC, to 1.65 for corresponding temperatures of -1.4°C and 30.3°C .

Oguz and Ozkadi (2000) investigated the performance characteristics of two prototype free-piston Stirling coolers (#1 and #2) from Global Cooling for cold head temperatures ranging from about -40°C to 0°C . The warm head temperature was kept around 30°C but varied slightly (i.e. 28 to 31°C). In the experimental set up the heat load on the cooler was simulated by electrical resistance heaters mounted on the cold head, which was enclosed in a heavily insulated box. Water cooling was applied to the warm (heat rejection) head. The results obtained for refrigeration capacity and coefficient of performance are shown in Figure 4.10 and Figure 4.11 respectively, where the voltages shown as a parameter in the legends refer to the FPSC input voltage.

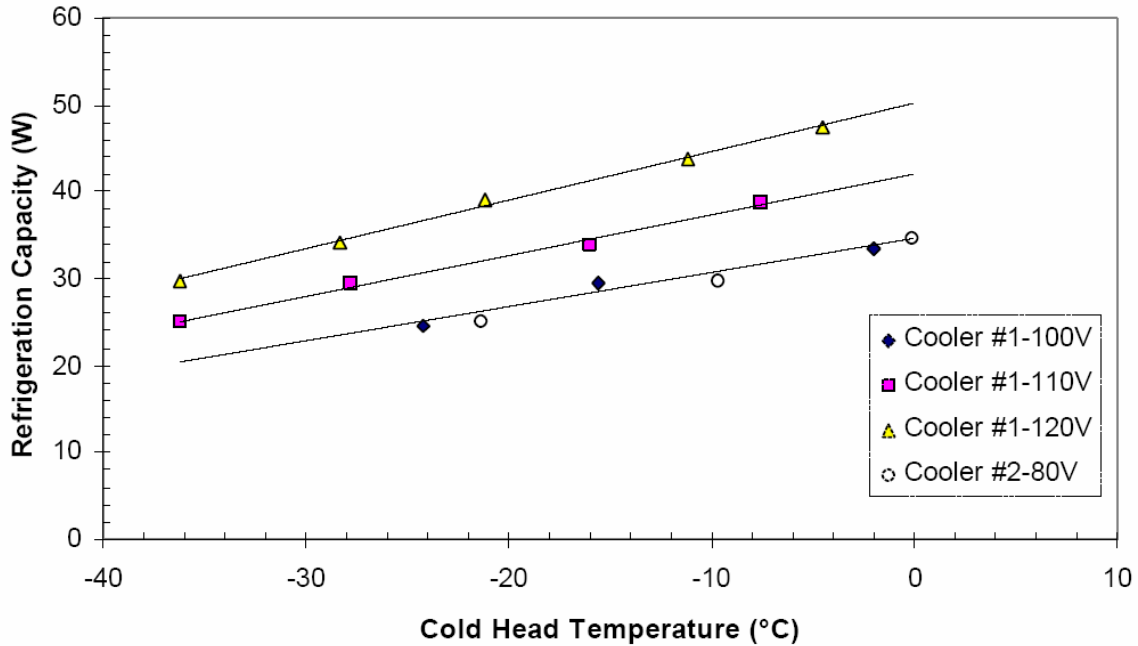


Figure 4.10 Refrigeration capacities of two prototype free-piston Stirling coolers; warm head temperature $\approx 30^{\circ}\text{C}$ (from Oguz and Ozkadi, 2000)

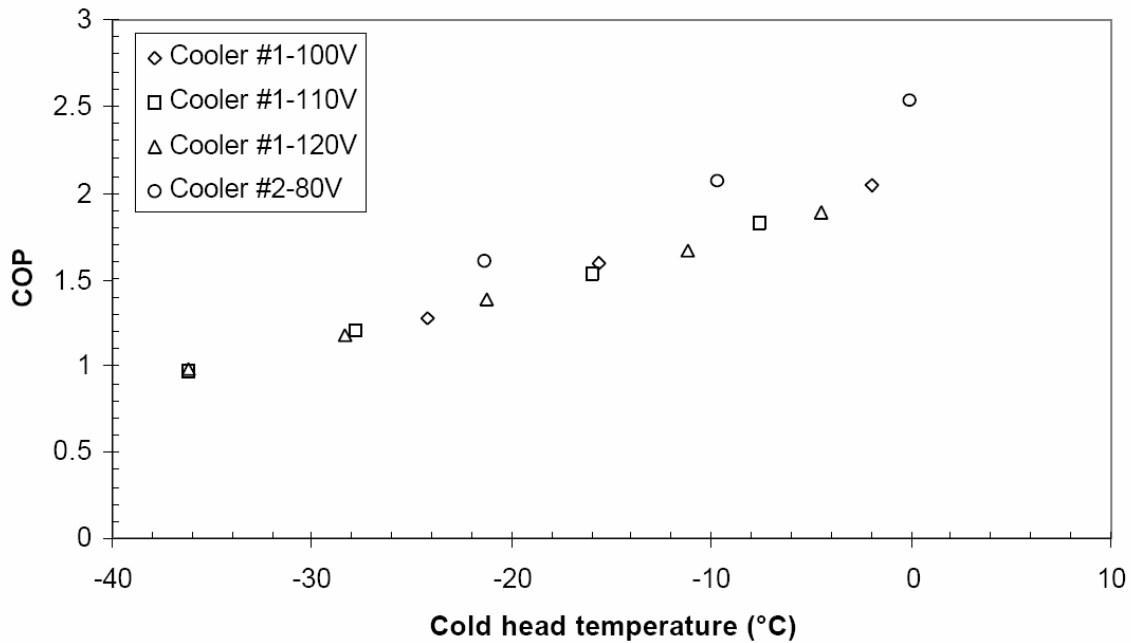


Figure 4.11 Coefficients of performance for two prototype free-piston Stirling coolers; warm head temperature $\approx 30^{\circ}\text{C}$ (from Oguz and Ozkadi, 2000)

A joint presentation by Sharp Corporation and Fuji Electric Company (2004), prepared for the Refrigerants, Naturally! technical conference held in Brussels in June 2004, shows the application of a FPSC to an 18 selection beverage can vending machine as illustrated in Figure 4.12.

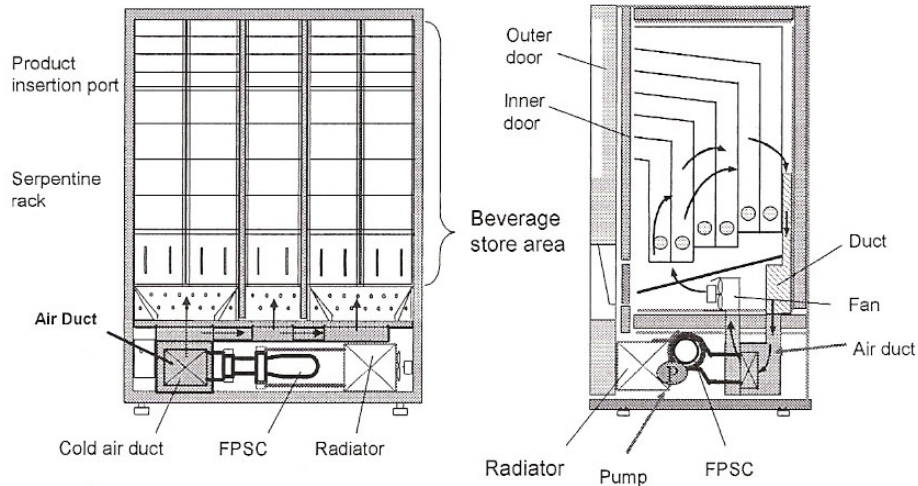


Figure 4.12 FPSC vending machine (*Sharp Corp/Fuji Electric, 2004*)

FPSC based products

The purpose of this section is to present examples of commercial products based on the free-piston Stirling cooler (FPSC) technology.

Figure 4.13 shows the SC-TD08 80 W Stirling Cooler manufactured by the Twinbird Corporation in Japan under licence from Global Cooling BV. This model can be used for applications down to -80°C and uses $90\text{ W}\pm 20\text{ W}$ of power from a 24 V DC supply. The FPSC is fitted with heat rejection fins and is supplied with a drive PCB (also shown in Figure 4.13) incorporating the cooling modulation circuit. The cooler has an approximate mass of 2.5 kg and overall dimensions of 130 mm diameter (max) x 280 mm high. Twinbird also assemble the FPSC and PCB described above into a casing with an exhaust cooling fan as the SC-UD08 80 W free-piston Stirling cooler module which is illustrated in Figure 4.14. The module assembly has an approximate mass of 3.5 kg and is 175 mm wide x 195 mm deep x 288 mm high.



Figure 4.13 SC-TD08 80 W Stirling Cooler (*Twinbird Corporation*)



Figure 4.14 SC-UD08 80 W FPSC module (*Twinbird Corporation*)

The cooling performance of the above FPSC units measured by Twinbird is shown in Figure 4.15. At an ambient temperature of 25°C, the cooling capacity is about 60 W at a cold head temperature of -23.3°C, and about 25 W at a cold head temperature of -80°C. Less powerful models of the above products, giving more than 35 W of cooling at a cold side temperature of -23.3°C and an ambient temperature of 25°C, are available from Twinbird.

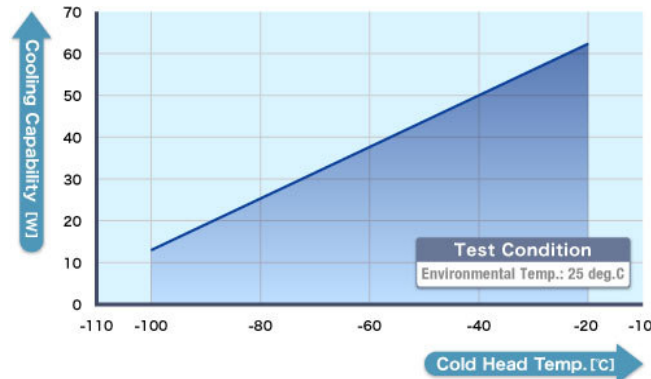


Figure 4.15 Cooling capacity versus cold head temperature for SC-TD08 80 W and SC-UD08 80 W module (Twinbird Corporation)

Twinbird Corporation also manufactures cool boxes utilizing FPSC technology. The SC-DF25 Deep Freezer shown in Figure 4.16 has a 25 litre capacity and its construction features vacuum insulation panels. The interior temperature can be set at 1°C intervals from 10°C down to a minimum of -40°C (at an ambient temperature of 25°C). The freezer box runs from a 12 V DC supply and consumes approximately 48 W.



Figure 4.16 25 litre capacity SC-DF25 Deep Freezer box (Twinbird Corporation)

Other 25 litre capacity cool boxes manufactured by Twinbird include the standard SC-C925 model, providing five set interior temperatures from 10°C down to -18°C, and a special model with a set interior temperature of 4°C ±2°C for transporting blood cargo. In addition, Twinbird has announced (in April 2007) that it is developing “Cool Cargo” boxes with much larger capacities and an interior temperature of -18°C for transporting

and/or preserving products such as pharmaceutical/medical goods and industrial/scientific products. It is further noted that under the terms of their license agreement with Global Cooling restrictions apply to the fields of use, manufacture and sale of FPSC based products manufactured by Twinbird. Specifically, all applications in the fields of refrigeration, preservation and transport of food, beverages and water are prohibited with the exception of outdoor leisure use with cooling capacities up to 50 W, and the following specific applications with cooling capacities up to 50 W: portable cool box, minibar refrigerator for hotel use, watercooler and wine cellar.

In the USA, two companies linked with Global Cooling, the outdoor company Coleman and the marine refrigeration specialist AvXcel, market 25 litre capacity FPSC cool boxes for temperatures down to -18°C (almost identical in appearance to the Twinbird standard SC-C925 model) for a retail price around \$600.

AvXcel also offer the TropiKool 40 system shown in Figure 4.17 for the marine refrigeration market. The system is rated to maintain a temperature below -45°C in a 170 litre insulated cabinet and comprises a free-piston Stirling cooler (apparently a Twinbird FPSC unit) fitted with a cooling fan and heat rejection fins, an electronic cooling capacity modulation unit and thermosyphon components, including a microchannel evaporator panel for installation in the cooled space and a condensing jacket for fitting to the cold head of the FPSC. Carbon dioxide is used as the heat transfer fluid in the two-phase thermosyphon circuit. The TropiKool system is advertised for sale at \$2200.

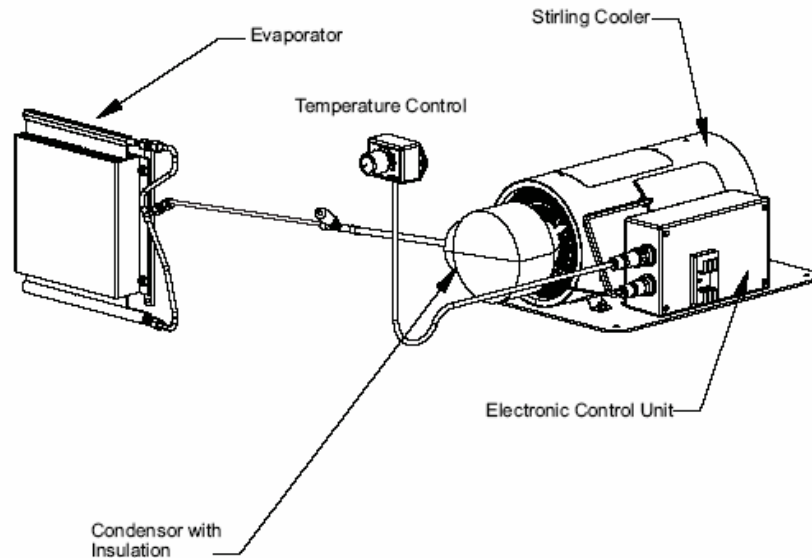


Figure 4.17 TropiKool 40 system with free-Stirling cooler and cold-side CO_2 thermosyphon (AvXcel)

Other Stirling cycle refrigeration research

Green et al (1996) report on the testing of a 'proof of concept' Stirling cycle cooled domestic freezer jointly developed by Oxford University and EA Technology, Capenhurst. The freezer was designed to provide a cooling duty of 60 W and a cabinet

temperature of -20°C at an ambient temperature of 25°C with a target COP of 0.95. The Stirling cycle cooler used, shown in Figure 4.18, was developed by Oxford University and features a linear motor driven piston with the displacer in a separate cylinder (γ -type configuration). Both the compressor piston and displacer are supported on spiral disk springs.

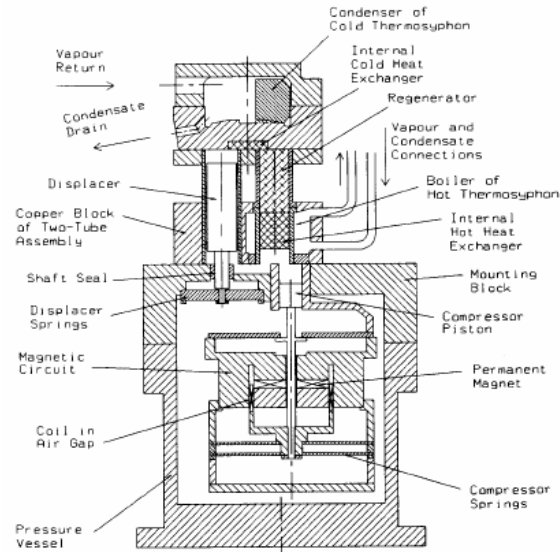


Figure 4.18 Stirling cycle cooler developed at Oxford University (from Green et al, 1996)

The Stirling cooler was fitted to a standard under-worktop, frost-free freezer of 80 litre nominal storage capacity. The original forced convection evaporator in the freezer cabinet was retained but a more efficient air recirculation fan was fitted. The evaporator was connected to the cold end of the cooler by a two-phase thermosyphon loop filled with isobutane (vapour pressure 3.7 bar at 25°C and 0.5 bar at the working temperature of -30°C). On the heat rejection side, the original wire-on-tube natural convection cooled condenser was replaced by a similar type with larger diameter tubes. The condenser was connected to the hot end of the cooler unit to form a second two-phase thermosyphon loop filled with sub-atmospheric water.

Tests on the Stirling cycle cooled freezer at the design condition (-20°C cabinet interior, 25°C ambient) showed a 17% reduction in energy consumption (including fan power and defrost energy) compared with the original vapour compression system (1.48 kWh/24h compared to 1.8 kWh/24h). Even when the effects of the more efficient fan and the different defrost interval were taken into account the energy saving was still 12%. A coefficient of performance of 0.9 was determined based on an estimate of the heat leakage rate into the cabinet. However, separate tests on an instrumented cooler unit, allowing accurate determination of the cooling capacity, gave a COP of just over 1.0 under similar temperature conditions.

Green et al (1976) conducted further tests on the instrumented cooler in an environmental chamber, at both full and reduced power, with constant hot and cold end temperatures of 55°C and -25°C and an environmental temperature of 32°C (corresponding to

CECOMAF conditions for standard rating of refrigerant compressors). As the cooling duty was decreased, the Stirling cooler demonstrated significant energy savings, and correspondingly higher (up to 80%) part-load *COP* values, compared with small appropriately rated vapour compression systems. This result was regarded as being especially important in view of the trend towards the improved insulation of refrigerator cabinets.

CONCLUDING REMARKS

- A review of Stirling cycle refrigeration has identified two main types of equipment of relevance to food refrigeration applications: (i) Stirling cycle process cryogenerators, and (ii) free-piston Stirling coolers.
- Cryogenerators: An established technology, originally developed by Philips, now produced by Stirling Cryogenics & Refrigeration BV. Process cryogenerators are single-stage, closed-cycle, water-cooled, shaft-driven (kinematic) Stirling refrigeration machines of the piston-displacer type. Available in 1- and 4-cylinder versions for process cooling of a liquid or a gas in the temperature range 65-200 K, including liquefaction. Process cryogenerators are the central component in stand-alone liquid nitrogen production plants (capacities up to 150 litre/h) used to supply LN₂ to tunnels used in the food industry for freezing high value products with high quality requirements. Coefficient of performance falls with cold head temperature from approximately 0.72 at 250 K to about one-tenth of that value at 70 K.
Stirling Cryogenics & Refrigeration BV (<http://www.stirling.nl>)
- Free-piston Stirling coolers: This relatively recent development of free-piston technology, originated at Sunpower, for cooling applications above 150 K is now led by Global Cooling. FPSCs are compact, helium filled (to 20-30 atm), hermetically sealed Stirling refrigeration machines of the piston-displacer type, the piston being driven by a moving magnet linear motor. Heat exchangers must be attached to the cold and warm heads of the FPSC unit to facilitate heat absorption and heat rejection respectively. FPSC units with nominal maximum cooling capacities of 40 W and 100 W have been produced, with larger capacity units, up to 300 W, reported to be under development. FPSCs have been evaluated experimentally by Global Cooling and appliance manufacturers for application to domestic and portable refrigerators and freezers as well as a beverage can vending machine. FPSC based products, including freezer boxes and a system for the marine refrigeration market, have been developed by licensees. Coefficients of performance measured for FPSCs with warm head temperatures close to 30°C vary with the cold head temperature. Values of *COP* between 2 and 3 have been reported for cold head temperatures around 0°C, and values around 1 for cold head temperatures approaching -40°C.
Global Cooling (<http://www.globalcooling.nl>; <http://www.globalcooling.com>)

REFERENCES

D.M. Berchowitz, Maximised performance of Stirling cycle refrigerators, IIR conference, Oslo, Norway, 1998.

D.M. Berchowitz, J. McEntee and S. Welty, Design and testing of a 40 W free-piston Stirling cycle cooling unit, 20th Int. Congress on Refrigeration, Sydney, 1999.

R.H. Green, P.B. Bailey, L. Roberts and G. Davey, The design and testing of a Stirling cycle domestic freezer, IIR conference, 2nd Int. Conf. on the Use of Non-Artificial Substances, Aarhus, Denmark, 1996.

S-Y Kim, W-S Chung, D-K Shin and K-S Cho, The application of Stirling cooler to refrigeration, IECEC-97, Proc 32nd Intersociety Energy Conversion Engineering Conf., Honolulu, Hawaii, 27 July–1 August, 1997, Vol. 2, 1023-1026.

Y-R Kwon and D.M. Berchowitz, Operational characteristics of Stirling machinery, International Congress of Refrigeration, Washington, D.C., 2003.

N.W. Lane, Commercialization status of free-piston Stirling machines, 12th International Stirling Engine Conference, Durham, UK, September 2005.

E. Oguz and F. Ozkadi, An experimental study on the refrigeration capacity and thermal performance of free-piston Stirling coolers, Proc. 8th Int. Refrigeration Conf., Purdue University, West Lafayette, Indiana, USA, 497-504, 2000.

Sharp Corporation/Fuji Electric Company, Vending machine using FPSC, Presented at Refrigerants, Naturally! Technical Conference, Brussels, June 2004. (available at <http://www.refrigerantsnaturally.com/june-2004.php>).

5. THERMOELECTRIC REFRIGERATION

INTRODUCTION

Peltier effect

Thermoelectric cooling devices utilise the Peltier effect, whereby the passage of a direct electric current through the junction of two dissimilar conducting materials causes the junction to either cool down (absorbing heat) or warm up (rejecting heat), depending on the direction of the current.

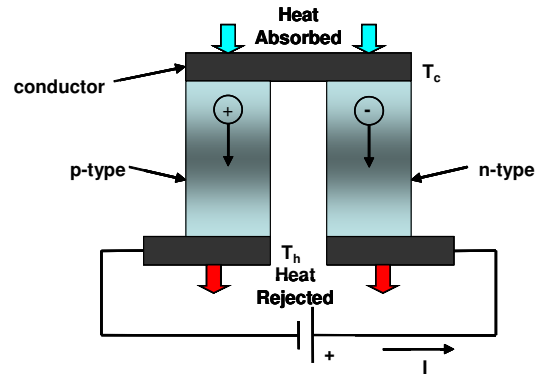


Figure 5.1 Thermoelectric cooling (or Peltier) couple

Figure 5.1 shows a pair of adjacent thermoelement legs joined at one end by a conducting metal strip forming a junction between the legs. Thus, the legs are connected in series electrically but act in parallel thermally. This unit is referred to as a thermoelectric couple and is the basic building block of a thermoelectric (or Peltier) cooling module. The thermoelement materials are doped semiconductors, one n-type with a majority of negative charge carriers (electrons) and the other p-type with a majority of positive charge carriers (holes). The majority of commercially available thermoelectric cooling modules are assembled from n-type and p-type thermoelements cut from bismuth telluride (Bi_2Te_3) based bulk materials.

A thermoelectric couple can be regarded as a solid state heat pump. When a direct current I passes through the junction, from the n-type material to the p-type material, the majority charge carriers in both materials flow, and transport energy, away from the junction. As a result the junction cools to a temperature T_c and absorbs heat from the cold source to maintain conservation of energy and charge. The energy pumped from the low temperature side by the electrons and holes produces a temperature rise at the opposite ends of the thermoelements, establishing hot junctions at T_h , where heat is rejected to the sink.

The Peltier coefficient is defined as the ratio of the rate of heat absorption by the cold junction to the electric current, or $\pi_{np} = \dot{Q}/I$, and has units of watts per ampere (or volts). It should be noted that changing the polarity of the d.c. power source, so that the electric current flows in the opposite direction, also reverses the direction of heat pumping and the junction temperatures.

Mention should also be made of the Seebeck effect which is the reverse of the Peltier effect. If instead of passing a current through the thermoelectric couple, as shown in Figure 5.1, a temperature difference $\Delta T = (T_h - T_c)$ is imposed between the ends of the thermoelements then an open-circuit voltage V is generated. This is the Seebeck voltage familiar from thermocouple temperature measurement but also exploited as the basis for thermoelectric power generation. The ratio of the V and ΔT defines the Seebeck coefficient of the thermoelectric couple, $\alpha_{np} = V/\Delta T$, which has units of V/K.

The Peltier and Seebeck coefficients of a thermoelectric couple are related by

$$\pi_{np} = \alpha_{np} T$$

5.1

where T is the absolute temperature of the junction.

Performance of a thermoelectric refrigerator

The cooling performance of a thermoelectric refrigerator is expressed in terms of its cooling capacity and coefficient of performance. In the simplified theory of a thermoelectric module, available in standard books on thermoelectrics (Rowe and Bhandari, 1983; Rowe, 2006), the relationships presented below are derived under the following assumptions[†]:

- electrical contact resistances at the thermoelement-conductor junctions can be neglected;
- thermal resistances at the hot and cold sides of the thermoelectric couple can be neglected;
- temperature-averaged values of thermal conductivity, electrical resistivity and Seebeck coefficient can be employed for the thermoelement leg materials.

(i) Rate of heat absorption from the cold source, \dot{Q}_c

In the absence of heat conduction from the hot junctions and ohmic heating of the thermoelements, \dot{Q}_c would simply equal the Peltier cooling effect at the cold junction given by $\pi_{np}I$. Taking account of these two irreversible effects, which act in opposition to the Peltier heat pumping, and using Equation 5.1, it can be shown that the actual rate of heat absorption by a single thermoelectric couple, as depicted in Figure 5.1, is given by

$$\dot{Q}_c = \alpha_{np} T_c I - K(T_h - T_c) - \frac{1}{2} I^2 R$$

5.2

where R is the electrical resistance of the thermoelement pair in series and K is the thermal conductance of the thermoelement pair in parallel. For a Peltier cooling module containing multiple thermoelectric couples Equation 5.2 must be multiplied by the number of couples.

[†] A third thermoelectric effect, the Thompson effect, responsible for heating or cooling when a current flows along a conductor with temperature gradient, is neglected here.

The RHS of Equation 5.2 shows that the Peltier cooling effect is proportional to the current I , whereas ohmic heating is proportional to I^2 . As I is increased, with fixed values of T_h and T_c , the net rate of cooling \dot{Q}_c increases initially, reaching a maximum when the rate of increase due to the Peltier effect is balanced by the rate of reduction due to the other two terms. Differentiating Equation 5.2 and setting the result to zero shows that this maximum occurs when the current is equal to $\alpha_{np}T_c/R$. Any further increase in the current would produce faster growth of ohmic heating, causing a decrease in \dot{Q}_c . Alternatively, keeping the current fixed and increasing the temperature difference between the hot and cold junctions, $(T_h - T_c)$, thereby increasing heat conduction towards the cold junction, produces a steady decrease in \dot{Q}_c . This eventually leads to zero net cooling ($\dot{Q}_c = 0$) at the cold junction when the Peltier cooling is equalled by the combination of ohmic heating and heat conduction. The corresponding maximum theoretical temperature difference $\Delta T_{max} = (T_h - T_c)_{max}$ that can be achieved by a thermoelectric couple occurs for $\dot{Q}_c = 0$ and $I = I_{max} = \alpha_{np}T_c/R$ (see above), where I_{max} denotes the current resulting in the greatest value of ΔT ($= \Delta T_{max}$). Substitution in Equation 5.2 gives

$$\Delta T_{max} = \frac{1}{2} \left(\frac{\alpha_{np}^2}{RK} \right) T_c^2 = \frac{1}{2} Z_{np} T_c^2$$

5.3

where Z_{np} is defined as the figure of merit of the thermoelectric couple. At the other extreme the maximum rate of cooling $\dot{Q}_{c,max}$ occurs when $\Delta T = 0$ and $I = I_{max}$.

(ii) Coefficient of performance, COP

This is equal to the rate of heat absorption, given by Equation 5.2, divided by the electrical power input \dot{W}_e consumed in ohmic heating of the thermoelements and balancing the Seebeck effect generated by the temperature difference $\Delta T = (T_h - T_c)$ between the junctions. Hence, in general COP is given by

$$COP = \frac{\dot{Q}_c}{\dot{W}_e} = \frac{\alpha_{np}T_c I - K(T_h - T_c) - I^2 R / 2}{\alpha_{np} \Delta T I + I^2 R}$$

5.4

Equation 5.4 shows that for a given thermoelectric couple with specific dimensions and physical properties, and fixed values of T_h and T_c , the coefficient of performance depends only on the current I . Using $\partial(COP)/\partial I = 0$ to obtain an expression for the current at maximum COP leads to the following result:

$$COP_{max} = \left(\frac{T_c}{\Delta T} \right) \left[\frac{(1 + Z_{np} T_m)^{1/2} - T_h / T_c}{(1 + Z_{np} T_m)^{1/2} + 1} \right]$$

5.5

where $T_m = (T_h + T_c)/2$. The maximum possible COP, for given T_h and T_c , is therefore equal to the coefficient of performance of a reversed Carnot cycle working between the same temperatures multiplied by the expression in square brackets which is clearly always less than 1. It should be noted that, for given values of T_h and T_c , COP_{max} occurs at an input current lower than that for maximum cooling capacity.

Equation 5.3 and Equation 5.5 show that both ΔT_{max} and COP_{max} depend on, and increase with, the figure of merit of the thermoelectric couple $Z_{np} = \alpha_{np}^2 / (RK) = (\alpha_p - \alpha_n)^2 / (RK)$, where R and K are determined by the dimensions and properties of the thermoelements. However, the magnitudes of the Seebeck coefficients, thermal conductivities and electrical resistivities of the n-type material and the p-type material are approximately equal in practice, although of opposite sign in the case of the Seebeck coefficients. It follows that Z_{np} can be replaced in the above equations by the figure of merit of the thermoelectric material Z defined by

$$Z = \frac{\alpha^2}{\rho k}$$

5.6

where α , ρ and k are the Seebeck coefficient, electrical resistivity and thermal conductivity of the thermoelectric material respectively. The units of Z (as defined in Equation 5.6) are K^{-1} , and consequently a dimensionless figure of merit ZT , where T is the absolute temperature, is often used to characterize thermoelectric materials. For the Bi_2Te_3 -based bulk materials used in commercial Peltier modules a figure of merit of $Z = 2.8 \times 10^{-3} K^{-1}$ is frequently used (e.g. Min and Rowe, 2000), corresponding to a dimensionless figure of merit $ZT = 0.84$ at $T = 300 K$.

Figure 5.2 shows how COP_{max} , given by Equation 5.5, varies with the temperature difference between the hot and cold sides for several values of the thermoelectric material figure of merit. The hot-side temperature of the thermoelements T_h is fixed as 300 K. Choosing a specific condition for comparison purposes, it is noted that the value of COP_{max} given by Equation 5.5 is just less than 1 for $\Delta T = 30 K$ and $Z = 2.8 \times 10^{-3} K^{-1}$. Putting this COP_{max} value in context, it is approximately 10% of the coefficient of performance for a reversed Carnot cycle operating between the same temperatures, whereas a conventional domestic refrigerator may achieve 30% of the reversed Carnot cycle efficiency (DiSalvo, 1999). For a thermoelectric refrigerator to achieve a comparable performance the thermoelectric material would need to have a Z value of approximately $0.01 K^{-1}$, i.e. approximately four times the current value obtained with Bi_2Te_3 -based materials.

It is evident from Figure 5.2 that it is desirable for the figure of merit of a thermoelectric material to be as high as possible to maximise the coefficient of performance for given temperatures. According to Goldsmid (2006) and DiSalvo (1999) the best available semiconductor materials for thermoelectric cooling near room temperature have a value of ZT equal to about 1, a figure that has not improved significantly over the 50 years since these materials were developed. Current research on thermoelectric materials is aimed at improving the figure of merit by reducing the lattice thermal conductivity and is concentrated in two areas: (i) finding new compounds exhibiting phonon glass-electronic crystal characteristics with favourable properties, and (ii) producing thermoelectric materials using low dimensional structures (quantum wells, quantum wires, quantum dots and superlattices). Brief summaries of the main approaches are given by Stockholm (1997), Riffat and Ma (2004) and Rowe (2006). A collection of recent in-depth reviews of specialist topics in thermoelectric materials research can be found in the CRC Thermoelectrics Handbook (2006).

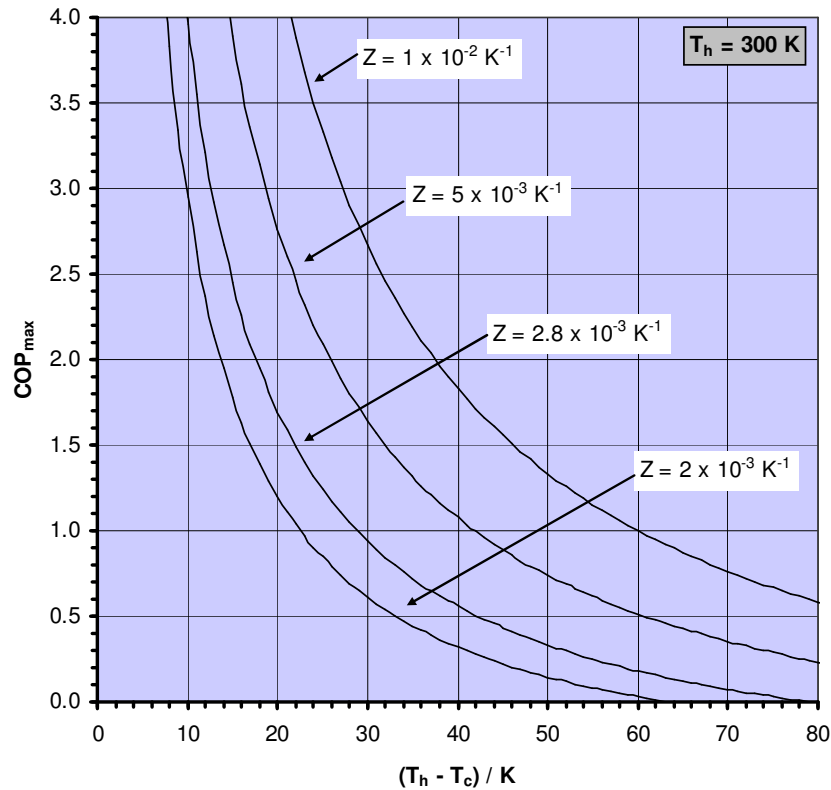


Figure 5.2 Maximum theoretical COP for a thermoelectric cooling module versus temperature difference for different values of the thermoelectric material figure of merit ($T_h = 300\text{ K}$)

The simplified theory of the thermoelectric refrigerator set out above assumes that electrical contact resistances at the hot and cold junctions can be neglected in comparison with the series resistance of the thermoelement legs. Furthermore, thermal resistances associated with substrate layers at the hot and cold sides of a thermoelectric module, and their associated temperature differences, are ignored. Nevertheless, the simplified model is considered to provide a reasonably adequate basis for modelling the behaviour of a thermoelectric cooling module if the thermoelements are relatively long. Using an improved model Min and Rowe (2000) demonstrated that the effect of the thermal and electrical contact resistances on the maximum coefficient of performance and the maximum heat pumping capacity becomes increasingly significant as the thermoelement length is reduced. In addition to the thermoelement length, the more realistic model employs three other parameters as follows: $n = 2\rho_c/\rho$, where ρ_c is the electrical contact resistivity, l_c the thickness of the substrate layers and $r = k/k_c$, where k_c is the thermal conductivity of the substrate layers. For a typical commercial thermoelement length of 1.5 mm, at $\Delta T = 30\text{ K}$ with $Z = 2.8 \times 10^{-3}\text{ K}^{-1}$, $n = 0.1\text{ mm}$, $l_c = 0.7\text{ mm}$ and $r = 0.20$ the value of COP_{max} calculated using the improved model is about 30% below that found using the simplified model.

Commercially available thermoelectric modules

The construction of a typical single-stage commercial thermoelectric cooling module is shown in Figure 5.3.

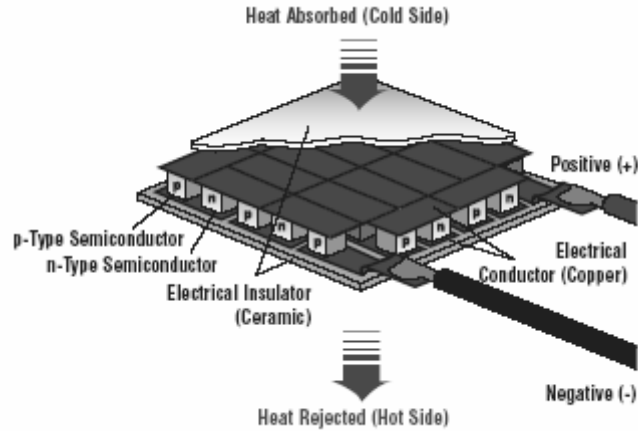


Figure 5.3 Construction of a typical thermoelectric (or Peltier) cooling module
(from *Melcor Thermoelectric Handbook*)

The semiconductor thermoelements (or ‘pellets’) are arranged in an array with alternate n-type and p-type elements and joined end-to-end by copper conductors to form a chain of thermoelectric couples. This assembly is sandwiched between electrically insulating ceramic substrates (usually ~ 0.6 mm thick alumina, Al_2O_3) that conduct heat being absorbed and rejected through the module faces, provide mechanical strength and have thermal expansion compatibility with the copper conductors.

Thermoelectric modules are available commercially to suit a wide range of small and medium cooling duties. Manufacturers’ lists include single-stage modules with maximum cooling capacities from less than one watt to 186 W. Module sizes vary from just a few millimetres square up to 62 mm x 62 mm and the number of thermoelectric couples N in a module from less than ten to 195. Maximum heat flux densities are mostly in the range 2-6 W/cm^2 but individual modules with up to 9 W/cm^2 are available. The maximum module size is limited by the stresses placed on the thermoelements and solder joints by differential thermal expansion between the hot and cold sides. Module thicknesses are normally between 2 mm and 6 mm.

Figure 5.4 shows an extract from the Melcor company literature giving information for the CP Series of standard single-stage modules. The physical dimensions and number of couples are listed for each module together with the following parameters for a fixed hot-side temperature of 25°C:

- ΔT_{max} maximum achievable temperature difference between the hot and cold sides (occurs at $I = I_{max}$, $\dot{Q}_c = 0$)
- I_{max} input current resulting in greatest ΔT ($= \Delta T_{max}$) at $\dot{Q}_c = 0$
- $\dot{Q}_{c,max}$ maximum cooling capacity (occurs at $I = I_{max}$, $\Delta T = 0$)
- V_{max} d.c. input voltage at ΔT_{max}

Other manufacturers and suppliers of thermoelectric cooling modules provide similar information. Module performance curves (in various formats) or software may also be

available for determining the relationships between \dot{Q}_c , ΔT , I and V for one or more hot-side temperatures to assist with module selection and system design. For example, Figure 5.5 shows performance curves for a Marlow Industries single stage module (model DT12-8) with nominal dimensions: 40 mm x 40 mm x 3.5 mm thick. The module provides a maximum cooling capacity $\dot{Q}_{c,max}$ (at $\Delta T = 0$) of 71 W at $T_h = 27^\circ\text{C}$ and 78 W at $T_h = 50^\circ\text{C}$. The maximum achievable temperature difference ΔT_{max} (at $\dot{Q}_c = 0$) is 66 K at $T_h = 27^\circ\text{C}$ and 74 K at $T_h = 50^\circ\text{C}$. The corresponding current I_{max} corresponding to these rated conditions is given as 7.4 A.

Catalog Number	Th = 25°C				N	Dimensions (mm)			
	Qmax ⁽¹⁾ (Watts)	I _{max} (Amps)	V _{max} (Volts)	ΔT _{max} (°C)		A	B	C	D ⁽²⁾
CP1.4-7-10L	1.8	3.9	0.85	68	7	9.4	9.4	9.4	4.7
CP0.8-31-06L	4.4	2.1	3.8	67	31	12	12	12	3.4
CP1.0-31-05L	8.2	3.9	3.8	67	31	15	15	15	3.2
CP1.0-63-06L	12.7	3.0	7.6	67	63	15	30	15	3.6
CP1.0-71-06L	14.4	3.0	8.6	67	71	23	23	23	3.6
CP0.8-127-06L	18.1	2.1	15.4	67	127	25	25	25	3.4
CP2-31-10L	18.8	9.0	3.8	68	31	30	30	30	5.6
CP0.85-127-06L	20.2	2.7	15.3	66	127	30	30	30	3.6
CP1.0-127-06L	25.7	3.0	15.4	67	127	30	30	30	3.6
CP1.4-71-06L	28.7	6.0	8.6	67	71	30	30	30	3.8
CP1.0-127-05L	33.4	3.9	15.4	67	127	30	30	30	3.2
CP1.4-127-10L	33.4	3.9	15.4	68	127	40	40	40	4.7
CP1.4-127-06L	51.4	6.0	15.4	67	127	40	40	40	3.8
CP1.4-127-045L	72.0	8.5	15.4	65	127	40	40	40	3.3
CP2-127-06L	120.0	14.0	15.4	67	127	62	62	62	4.6

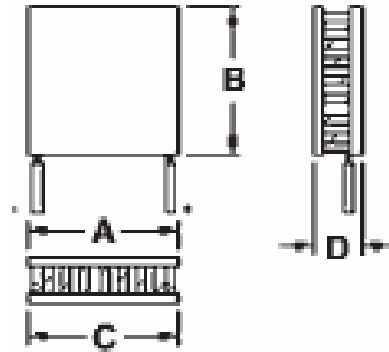


Figure 5.4 Standard commercially available thermoelectric single stage cooling modules (from Melcor)

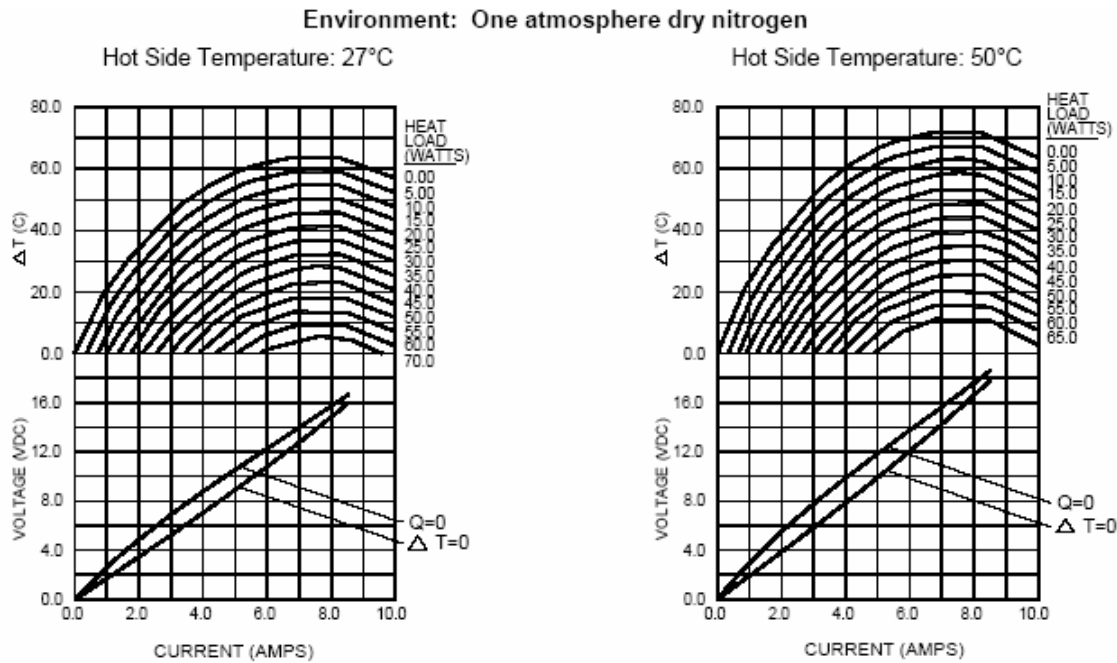


Figure 5.5 Performance curves for a single stage thermoelectric cooling module at two hot side temperatures (from Marlow Industries)

It must be emphasized that the rated conditions ΔT_{max} (at $I = I_{max}$, $\dot{Q}_c = 0$) and $\dot{Q}_{c,max}$ (at $I = I_{max}$, $\Delta T = 0$) quoted by the module manufacturer for a given hot-side temperature T_h represent opposite extremes of operation in terms of the temperature difference obtained

and the heat removal capacity. The full range of module operating conditions for a typical commercial module is illustrated by the performance characteristics presented in Figure 5.6 and Figure 5.7 and show how \dot{Q}_c and COP , respectively, vary for various values of ΔT as the module input current increases from 0 to I_{max} . These graphs apply to a Ferrotec single-stage module nominally 40 mm square by 4 mm thick containing 127 thermoelectric couples. The module is rated as follows: $\dot{Q}_{c,max} = 80$ W, $\Delta T_{max} = 72$ K and $I_{max} = 8.5$ A. The legend (shown on Figure 5.6) indicates the temperature difference associated with each curve in Figure 5.6 and Figure 5.7, starting with $\Delta T = 0$ for the top curve in each figure.

It can be seen from Figure 5.6 that, in general, the cooling capacity \dot{Q}_c increases with either an increase in input current I or a decrease in the temperature differential ΔT between the hot and cold sides of the module. Figure 5.7 shows that the coefficient of performance COP also increases as ΔT is reduced (with the input current held constant) and exhibits a maximum value COP_{max} as the input current is varied at a fixed ΔT . Furthermore, the magnitude of COP_{max} increases and its position moves progressively to lower values of I as ΔT is decreased.

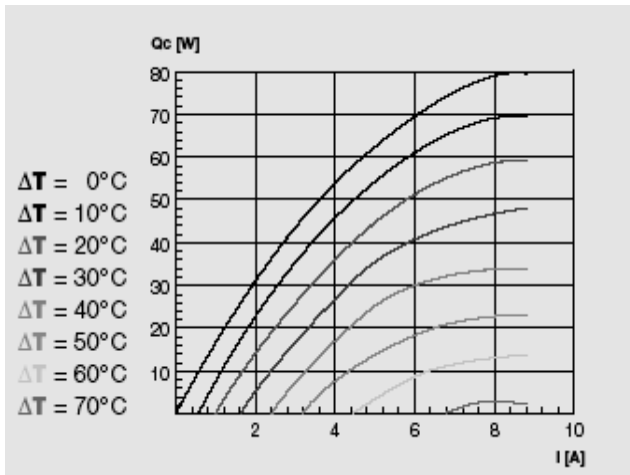


Figure 5.6 Cooling capacity versus input current at various ΔT values for a single-stage module with $\dot{Q}_{c,max} = 80$ W, $\Delta T_{max} = 72$ K and $I_{max} = 8.5$ A
(from Ferrotec)

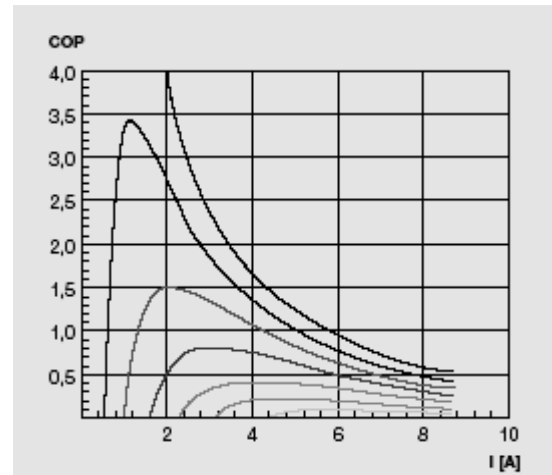


Figure 5.7 COP versus input current at various ΔT values for a single-stage module with $\dot{Q}_{c,max} = 80$ W and $I_{max} = 8.5$ A
(from Ferrotec)

It should be clear from the foregoing discussion that a specific pair of values for \dot{Q}_c and ΔT within the boundaries of the performance characteristics defines a unique operating point for a module, allowing the required input current and the corresponding coefficient of performance to be found. The design of a thermoelectric refrigeration system to provide the necessary rate of heat removal (\dot{Q}_c) for maintaining a required cold space temperature includes the selection of an appropriate cooling module (or modules). In addition to the characteristics of available modules, the ambient temperature for the application and the thermal resistances of peripheral heat exchange systems must be

taken into account as they have a significant influence on the temperature difference ΔT across the module.

In practice, operation with an input current close to I_{max} is generally avoided due to the poor efficiency (low COP) associated with the dominating effect of ohmic heating as the cooling capacity peaks. According to the Melcor Thermoelectric Handbook most thermoelectric coolers are operated somewhere between 40% and 80% of the maximum input power. Similar information issued by the Tellurex Corporation states that in ninety percent of applications the module current is between 70% and 80% of I_{max} .

For applications where the required cooling load exceeds the heat pumping capacity available with one module, multiple modules can be mounted in parallel thermally and connected electrically in series or series-parallel.

The maximum temperature difference ΔT_{max} (at $\dot{Q}_c = 0$) achievable with a single-stage thermoelectric cooling module can be estimated from Equation 5.3 and is limited to around 70 K. Multi-stage (or cascade) modules are available, usually for fairly low cooling capacities, with up to 6 stages for situations where higher temperature differentials of up to about 130 K are required. Most multi-stage modules are pyramidal in profile, as shown in Figure 5.8, with each successive higher-temperature stage absorbing heat rejected from the previous stage. Some two-stage modules, however, are manufactured with equal area stages and are capable of reaching a ΔT_{max} of over 80 K.

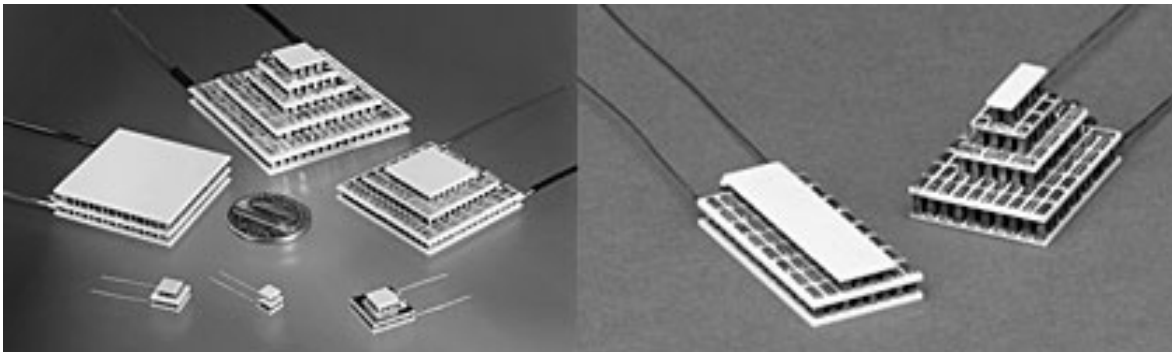


Figure 5.8 Multi-stage thermoelectric cooling modules (*from Melcor*)

Applications of thermoelectric cooling

Thermoelectric modules and systems have been extensively applied in numerous fields, handling cooling loads from milliwatts up to tens of kilowatts with temperature differences from almost zero to over 100 K (Stockholm, 1997). Although they are not the appropriate choice in all situations, thermoelectric coolers have the following significant advantages compared to other cooling methods which favour their adoption for certain applications:

- Solid-state construction.
 - absence of moving parts;
 - high reliability and life (MTBF > 200 000 h);
 - virtually maintenance-free;

- acoustically silent, no vibration, negligible electrical interference;
- environmentally friendly – no refrigerant gases involved.
- Compactness and low weight.
- Precise temperature control can be achieved with appropriate circuitry.

Riffat and Ma (2003) conducted a recent review of the applications and prospects of thermoelectric energy conversion devices for cooling (Peltier effect) and power generation (Seebeck effect). Other contributions on the uses of thermoelectric cooling include the review of Peltier cooling technology by Stockholm (1997), where applications are categorized according to cooling capacity range, and the CRC Thermoelectrics Handbook chapter by Davis et al (2006) dealing with mass-market applications. In addition, manufacturers and suppliers (see for example the Kryotherm and Marlow Industries web sites) list a wide variety of applications where thermoelectric products or solutions have been developed for cooling or temperature stabilization. Applications cover a diverse range of areas including electronics, computers and telecommunications, defence and space, medical and biological applications, laboratory and scientific equipment, air conditioning, food and beverage, and consumer products. Table 5.1 lists equipment incorporating thermoelectric cooling technology relevant to the scope of this review.

Table 5.1 Equipment utilising thermoelectric cooling for food and/or drink related uses

-
- | | |
|---|---|
| <ul style="list-style-type: none"> • domestic refrigerators; • refrigerator/freezer; • hotel room (mini-bar) refrigerators; • refrigerators for mobile homes, trucks, recreational vehicles and cars; • food service refrigerators for airborne application; • portable picnic coolers; | <ul style="list-style-type: none"> • wine coolers; • beer keg cooler; • beverage can cooler; • drinking water coolers; • milk cooler; • cream dispenser; • cooled conical fermenters for brewing; • point-of-sale vitrines. |
|---|---|
-

THERMOELECTRIC REFRIGERATION SYSTEMS

In a thermoelectric refrigeration system the Peltier module (or modules) must be interfaced with heat exchange systems to facilitate heat removal from the refrigerated space to the cold-side and heat rejection from the hot-side to the surroundings. The thermal resistances introduced by the heat exchange systems have a significant influence on the coefficient of performance of the refrigeration system. Some recent studies on the performance of prototype thermoelectric refrigerators and associated heat transfer systems are described in the following two sections.

Performance tests on thermoelectric refrigerators

Bansal and Martin (2000) measured the performance of three different types of domestic refrigerator: (i) a R134A vapour compression cycle fitted with heat exchange between the capillary tube and the suction line, (ii) an ammonia-water absorption cycle, and (iii) a thermoelectric unit fitted with pumped ethylene glycol heat exchanger loops at both the

cold and hot sides of the Peltier module to assist heat transfer from the air inside the refrigerator cabinet and to the environment respectively (see Figure 5.9).

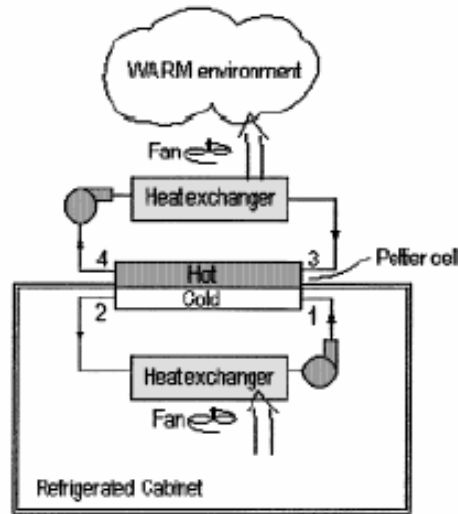


Figure 5.9 Schematic of thermoelectric refrigerator (from Bansal and Martin, 2000)

The internal volumes of the three refrigerator cabinets were only roughly similar and heat loss tests showed markedly different values of overall heat conductance, UA , between the interior air and the surrounding ambient as follows: (i) vapour compression; capacity = 45 litre, $UA = 1.01 \text{ W K}^{-1}$, (ii) absorption; capacity = 60 litre, $UA = 0.69 \text{ W K}^{-1}$, and (iii) thermoelectric; capacity = 40 litre, $UA = 0.78 \text{ W K}^{-1}$. The coefficient of performance values determined from the test results, for a cabinet temperature of 5°C and an ambient temperature of 16.6°C , were 2.59 for the vapour compression system, 0.47 for the absorption system and 0.69 for the thermoelectric system. An energy consumption comparison for the three refrigerators showed that the $\text{NH}_3\text{-H}_2\text{O}$ absorption system required the highest power input, despite its superior thermal resistance and hence lower heat removal requirement. The energy consumption values for the thermoelectric and vapour compression systems were about 80% and 33% of that for the absorption system respectively.

Cost comparisons showed that the purchase price of the thermoelectric system was approximately 5% more than for the absorption system, and more than 2.5 times the cost of the vapour compression system. For an assumed life time of 20 years it was shown that the total cost (purchasing plus operating costs) of the thermoelectric system would be marginally less than for the absorption system because of the greater energy costs for the latter. However, the total life time cost for the cheaper and more efficient vapour compression system would be about 37% of total cost for either of the other two systems.

Davis et al (2004) of Hydrocool Pty, Australia, a company specializing in heat transfer and thermoelectric research, described the design, build and performance of a prototype 126 litre thermoelectric refrigerator/freezer, incorporating a 36 litre freezer compartment, developed in collaboration with the Matsushita Refrigeration Company of Japan. Design operating temperatures of 0°C and -25°C were specified for the refrigerator and freezer

respectively. The unit, shown in Figure 5.10, features vacuum insulation panels to limit the heat load on the freezer and pumped recirculation liquid (a potassium formate solution) heat exchange circuits on both the hot and cold sides (see Figure 5.11). Heat is transferred by Hydrocool micro-channel heat exchangers between the thermoelectric modules and liquid, and finned-tube heat exchangers (with fans) between air and liquid.



Figure 5.10 126 litre thermoelectric refrigerator/freezer prototype (from Davis et al, 2004)

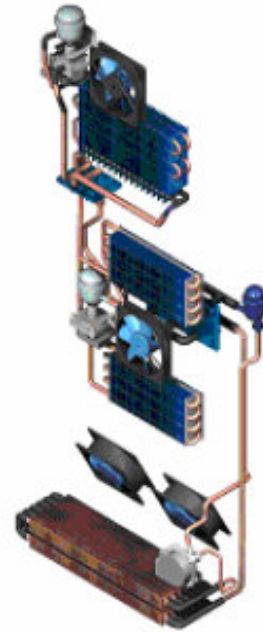


Figure 5.11 Layout of heat exchange systems for 126 litre thermoelectric refrigerator/freezer prototype (from Davis et al, 2004)

The unit uses a total of four thermoelectric modules, one module pumping heat from the freezer to the fridge and three other modules removing heat from the fridge to ambient. On test, the prototype refrigerator/freezer achieved an overall coefficient of performance of 0.44. Hydrocool (see <http://www.hydrocool.com/>) have recently announced the achievement of a *COP* of 1.2 for a 250 litre prototype thermoelectric refrigerator.

In a recent investigation Min and Rowe (2006) measured the performances of three prototype thermoelectric domestic refrigerators (designated TER-1, TER-2 and TER-3) with different heat exchanger arrangements as detailed in Table 5.2. For comparison purposes, a conventional vapour compression refrigerator with a total internal cabinet volume of 115 litre (including a 25 litre, -15°C freezer compartment) was also tested. This unit was found to achieve a *COP* of about 0.8 for a cabinet interior-to-ambient temperature difference, $\Delta T = 16\text{ K}$ and an ambient air temperature, $T_a = 23^{\circ}\text{C}$, although it was noted that a higher value of *COP* would be expected if only a fridge compartment was involved. The *COP* of the thermoelectric refrigerator TER-1, shown in Figure 5.12, was about 0.5 for the same conditions, exhibiting an almost linear increase from 0.36 to 1.16 as the temperature difference was reduced from 17.1 K to 9.7 K.

Table 5.2 Details of prototype thermoelectric domestic refrigerators tested by Min and Rowe, 2006.

	Cold-side heat exchanger	Hot-side heat exchanger	Cabinet internal volume/ litre
TER-1	fan-assisted (1 fan) aluminium heat exchanger (100 x 100 x 30)* with 24 bonded fins (100 x 20 x 1)* (see Figure 5.12)	fan-assisted (2 fans) aluminium heat exchanger (200 x 150 x 70)* with 33 bonded fins (200 x 60 x 1)* (see Figure 5.12)	115**
TER-2	fan-assisted (1 fan) extruded aluminium heat exchanger, similar to TER-1 but lower fin density (see Figure 5.13)	closed-loop pumped liquid heat exchange circuit (see Figure 5.13)	115**
TER-3	closed-loop pumped liquid heat exchange circuit	closed-loop pumped liquid heat exchange circuit	40

* all dimensions in mm; ** TER-1 and TER-2 cabinets were identical to the vapour compression unit.

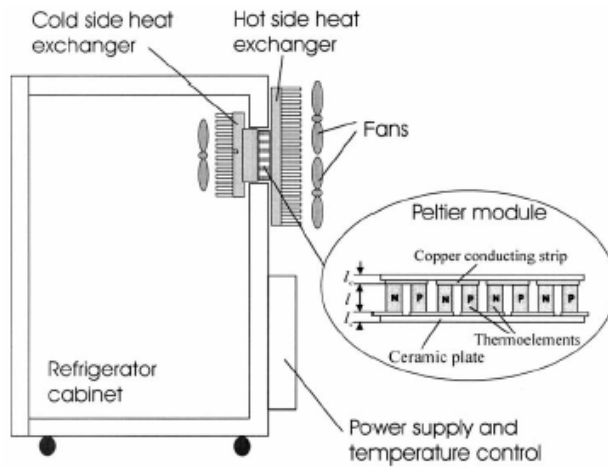


Figure 5.12 Thermoelectric refrigerator TER-1 with finned heat exchangers (from Min and Rowe, 2006)

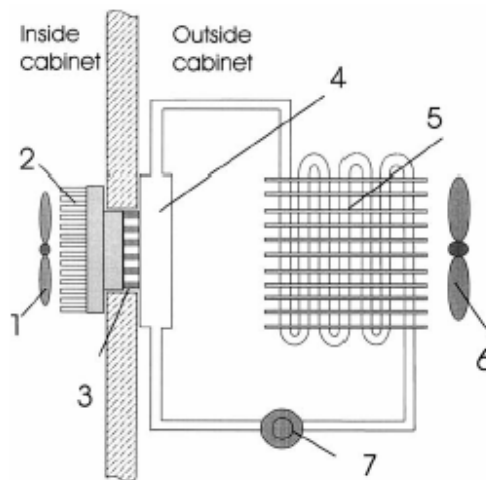


Figure 5.13 Thermoelectric refrigerator TER-2 with closed-loop liquid heat exchanger on the hot-side (from Min and Rowe, 2006)

In comparison with the TER-1 performance, Min and Rowe (2006) reported that the thermoelectric refrigerators employing a liquid heat exchange system on one or both sides achieved significantly lower *COP* values; approximately 0.3 at $\Delta T = 10$ K for TER-2 and 0.2 at $\Delta T = 14$ K for TER-3. The authors attributed the poor efficiency values measured for TER-2 and TER-3 to the limited heat pumping capacity of the thermoelectric modules, which in both cases were operated near to the maximum temperature difference where *COP* is relatively low.

Heat exchange systems for thermoelectric refrigerators

Riffat and Ma (2003) reviewed research on methods of improving the *COP* of thermoelectric cooling systems, including the use of heat exchangers with lower thermal resistances to reduce the temperature difference across the Peltier module. Natural convection and forced convection air-cooled heat sinks, water-cooled heat exchangers, heat pipes, a thermosyphon reboiler-condenser system and a system incorporating a phase change material are discussed. Other recent studies of liquid-cooled and two-phase thermosyphon heat exchangers are described in this section.

Davis et al (2006) examined the achievable performance of thermoelectric refrigeration systems employing state of the art air-cooled and liquid-cooled heat exchange systems. They noted that the recent development of inexpensive heat exchange systems with improved efficiency has facilitated increased heat flux densities, thus reducing the number of thermoelectric modules required. It is concluded that the cost reductions associated with using fewer modules, plus the availability of cheaper modules and affordable heat exchanger systems have significantly enhanced the commercial viability of thermoelectric cooling applications.

A paper by Nishihata et al (2002) of the Matsushita Refrigeration Company in Japan describes an enhanced liquid cooling system developed for application in Panasonic thermoelectric wine cellar cabinets and other Peltier cooled products. Figure 5.14 and Figure 5.15 illustrate the main features of the new design, which utilizes a single circular thermoelectric module of diameter 62 mm and integrates the circulation pump directly into the liquid heat exchanger manifold fitted to the heat rejection face of the module.

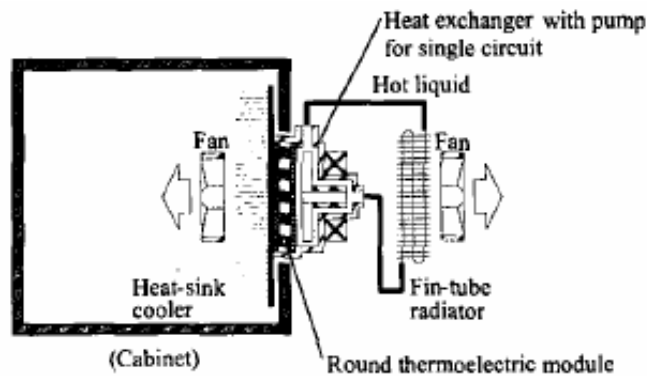


Figure 5.14 Schematic of Matsushita/Panasonic enhanced liquid cooling system (from Nishihata et al, 2002)

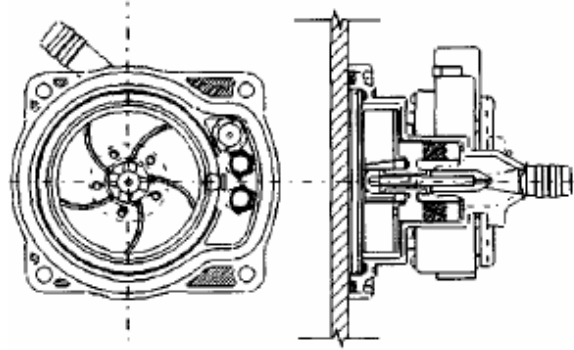


Figure 5.15 Matsushita/Panasonic liquid heat exchanger manifold with integrated circulation pump (from Nishihata et al, 2002)

Nishihata et al (2002) presented a comparison between two thermoelectric refrigerators using different liquid heat exchange systems: (i) the new enhanced system with integrated circulation pump described above, and (ii) a previous design using three 40 mm x 40 mm thermoelectric modules fitted with separate liquid manifolds, incorporating turbulence promoters, connected in series. A fan-assisted finned heat exchanger is employed on the heat absorption side of the thermoelectric module inside the refrigerated cabinet. The same values of cooling capacity (= 40.6 W), ambient air temperature (= 30°C) and cabinet temperature (= 11°C) were assumed for both systems. The comparison showed that the total fan plus pump power input was marginally higher with the enhanced system, at 7.5 W compared to 6.7 W, but the power input for the thermoelectric module reduced by more than 50%, from 135.7 W to 60.3 W. This improvement was reflected in the coefficient of performance which increased by a factor of 2.1, from 0.28 to 0.60.

Astrain et al (2003) developed a novel heat exchange device, as illustrated in Figure 5.16, incorporating a two-phase open-loop thermosyphon. The underlying principle of the device is redistribution of heat rejected from the relatively small face area of the Peltier cooler to the much larger fan-cooled finned outer surface. Thus, improved heat dissipation is achieved through a reduction in thermal resistance compared to a directly attached conventional finned heat sink.

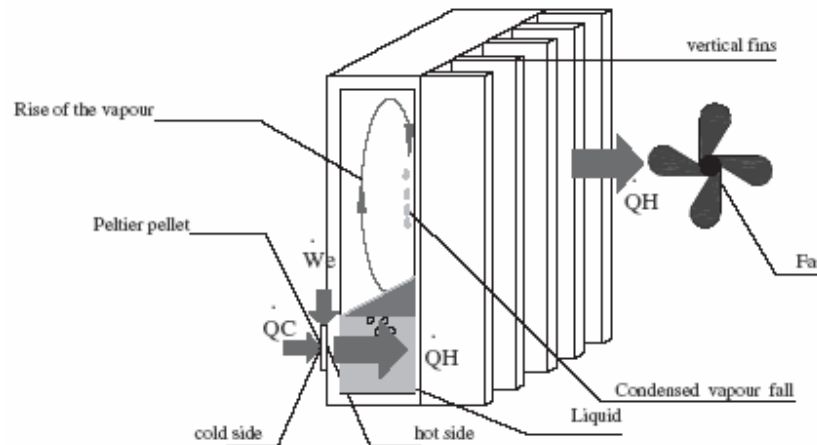


Figure 5.16 Hot-side heat exchanger incorporating thermosyphon (from Astrain et al, 2003)

An optimized prototype was constructed from aluminium sections with overall dimensions of 400 mm high x 155 mm wide, and 50 mm long x 1 mm thick fins spaced 3 mm apart. The thermosyphon cavity internal dimension was 11 mm between the condensing and boiling surfaces, the latter with V-shaped scratches to promote heat transfer. Refrigerant R-141b was used as the working fluid.

Experiments were performed using the prototype thermosyphon heat exchange device for a heat dissipation rate of 50 W from a 40 mm x 40 mm Peltier module. The results indicated that total thermal resistance from the Peltier module hot face to ambient varied with ambient temperature from 0.125 K/W at 293 K to 0.079 K/W at 308 K, corresponding to an improvement compared to a conventional finned heat sink of between 23.8% and 51.4% respectively.

Astrain et al (2003) also tested and compared two versions of a prototype 198 litre thermoelectric refrigerator, one employing the optimized thermosyphon heat exchange device described above and the other using a conventional heat sink. It was found that use of the thermosyphon device resulted in lower cabinet interior temperatures and increased the refrigerator *COP* by between 21.3% (at 292 K ambient) and 36.5% (at 303 K ambient). The maximum *COP* value measured, however, was only 0.32 (at 303 K ambient).

Chandratilleke et al (2004) presented results from simulation models and experiments for micro-channel heat exchangers developed by Hydrocool for thermoelectric refrigeration applications, for example the 126 litre prototype refrigerator/freezer discussed in the previous section (Davis et al, 2004). Tests conducted on the heat exchangers using water as the heat transfer fluid to remove 15-20 W over a base area of 40mm x 40 mm indicated that thermal resistances of the order 0.01–0.02 K/W could be achieved, claimed to be the lowest R values reported for heat exchangers designed for thermoelectric modules.

Other thermoelectric cooling products

In addition to the equipment already listed in Table 5.1, manufacturers of thermoelectric cooling equipment produce a wide variety of other Peltier based cooling products, including cold plates, liquid chillers and air-to-air coolers, for a broad range of applications. Some of these products may conceivably be applied, or the technology adapted, for food and drink related applications. Two examples are described below.

Figure 5.17 shows an air-to-air thermoelectric cooling unit (Model AC-162) manufactured by TE Technology, Inc. Both larger and smaller units are available and similar units are available from other manufacturers. The unit shown incorporates six thermoelectric cooling modules and extender blocks, together with bonded fin heat exchangers and fans on both the hot and cold sides. Typical applications include cooling of electronic enclosures, refrigerators, vending machines and environmental chambers. At 25°C ambient temperature the unit has a rated cooling capacity of 162 W at zero temperature difference. The temperature of an enclosure can be reduced to 45 K below ambient at zero load. For intermediate temperature differences the cooling capacity reduces linearly and, for example, would still be about 75 W for a 25 K differential. The

cooling unit is powered by a 24 V DC supply and draws a total current of approximately 18 A at its rated capacity. The cost quoted per unit is \$675.

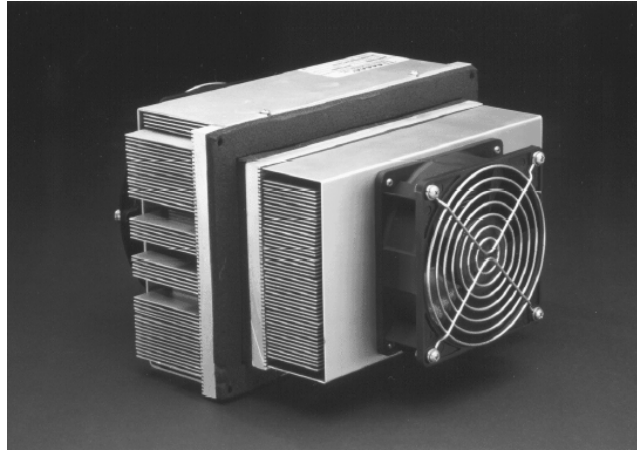


Figure 5.17 Thermoelectric air-to-air cooling unit (from *TE Technology, Inc.*)

Figure 5.18 shows a thermoelectric liquid-to-air cooler (Model LC-200), also manufactured by TE Technology, Inc. The cooler is suitable for a variety of laboratory and other applications including recirculating water chillers, in-process cooling, laser diode cooling and temperature baths. The unit features an 8-pass liquid heat exchanger, a high-density bonded fin heat sink and cooling fan on the air side and uses six thermoelectric cooling modules. The cooler can be supplied with swirl inserts on the liquid side of the heat exchanger to improve heat transfer at low flow rates. At an ambient temperature of 25°C the rated cooling capacity is nearly 200 W, based on zero temperature difference between the liquid inlet and ambient temperatures and a water flow rate of 1.6 litre/minute. For a liquid inlet temperature of 0°C, for example, and the same ambient temperature the cooling capacity would be just less than 100 W. The unit is powered by a 24 V DC supply and draws a total current of approximately 17.65 A at its rated capacity. The cost quoted per unit is \$609.

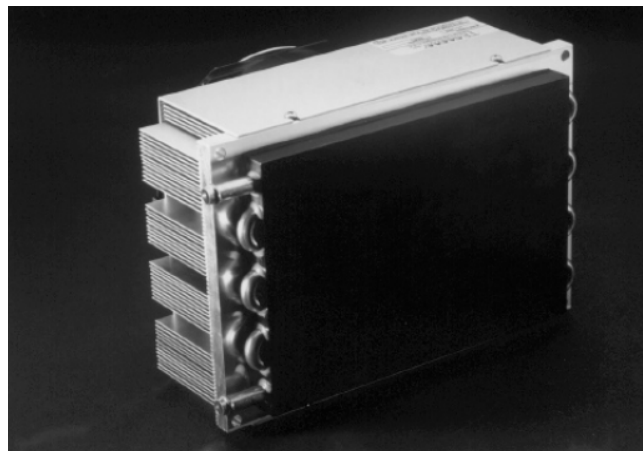


Figure 5.18 Thermoelectric liquid cooling unit (from *TE Technology, Inc.*)

Large thermoelectric cooling systems

Some large thermoelectric cooling systems have been built, mainly for special applications, to satisfy cooling loads (with combined heating in some cases) in the kilowatt range using multiple Peltier modules. Stockholm (1997) describes some past applications, including a building air conditioning installation with 30 units, each providing 1.5 kW of cooling and 1.8 kW of heating, a railway carriage air conditioning system with 20 kW of cooling and 32 kW of heating used on the French railways, and a 15 kW cooling system for producing chilled water in a submarine. Stockholm (1997) states that these systems demonstrated their reliability but were uneconomic, concluding that further applications for thermoelectric cooling with cooling loads in the tens of kW range will not be economic until thermoelectric materials with at least double the current figure of merit become available for industrial use.

A further example is the thermoelectric gas cooling system installed in the radioactive gas activity suppression plant at the Leningrad nuclear power facility (Lebedev et al, 2002). The system cools 300 m³/h of gas from 35°C to -20°C and rejects heat to sea water. The gas flows in 40 parallel streams, each with 6 cooling units connected in series, and each unit containing 18 Kryotherm thermoelectric cooling modules.

CONCLUDING REMARKS

- A review has been conducted of information on thermoelectric (or Peltier) refrigeration technology covering fundamentals, commercially available thermoelectric cooling modules, applications, thermoelectric refrigerators, associated heat exchange systems and other thermoelectric cooling products.
- Thermoelectric coolers (TECs) are lightweight, compact, d.c. powered, solid-state devices incorporating one or more semiconductor thermocouples. They contain no moving parts and are reliable, virtually maintenance-free, silent and vibration-free in operation. No refrigerant gases are involved. TECs can be used for heating as well as cooling and integration with temperature control circuitry is simple.
- The main drawback of thermoelectric cooling is the intrinsically low coefficient of performance which is linked to the properties of the thermoelement materials and characterized by the dimensionless figure of merit, ZT . Nearly all commercially available TECs are constructed from bismuth telluride (Bi_2Te_3) based bulk materials. The best materials of this type have a ZT approaching unity. Approximately four times this value would be required for thermoelectric coolers to achieve efficiencies comparable with vapour compression systems. Research directed towards achieving higher values of the figure of merit is focused on: (i) finding new materials with improved thermoelectric properties and (ii) fabricating low-dimensional thermoelectric structures.
- A wide range of single-stage thermoelectric modules is available commercially with maximum cooling capacities from less than one watt up to nearly 200 W. Module dimensions vary from a few millimetres square up to 62 mm x 62 mm, with module

thicknesses normally between 2 mm and 6mm. The number of couples per module varies from less than ten to nearly 200. Each module is rated for the extreme conditions ΔT_{max} and $\dot{Q}_{c,max}$ (both at I_{max}), although in most applications modules are operated below 80% of I_{max} to avoid poor efficiency. The maximum achievable temperature difference ΔT_{max} for a single-stage TEC is around 70 K. Multi-stage (or cascade) modules, with up to six stages stacked in series one on top of another, are available for situations where larger temperature differences are required. Thermoelectric modules are extensively applied for the cooling or temperature stabilization of electronic devices where small size and high reliability are of often greater importance than efficiency

- Modules can be mounted in parallel for applications where cooling loads beyond the capacity of a single module must be satisfied. Typical thermoelectric cooling systems where multiple modules may be used include refrigerators, air conditioners, electronic enclosures, cold plates and liquid chillers.
- TEC based products developed, or under development, for food and/or drink related uses include domestic refrigerators (and a fridge/freezer), refrigerators for hotel rooms (preferred for their silent operation), mobile homes, trucks and other vehicles, portable cool boxes, drinking water coolers, beer/wine cabinets and food service items.
- Coefficients of performance reported from tests conducted on various prototype domestic thermoelectric refrigerators, with internal volumes from 40 litres to 250 litres, vary widely from approximately 0.2 up to 1.2. An overall *COP* of 0.44 was recorded for a 126 litre prototype unit operating with fridge (90 litre) and freezer (36 litre) compartment temperatures of 0°C and -25°C respectively.
- The design of a thermoelectric refrigeration system should specify the use of low-thermal resistance heat exchangers interfaced to the hot and cold sides of the TEC modules in order to achieve the best possible system performance.
- Large thermoelectric cooling systems with cooling capacities into the tens of kW range have been built and operated satisfactorily, albeit uneconomically, for special applications. Further applications on this scale are not anticipated without a significant breakthrough in improving the figure of merit of thermoelectric materials.

REFERENCES

- D. Astrain, J.G. Vian and M. Dominguez, Increase of COP in the thermoelectric refrigeration by the optimization of heat dissipation, *Applied Thermal Engineering*, 23, 2183-2200, 2003.
- P.K. Bansal and A. Martin, Comparative study of vapour compression, thermoelectric and absorption refrigerators, *International Journal of Energy Research*, 24, 93-107, 2000.
- T. Chandratilleke, B. Banney and P. Clarke, High performance heat exchanger for thermoelectric cooling with large heat loads, 23rd International Conference on Thermoelectrics, Adelaide, 2004.
- M.C. Davis, B.P. Banney, P.T. Clarke, B.R. Manners and R.M. Weymouth, Thermoelectric refrigeration for mass-market applications, Section V, Chapter 59: Thermoelectrics Handbook: Macro to Nano, (Ed: D.M. Rowe), CRC Press, 2006.
- M. Davis, B. Manners and P. Clarke, Design of a 126 litre refrigerator/freezer commercial prototype, 23rd International Conference on Thermoelectrics, Adelaide, 2004.
- F.J. DiSalvo, Thermoelectric cooling and power generation, *Science*, 285 (5428), 703-706, 1999.
- H.J. Goldsmid, A new upper limit to the thermoelectric figure-of-merit, Section I, Chapter 10: Thermoelectrics Handbook: Macro to Nano, (Ed: D.M. Rowe), CRC Press, 2006.
- V.I. Lebedev, L.I. Tyomkin, V.E. Baukin and A.P. Vyalov, The 150 kW thermoelectric gas cooling system. Results of operation, Proc. 21st International Conference on Thermoelectronics, 25-29 Aug. 2002, 558 – 560.
- G. Min and D.M. Rowe, Improved model for calculating the coefficient of performance of a Peltier module, *Energy Conversion & Management*, 41, 163-171, 2000.
- G. Min and D.M. Rowe, Experimental evaluation of prototype thermoelectric domestic-refrigerators, *Applied Energy*, 83, 133-152, 2006.
- H. Nishihata, O. Kido, T. Ueno, Peltier cooling system utilizing liquid heat exchanger combined with pump, Proc. 21st International Conference on Thermoelectrics, Long Beach, CA, USA, August 2002
- S.B. Riffatt and X. Ma, Thermoelectrics: a review of present and potential applications, *Applied Thermal Engineering*, 23, 913-935, 2003.
- S.B. Riffatt and X. Ma, Improving the coefficient of performance of thermoelectric cooling systems: a review, *International Journal of Energy Research*, 28, 753-768, 2004.

D.M. Rowe, General Principles and Basic Considerations, Section I, Chapter 1:
Thermoelectrics Handbook: Macro to Nano, (Ed: D.M. Rowe), CRC Press, 2006.

D.M. Rowe and C.M.Bhandari, Modern Thermoelectrics, Holt, Rinehart and Wilson,
1983.

J.G. Stockholm, Current state of Peltier cooling, Proc. 16th International Conference on
Thermoelectrics, Dresden, Germany, 1997, 37-46.